

# The Solid State of Rare Gases

GERALD L. POLLACK

National Bureau of Standards, Washington, D. C.

## CONTENTS

Introduction.....	748
I. Structure.....	749
A. X-Ray Diffraction Experiments.....	749
(1) Introduction.....	749
(2) Powder Methods and Results.....	750
(3) Other Techniques.....	753
B. Density and Expansivity.....	753
C. Theory of the Solid Structure.....	755
II. Melting and Crystallization.....	758
A. Melting.....	758
(1) General and Theoretical.....	758
(2) Experimental.....	760
B. Crystallization.....	763
III. Thermodynamic Properties.....	765
A. Intermolecular Potentials.....	765
B. Law of Corresponding States and Applications.....	771
(1) Law of Corresponding States.....	771
(2) Vapor Pressure.....	774
(3) Thermal Conductivity.....	778
C. Specific Heat.....	781
(1) Vacancy Effects.....	784
(2) Anharmonicity and Grüneisen's Constant.....	785
D. Zero-Point Properties.....	786
E. Compressibility.....	789
Acknowledgments.....	791

## INTRODUCTION

The study of the solid state of rare gases is doubly and uniquely interesting. First, the forces between identical molecules are weak, short range, much investigated, and rather well understood so that critical tests of appropriate theories by their ability to predict properties of rare gas crystals are comparatively simple. Second, these same forces make it necessary to carry out experiments on the rare-gas solids at low temperatures, high pressures, or both so that accurate measurements of the predicted properties are difficult. Partly on account of the theoretical advantages and notwithstanding the experimental difficulties much interest has centered around these studies since the beginning of this century, shortly following the discovery of the gases themselves, and increasingly in the last fifteen years. The purpose of this paper is to review both experimental and theoretical work on solid Ne, Ar, Kr, Xe, and Rn with special emphasis on advances since the well-known review<sup>1</sup> of this kind on Ar.

<sup>1</sup> E. R. Dobbs and G. O. Jones, Repts. Progr. Phys. **20**, 516 (1957).

Rare-gas crystals are prototype<sup>2-4</sup> molecular crystals, one of the classic solid types.<sup>5-7</sup> For our purposes molecular crystals may be characterized thus: (a) all lattice points are occupied by identical molecules, and (b) the lattice molecules interact with weak forces, principally van der Waals attractions ( $r^{-6}$ ). In more complicated molecular crystals the forces may be strongly noncentral, or covalent effects may become important. Actually these contributions are present even in rare-gas crystals but their effects are quantitatively small (see, however, I.C. Theory of the Solid Structure). The properties of rare-gas solids usually change in an ordered and frequently predictable fashion (see, e.g., III.B.1 Law of Corresponding States) as the tables and figures show. This has been used, for example, to study effects of isotopes and zero-point energy and also as a basis for calculating properties of other not quite so ideal molecular crystals. Using more specific theories, experiments on rare-gas solids yield much knowledge on the details of molecular interaction especially departures from simple inverse-power potentials, anharmonicity, and electron exchange. Most recently, effects of lattice imperfections have been observed and studied in rare-gas crystals. We have attempted in what follows to discuss the main ideas in these and in other modern currents of rare-gas solid research. Although He is a rare gas and should properly be included in the discussion, its small molecular mass and large ratio of zero-point energy to static-lattice energy give the solid and the liquid many well-known and appreciated unique properties. These have been copiously reviewed by others and therefore any but casual mention of He is omitted here. Experiments on solid and liquid Rn in contrast have been very few; these have been included. A clear and concise survey of experimental properties of liquid and solid rare gases including He has been given by Hollis Hallett<sup>8</sup> as part

<sup>2</sup> G. O. Jones, Z. Physik. Chem. **16**, 267 (1958).

<sup>3</sup> A. V. Stepanov, *Krystallografiya* **3**, 392 (1958) [English transl.: Soviet Phys.—Cryst. **3**, 395 (1958)].

<sup>4</sup> E. R. Dobbs, Am. J. Phys. **28**, 243 (1960).

<sup>5</sup> F. Seitz, *The Modern Theory of Solids* (McGraw-Hill Book Company, Inc., New York, 1940).

<sup>6</sup> C. Kittel, *Introduction to Solid State Physics* (John Wiley & Sons, Inc., New York, 1956).

<sup>7</sup> P. W. Anderson, *Concepts in Solids* (W. A. Benjamin, Inc., New York, 1963).

<sup>8</sup> A. C. Hollis Hallett, in *Argon, Helium, and the Rare Gases*, edited by G. A. Cook (Interscience Publishers, Inc., New York, 1961), Vol. I, pp. 313-385.

of an exhaustive treatment of He and the rare gases.<sup>9</sup> For further, general information on the rare gases the reader is referred to two recent books.<sup>10,11</sup>

This paper is divided into the following main parts: I. Structure, II. Melting and Crystallization, and III. Thermodynamic Properties, each with several sub-headings. Under these headings a comprehensive review, within limits of coherence, of both the experimental and theoretical literature has been attempted with enough background material to facilitate understanding by workers in other fields. The theoretical discussions aim at presenting the main ideas in sufficient detail to enable at least qualitative and where feasible quantitative comparison of different approaches among themselves and with experiment. Some advantage has been taken of the excellent discussions in the earlier review of Dobbs and Jones<sup>1</sup> in avoiding unnecessary duplication. The experimental discussions are aimed at describing the techniques and their limitations, presenting the results as far as they are known in figures and tables, and pointing up directions for further progress of especial interest. Relevant theoretical work has been discussed either interwoven with or else closely following the experiments. Since it was clear from the outset that there were many more theoretical papers than experimental ones to be reviewed, preference was shown toward these latter, our stated aim being to encourage further experiments on rare-gas solids.

## I. STRUCTURE

### A. X-Ray Diffraction Experiments

#### 1. Introduction

Of all the kinds of measurements which have been made on solid rare gases the most complete are those of x-ray diffraction studies. From these and related experiments it is known that the rare gases crystallize into the cubic close-packed structure common to many metals, e.g., Cu and Ag, and to other molecular crystals, e.g., HCl and CH<sub>4</sub>.

In a cubic close-packed molecular crystal the lattice may be conveniently pictured as built up of layers of spheres, each sphere representing one molecule. Let all the centers of a large number of identical spheres be coplanar and let the spheres be closest packed in the plane so that every sphere touches six others, i.e. every sphere has six nearest neighbors in the plane. If many such identical planes are layered upon each other so that the interstitial volume is minimized (each sphere

touches three spheres in the plane below and three spheres in the plane above) and the spheres of any plane are vertically aligned with the spheres in the planes twice removed, i.e. an ordering ABCABC . . . , we have a representation of the geometry involved.<sup>12</sup> The equilibrium molecular crystal structure is in general a function of the external conditions, e.g., temperature and pressure, and although there has only most recently been experimental evidence for any phase other than the cubic close-packed one for rare-gas solids, much theoretical work has been done on a postulated hexagonal close-packed (hcp) phase. This is another rather commonly observed structure in metals, e.g., Mg and Zn, but less commonly observed in molecular crystals. The hcp structure has, however, been observed in H<sub>2</sub> and recently<sup>13</sup> in N<sub>2</sub>. It is characterized by closest-packed planes layered so as to minimize the interstitial volume but with an ordering ABAB. . . .<sup>12</sup>

The equilibrium crystal configuration under a set of conditions is that for which the Gibbs free energy ( $G = E + PV - TS$ ) is a minimum. Under certain conditions, notably at 0°K and at zero pressure, there are theoretical grounds for the stability of an hcp over a cubic close-packed structure for rare-gas crystals. Much has been learned from calculations of this kind and we discuss them in detail below (I.C.). It is to be emphasized that problems of phase change are much more easily treated in rare-gas crystals than in the other less symmetric molecular crystals whose Gibbs functions must contain important terms for relative orientation, rotational and vibrational energy, etc. In such substances discontinuities in solid-state properties are more difficult to trace down and they occur frequently. In a rare-gas crystal on the other hand almost any discontinuity in physical properties should be detected by a change in crystal structure, i.e. by x-ray observation. Principal exceptions are higher energy phenomena which involve electron distribution and these too may in principle be observed by x-ray techniques. Thus, for the study of the solid state of rare gases x rays are a uniquely powerful probe.

For understanding the results of x-ray structure studies it is necessary to fix attention on the unit cell of the rare-gas crystals. For these cubic close-packed structures, the unit cell is face-centered cubic (fcc), i.e., a cube of side  $a_0$  the lattice parameter, with a molecule of rare gas more or less loosely bound to each of its corners and another in the center of each face. The relation between a molecule in the center of a face and each of the four molecules at the corners of that face is that of nearest neighbor, and the relation between a molecule at the corner of a face and the molecules at

<sup>9</sup> *Argon, Helium, and the Rare Gases*, edited by G. A. Cook (Interscience Publishers, Inc., New York, 1961), Vols. I and II.

<sup>10</sup> P. Lafitte and H. Brusset, *Les Gas Inertes, l'Hydrogène, les Halogènes* (Masson et Cie., Paris, 1955).

<sup>11</sup> D. N. Finkel'shtein, *Inertnye Gazy* (Izdatel'stvo Acad. Nauk U.S.S.R., Moscow, 1961).

<sup>12</sup> The geometry is made much clearer by reference to diagrams. L. Pauling, *Nature of the Chemical Bond* (Cornell University Press, Ithaca, New York, 1948), 2nd ed., pp. 373, 374.

<sup>13</sup> W. E. Streib, T. H. Jordan, and W. N. Lipscomb, *J. Chem. Phys.* **37**, 2962 (1962).

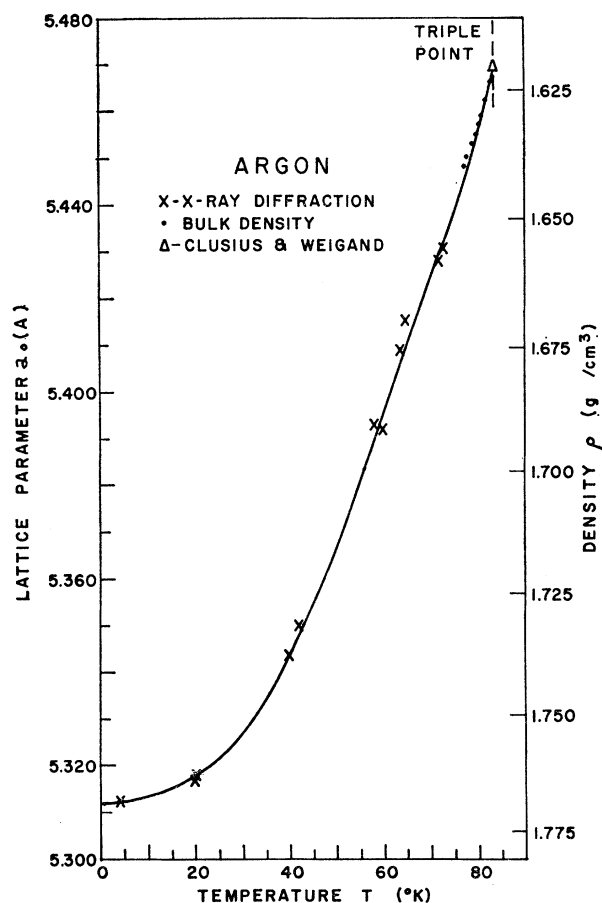


FIG. 1. Lattice parameter  $a_0$  (Å) and density  $\rho$  ( $\text{g/cm}^3$ ) of argon as function of temperature  $T$  ( $^\circ\text{K}$ ). The experimental uncertainty in the best modern values, which are represented by the solid curve, is about 0.002 Å. Most of the measurements shown were carried out on argon samples 99.999% pure. The x-ray diffraction data is that of Dobbs *et al.* (Ref. 26), and Bolz and Mauer (Ref. 28); the bulk-density data are that of Dobbs *et al.*, and Smith (Ref. 27); the density at the triple point is from Clusius and Weigand (Ref. 25).

adjacent corners of the face is that of second nearest neighbor. It may be seen that for a fcc crystal the number of nearest neighbors is 12 and the nearest-neighbor distance is  $a_0/\sqrt{2}$ . The number of second nearest neighbors is only 6 and the second nearest-neighbor distance is  $a_0$ .

Until recently the only x-ray measurements on rare gases were on powder samples and these have been the most productive experiments. The techniques and their results are discussed in more detail in the next section (I.A.2). X-ray measurements on single crystals offer the opportunity of determining  $a_0$  more accurately. So far very few experiments of this kind have been reported, but such work is being undertaken in some laboratories. Sec. I.A.3 therefore discusses briefly what is involved in single crystal measurements on rare gases and related experiments.

## 2. Powder Methods and Results

The Debye-Scherrer-Hull powder technique<sup>14,15</sup> and variants of it have been the most productive for x-ray study of rare-gas solid structure. Briefly described, the low-temperature Debye-Scherrer-Hull camera beams monochromatic, collimated, x rays at a powdered sample in the center of a cylindrical cell. The powder is usually deposited in a uniform, thin layer on the surface of a small, hollow, thin-walled metal cylinder filled with an appropriate coolant, e.g., liquid nitrogen or liquid helium. The beam is diffracted from the crystallites in the powder and the diffracted x rays impinge on a film strip which is concentric with the sample and which is placed around the camera so as to subtend the largest possible angle measured from the cylinder axis. If the crystallites of the powder are sufficiently small and randomly oriented, the type of crystal structure and lattice parameter  $a_0$  may be determined from the spacings and relative intensities of the lines on the developed film. A powder satisfying these conditions is formed when rare gas is condensed from a pressure below its triple-point vapor pressure onto a sufficiently cold surface. Slow condensation of Ar vapor onto a 4°K cold surface for example, gives crystal sizes of a few hundred angstroms. Crystals smaller than 100 Å are usually not observable on powder patterns.

The earliest x-ray determinations of rare-gas solid structure were made with such cameras,<sup>16</sup> at isolated temperatures, almost concurrently in Germany<sup>17</sup> and Holland<sup>18</sup> on Ar, the most widely available of the rare gases. Subsequently the techniques were extended to Ne<sup>19</sup> and Kr<sup>20</sup> by Dutch workers and to Xe<sup>21</sup> and Kr<sup>22</sup> in Italy. These experiments all identified the fcc structure of the solids but their determinations of  $a_0$  were all rather unreliable by modern standards. Inaccuracies in measurement of  $a_0$  were probably due to several causes. In general, the beams were not well collimated. This, along with large sample radius and eccentricity, tends to spread out the diffraction maxima on the film strip, making accurate measurements of the angle of diffraction difficult. Not surprisingly these early devices lacked the flexibility of modern Debye-Scherrer-Hull cameras and no adequate provision could be made for assuring that the axis of the cylindrical specimen coincided with the axis of the film. The claimed uncertainties in  $a_0$  for this earlier work vary from about  $\pm 0.01$  Å to  $\pm 0.06$  Å

<sup>14</sup> A. H. Compton and S. K. Allison, *X-Rays in Theory and Experiment* (D. Van Nostrand Co., Inc., New York, 1935).

<sup>15</sup> L. V. Azároff and M. J. Buerger, *The Powder Method in X-Ray Crystallography* (McGraw-Hill Book Co., Inc., New York, 1958).

<sup>16</sup> F. Simon and C. von Simson, *Z. Physik* **21**, 168 (1924).

<sup>17</sup> F. Simon and C. von Simson, *Z. Physik* **25**, 160 (1924).

<sup>18</sup> J. De Smedt and W. H. Keesom, *Physica* **5**, 344 (1925).

<sup>19</sup> J. De Smedt, W. H. Keesom, and H. H. Mooy, *Commun. Kamerlingh Onnes Lab. Univ. Leiden* **18**, 203e (1930).

<sup>20</sup> W. H. Keesom and H. H. Mooy, *Nature* **125**, 889 (1930). W. H. Keesom and H. H. Mooy, *Proc. Acad. Sci. Amsterdam* **33**, 447 (1930).

<sup>21</sup> G. Natta and A. Nasini, *Nature* **125**, 457 (1930).

<sup>22</sup> A. Nasini and G. Natta, *Atti. Accad. Naz. Lincei, Rend.* **12**, 141 (1930).

but modern values of  $a_0$  fall in general well outside these limits.

Perhaps the most severe limitation in these pioneering researches was the necessity of working with the solids only at temperatures far below their triple points because of the high vapor pressures of the rare gases. For insufficiently low temperatures the appreciable vapor pressure in the camera conducted heat to the powder which melted it. This made the long exposures necessary for good powder patterns impossible. Investigation of  $a_0$  for Kr and Xe at temperatures nearer to their triple-point temperatures were undertaken by Ruhemann and Simon<sup>22</sup> with an apparatus which was the forerunner of modern low-temperature powder cameras. In this camera the deposition surface and the vapor in equilibrium with it were thermally isolated from ambient temperatures by a vacuum jacket. Beam ac-

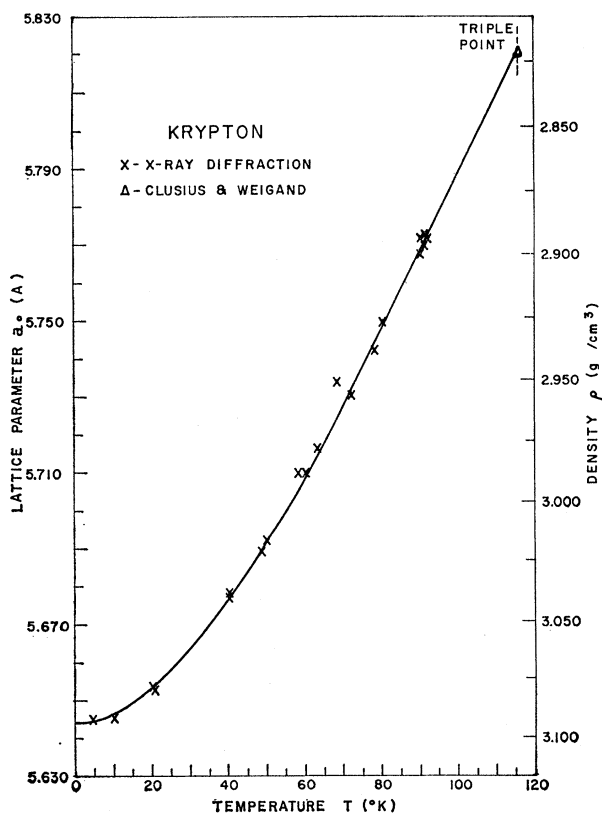


FIG. 2. Lattice parameter  $a_0$  (Å) and density  $\rho$  (g/cm<sup>3</sup>) of krypton as function of temperature  $T$  (°K). The solid curve represents the best modern values. The experimental uncertainty is about 0.001 Å in the range of the measurements. Most of the measurements shown were carried out on krypton samples 99.5% pure. The x-ray diffraction data is that of Dobbs and Luszczynski (Ref. 31), Cheesman and Soane (Ref. 32), Figgins and Smith (Ref. 33), Klug and Sears (Ref. 34), and Bolz and Mauer (Ref. 28). The density at the triple point is from Clusius and Weigand (Ref. 25).

<sup>22</sup> B. Ruhemann and F. Simon, *Z. Physik. Chem.* **B15**, 389 (1931).

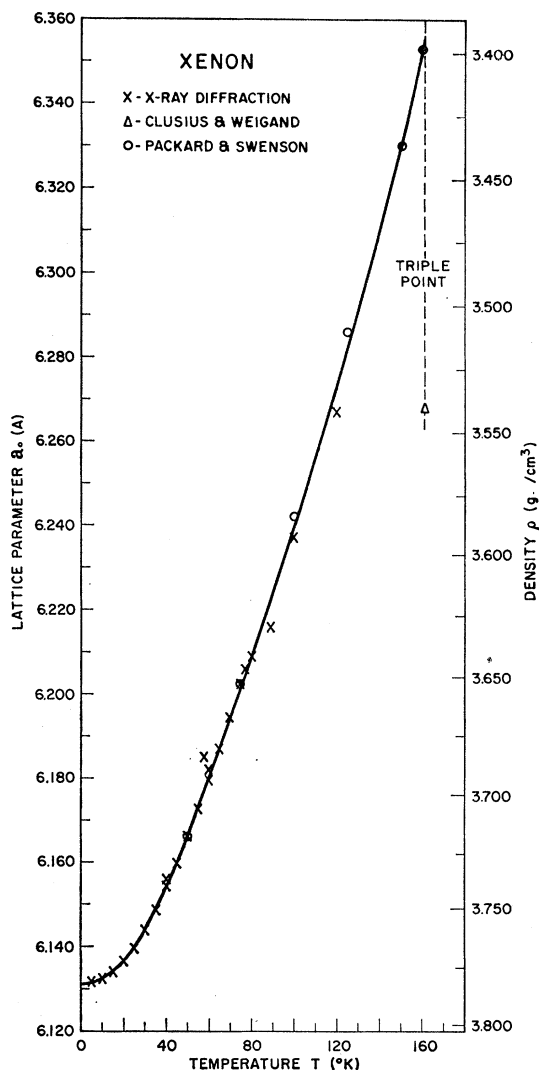


FIG. 3. Lattice parameter  $a_0$  (Å) and density  $\rho$  (g/cm<sup>3</sup>) of xenon as function of temperature  $T$  (°K). The solid curve represents the best modern values. The experimental uncertainty below 120°K is about 0.001 Å. Except for the determination of Clusius and Weigand (Ref. 25), which is uncertain, the only measurements of either  $\rho$  or  $a_0$  which have been reported above 120°K are the very recent ones of Packard and Swenson (Ref. 35) from compressibility experiments. The x-ray diffraction data are from Cheesman and Soane (Ref. 32), Eatwell and Smith (Ref. 36), Sears and Klug (Ref. 37), and Bolz and Mauer (Ref. 28).

cess to the condensed film was through vacuum tight but x-ray transparent windows.

The lattice parameter at the triple point was subsequently indirectly determined from thermodynamic considerations of the change in volume on freezing.<sup>24,25</sup> When the densities  $\rho$  of the solid-rare gases at the triple point obtained in this manner are used to recompute  $a_0$  with modern molecular weights the results, except for Xe, are impressive. These four values of  $a_0$  have been included in Figs. 1-4.

<sup>24</sup> K. Clusius, *Z. Physik. Chem.* **B31**, 459 (1936).

<sup>25</sup> K. Clusius and K. Weigand, *Z. Physik. Chem.* **B46**, 1 (1940).

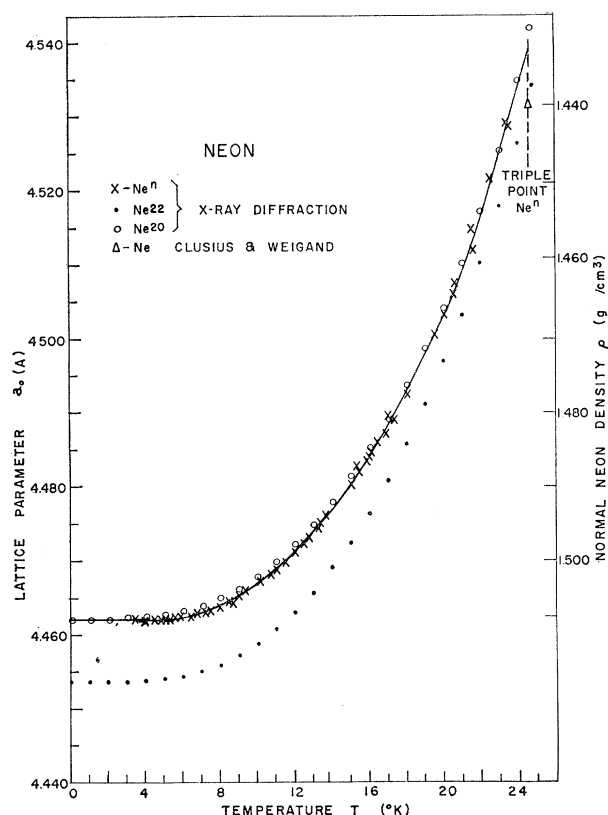


FIG. 4. Lattice parameter  $a_0$  (Å) and density  $\rho$  ( $\text{g}/\text{cm}^3$ ) of normal neon ( $^{20}\text{Ne}$ ), and lattice parameter of  $^{20}\text{Ne}$  and  $^{22}\text{Ne}$  as functions of temperature  $T$  ( $^\circ\text{K}$ ). The standard deviation of all the x-ray data is 0.0006 Å. The solid curve represents the best modern values for normal neon. Points for  $^{20}\text{Ne}$  and  $^{22}\text{Ne}$  were taken at 5 $^\circ\text{K}$  intervals from a least squares polynomial fit over the entire temperature range. Purities of the samples were:  $^{20}\text{Ne}$  99.96%,  $^{22}\text{Ne}$  98.6%, and  $^{22}\text{Ne}$  98.8%. The x-ray diffraction data is the work of Bolz and Mauer (Ref. 39); the density at the triple point is from Clusius and Weigand (Ref. 25).

During the last decade reliable values of  $a_0$  have become available over almost the entire temperature range from 0 $^\circ\text{K}$  to the triple point for the rare gases. The work on each of these is briefly discussed and the results shown on Figs. 1–4. Since  $\rho$  and  $a_0$  are connected for fcc crystals by the simple formula  $\rho = 4M/Na_0^3$ , where  $M$  is the molecular weight and  $N$  is Avogadro's number, results both of diffraction techniques which measure  $a_0$  and of measurements of the bulk density have been plotted on the same curves. Density and expansivity is discussed in I.B.

**Argon** The first modern work on  $a_0$  for Ar<sup>26</sup> as well as for Kr was done by a group at Queen Mary College in England. For temperatures from 20 to 60 $^\circ\text{K}$  the Debye-Scherrer-Hull technique was used but above 60 $^\circ\text{K}$  it was necessary to measure  $\rho$  by a bulk-density method.<sup>26,27</sup> At these higher temperatures the powder

<sup>26</sup> E. R. Dobbs, B. F. Figgins, G. O. Jones, D. C. Piercey, and D. P. Riley, *Nature* **178**, 483 (1956).

<sup>27</sup> B. L. Smith, *Phil. Mag.* **6**, 939 (1961).

recrystallizes and the grain size increases causing the patterns to become "spotty." X-ray powder measurements which are in good agreement with these have been made over a wider temperature range, 4.2 to 73 $^\circ\text{K}$ .<sup>28</sup> The results are all shown on Fig. 1. Notice that the density scale on the right of all the figures is cubic. A single determination by Henshaw<sup>29</sup> of  $a_0$  at liquid helium temperature using neutron diffraction gives a value smaller than the x-ray data. Meyer *et al.*<sup>30</sup> have recently observed, in x-ray powder patterns of Ar frozen from liquid, evidence for 1–5% metastable hcp structure mixed in with the fcc. The amount of hcp depends sensitively on impurities in the lattice. Lattice constants for the two phases show that the hcp is ideally close packed and that the planar spacing in both lattices is the same within experimental error. This is the first experimental evidence for hcp structure in rare-gas solids.

**Krypton** An accurate determination of  $a_0$  for Kr was first reported by Dobbs and Luszczynski<sup>31</sup> from x-ray diffraction of a powdered sample at 91 $^\circ\text{K}$ . This result was confirmed and extended by the same method in 1957,<sup>32</sup> and somewhat later by both x-ray and bulk density measurements.<sup>33</sup> Bolz and Mauer<sup>28</sup> have made thorough measurements from 4.2 to 92 $^\circ\text{K}$  confirming the above results using a modified powder diffractometer, and a single diffractometer measurement by Klug and Sears<sup>34</sup> at 48.4 $^\circ\text{K}$  is also in good agreement. All of these data have been plotted in Fig. 2.

**Xenon** Until now the single available measurement above 120 $^\circ\text{K}$  was the determination of Clusius and Weigand<sup>25</sup> at the triple point, calculated using an uncertain value of the liquid density. Most recently, however, Packard and Swenson<sup>35</sup> have determined Xe specific volumes accurate to probably better than 0.3% in the range 20 to 160 $^\circ\text{K}$  from piston displacement equation of state and compressibility measurements (see III.E. Compressibility). The earliest measurements<sup>32</sup> have been extended to the range 5.5 to 120 $^\circ\text{K}$  by x-ray techniques<sup>36,37</sup> and bulk-density measurements.<sup>36</sup> In order to get sharp x-ray patterns at temperatures near 120 $^\circ\text{K}$  where recrystallization and grain growth occur, the sample was rotated and vertically translated in the beam. Under these experimental conditions, the x-ray

<sup>28</sup> L. H. Bolz and F. A. Mauer (unpublished).

<sup>29</sup> D. G. Henshaw, *Phys. Rev.* **111**, 1470 (1958).

<sup>30</sup> L. Meyer, C. S. Barrett, and P. Haasen, *J. Chem. Phys.* **40**, 2744 (1964). Thanks are due the authors for graciously providing preprints of their work.

<sup>31</sup> E. R. Dobbs and K. Luszczynski, *Proc. Internat. Conf. Low Temp. Phys., Paris, 1955*, pp. 439–440.

<sup>32</sup> G. H. Cheesman and C. M. Soane, *Proc. Phys. Soc. (London)* **70B**, 700 (1957).

<sup>33</sup> B. F. Figgins and B. L. Smith, *Phil. Mag.* **5**, 186 (1960).

<sup>34</sup> H. P. Klug and D. R. Sears, AFOSR Contract Report #49(638)-575 (April, 1962).

<sup>35</sup> J. R. Packard and C. A. Swenson, *J. Phys. Chem. Solids* **24**, 1405 (1963). Thanks are due the authors for graciously providing a preprint of their work.

<sup>36</sup> A. J. Eatwell and B. L. Smith, *Phil. Mag.* **6**, 461 (1961).

<sup>37</sup> D. R. Sears and H. P. Klug, *J. Chem. Phys.* **37**, 3002 (1962).

determinations of  $a_0$  are more accurate than the bulk-density ones. These results are shown in Fig. 3.

*Neon* Because of its very low triple point very little accurate data have been available until recently on  $a_0$  for Ne. A determination by x-ray diffraction<sup>38</sup> of the lattice-parameter difference between <sup>20</sup>Ne and <sup>22</sup>Ne at 4.2°K had been made and at the same temperature  $a_0$  was determined from neutron diffraction experiments.<sup>29</sup> The most complete data are those of Bolz and Mauer<sup>39</sup> who determined  $a_0$  at frequent temperature intervals for normally occurring Ne (<sup>n</sup>Ne), <sup>20</sup>, and <sup>22</sup>Ne, from 4.2°K to the respective triple points. Their results are shown in Fig. 4. Their apparatus and technique<sup>40,41</sup> offer considerable improvements over those of other workers' and are worth mention. The powdered samples were deposited on a flat surface which could be accurately oriented both by translation and rotation. Temperature of the surface was measured by an imbedded thermocouple and controlled with an automatic feedback heating circuit. The diffracted beam (Ni filtered CuK $\alpha$  radiation) was detected over a wide angle by an electronic counter-diffractometer. This detector is faster than film detectors and transient effects can be better observed with it. The data from these experiments show a standard deviation of only 0.0006 Å.

### 3. Other Techniques

The study of single crystals of rare gases by x rays can potentially provide more information than has been obtained from powder methods. For most diffraction experiments of this kind single crystals about 1 mm on a side are sufficient and crystals of this size can be grown by slow freezing from the melt (see II.B. Crystallization). Technical difficulties in making such measurements are many and therefore relatively little progress has been reported. We present here very briefly what has been done and some potentialities.

For measurement of the lattice parameter the powder method gives at best<sup>42</sup> a reproducibility of 1 part in 10<sup>4</sup>. Using Bond's method<sup>43</sup> for determination of  $a_0$  from nearly perfect single crystals, an uncertainty of 4 p.p.m. may be achieved. It is to be emphasized that experiments on solid-rare gases whether powders or single crystals, must be performed under much more difficult conditions than obtained in the above experiments, which used standard substances at room

temperatures. Experiments on the orientation and x-ray diffraction of 1 mm single crystals of more complex molecular crystals<sup>44</sup> have been carried out well below liquid-nitrogen temperature. Rotating crystal measurements of the structures<sup>13</sup> have yielded much information on phase changes, molecular orientation, etc., although measurements of  $a_0$  are still uncertain due to difficulties in centering the samples. It is to be expected that experiments of this kind will eventually give results better than those now attainable with powder methods and that they will be carried over to rare-gas crystals. Single crystal  $a_0$  measurements may also be carried out closer to the triple-point temperature than powder measurements since no problems of recrystallization and grain growth arise.

Defect properties in solids are also best studied by single crystal x-ray measurements. Recent theoretical work<sup>45,46</sup> on symmetric point defects in solid argon, i.e., vacancies, substitution of other rare-gas atoms in the lattice and interstitially, and pairs of these defects, has predicted interesting quantitative and qualitative effects observable in such experiments. There is much of fundamental interest in studying these defects in solid-rare gases since the energies required for their creation are so small (see III.C.1).

### B. Density and Expansivity

Two techniques have been applied in determining the densities of solid-rare gases: the x-ray powder diffraction method, previously described, and the bulk-density method. The bulk-density method consists of measuring the mass of the gas, at some standard temperature and pressure, which condenses to a compact solid block free of macroscopic voids and defects. The solid is condensed, usually directly from the vapor, in a known volume at a known temperature below the triple-point temperature. The bulk-density method is preferred near the triple point where powder diffraction determinations are difficult and single-crystal diffraction methods not yet practical.

Agreement between these methods is in general excellent but it must be noted that the bulk density, especially, is sensitive to crystal defects of various kinds. Recent experiments in growing large crystals of rare gases and measuring their sizes (see II.B. Crystallization) have shown that compact crystalline solids free of macroscopic irregularities may be composed of grains of widely different average size depending on the crystal-growth parameters, in particular, the growth rate. This difficulty has been further pointed up by a bulk density determination<sup>47</sup> of solid Ar in which the solid was condensed from several pressures at fixed temperature from

<sup>38</sup> V. S. Kogan, B. G. Lazarev, and R. F. Bulatova, *Zh. Eksperim. i Teor. Fiz.* **40**, 29(1961) [English transl.: *Soviet Phys.-JETP* **13**, 19 (1961)].

<sup>39</sup> L. H. Bolz and F. A. Mauer, in *Advances in X-Ray Analysis*, edited by W. M. Mueller and M. Fay (Plenum Press, New York, 1963), Vol. 6, pp. 242-249.

<sup>40</sup> I. A. Black, L. H. Bolz, F. P. Brooks, F. A. Mauer, and H. S. Peiser, *J. Res. Natl. Bur. Stds.* **61**, 367 (1958).

<sup>41</sup> F. A. Mauer and L. H. Bolz, *J. Res. Natl. Bur. Stds.* **65c**, 225 (1961).

<sup>42</sup> W. Parrish, *Acta Cryst.* **13**, 838 (1960).

<sup>43</sup> W. L. Bond, *Acta Cryst.* **13**, 814 (1960).

<sup>44</sup> W. E. Streib and W. N. Lipscomb, *Proc. Natl. Acad. Sci. U. S. A.* **48**, 911 (1962).

<sup>45</sup> H. Kanzaki, *J. Phys. Chem. Solids* **2**, 24 (1957).

<sup>46</sup> H. Kanzaki, *J. Phys. Chem. Solids* **2**, 107 (1957).

<sup>47</sup> W. M. Hinds, M. S. thesis, University of Virginia, 1956.

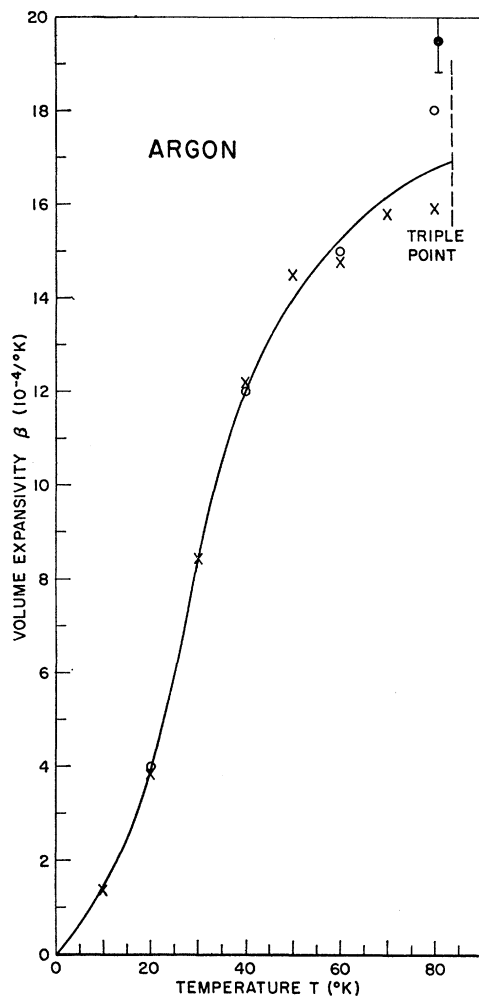


FIG. 5. Volume expansivity  $\beta$  ( $10^{-4}/^{\circ}\text{K}$ ) of argon as function of temperature  $T$  ( $^{\circ}\text{K}$ ). The open circles are the data of Dobbs *et al.* (Ref. 26), the crosses are the results of Bolz and Mauer (Ref. 28). The closed circle is an optical determination of Smith and Pings (Ref. 246). Uncertainty in the ordinate is about  $\pm 1 \times 10^{-4}/^{\circ}\text{K}$  at temperatures near the triple point and decreases somewhat at lower temperatures.

the liquid, and then from several lower pressures and at the same temperature from the vapor. The average density of the solid grown from the vapor was found in these experiments to be about 1% less than the solid grown from the liquid; the effect may be less important for purer samples. By comparison, the inherent uncertainties in bulk-density determinations are from 0.1% to 0.05%. This indicates that the crystalline solid condensed from the vapor may be more porous than when grown from the liquid; the result of voids too small to be seen or of lower density caused by small grain size in the bulk.

Volume expansivity  $\beta = V^{-1}(\partial V/\partial T)_P$  has been measured from the slope of  $\rho$  or  $a_0$  vs  $T$  curves for solid Ar,<sup>26,28</sup> Kr,<sup>28,33</sup> Xe,<sup>35-37</sup> and for Ne.<sup>39</sup> The results have

been plotted in Figs. 5, 6, 7, and 8, respectively. The large uncertainties and the scatter of the points result from insufficiently detailed knowledge of the variation of  $\rho$  or  $a_0$  with  $T$  for rare gases.

Expansivity measurements are of particular theoretical importance for these substances. The canonical means for calculating  $\beta$  in a region where it has not been measured but where the specific heat is known, is from Grüneisen's law:

$$\beta = (\gamma\chi/V) C_v, \quad (1)$$

where  $\chi$  is the compressibility,  $C_v$  the specific heat at constant volume,  $V$  the volume, and  $\gamma$  Grüneisen's constant. The usefulness of the law is that at low temperatures, say below the Debye temperature  $\Theta_D$ ,  $\gamma$  may frequently be taken as a constant or a slowly varying function of  $V$ ; in this range then,  $\beta \propto C_v$ , approximately. Detailed experiments have shown that  $\gamma$  varies more than is expected and theoretical work<sup>48</sup> has closely connected temperature variations in  $\gamma$  with the lattice vibration frequency spectrum of the solid. The predictions of the model are applied best to rare-gas solids at around  $0.2\Theta_D$  where the main deviations in  $\gamma$  should occur. This means that from accurate measurement of  $\beta$  information about the molecular vibrations can be obtained in a region where effects of anharmonicity in the interatomic potentials are unimportant.

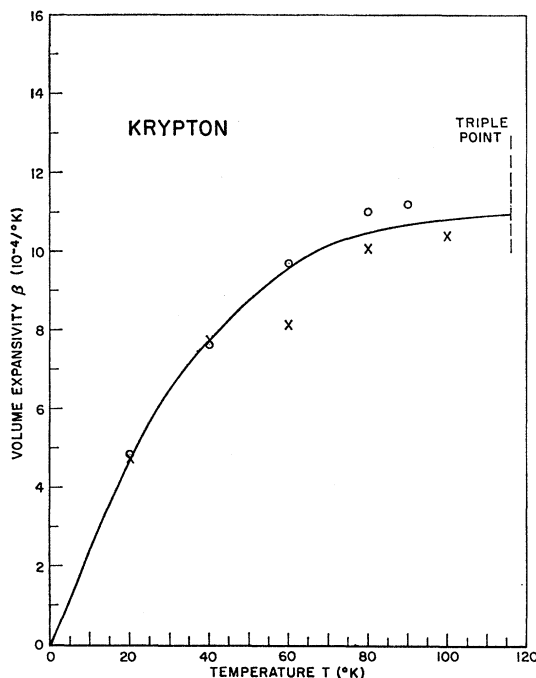


FIG. 6. Volume expansivity  $\beta$  ( $10^{-4}/^{\circ}\text{K}$ ) of krypton as function of temperature  $T$  ( $^{\circ}\text{K}$ ). The circles are the data of Figgins and Smith (Ref. 33), the crosses are the results of Bolz and Mauer (Ref. 28).

<sup>48</sup> T. H. K. Barron, *Phil. Mag.* **46**, 720 (1955).

### C. Theory of the Solid Structure

The general problem of structure of molecular solids may be stated thus: from detailed knowledge of the forces among the molecules and of appropriate molecular properties, e.g. mass, polarizability, molecular structure, find the equilibrium arrangement over all temperatures and pressures for which the solid phase exists. The problem is not yet capable of accurate quantitative treatment but for the rare gases it is known (see III.A. Intermolecular Potentials) that to a good approximation the forces among the molecules are well represented by two-body central potentials of the Mie-Lennard-Jones type. This potential function is of the general form

$$\phi(r) = \frac{\epsilon nm}{m-n} \left[ m^{-1} \left( \frac{r_0}{r} \right)^m - n^{-1} \left( \frac{r_0}{r} \right)^n \right], \quad (n > m), \quad (2)$$

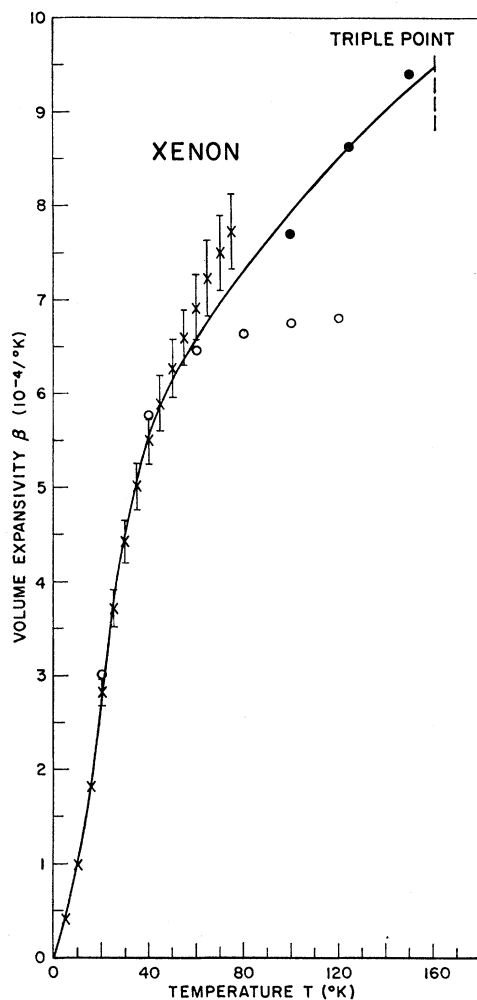


FIG. 7. Volume expansivity  $\beta$  ( $10^{-4}/^{\circ}\text{K}$ ) of xenon as function of temperature  $T$  ( $^{\circ}\text{K}$ ). The open circles are the data of Eatwell and Smith (Ref. 36), the crosses are the results of Sears and Klug (Ref. 37), the closed circles are results of Packard and Swenson (Ref. 35).

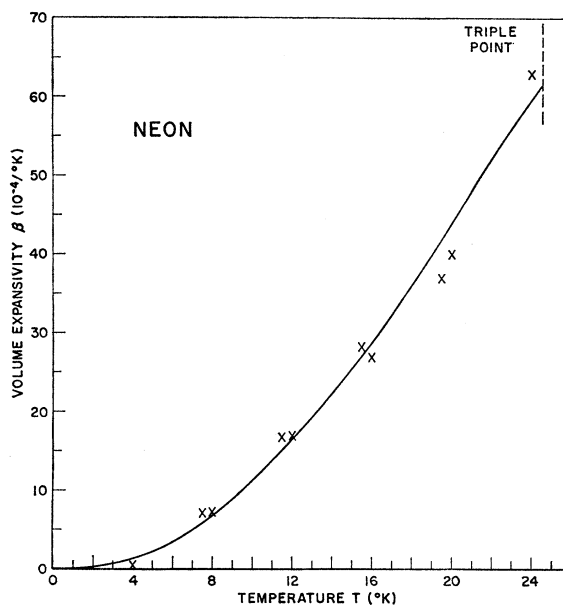


FIG. 8. Volume expansivity  $\beta$  ( $10^{-4}/^{\circ}\text{K}$ ) of neon as function of temperature  $T$  ( $^{\circ}\text{K}$ ). All points are results of Bolz and Mauer (Ref. 39). The curve is to be regarded as approximate.

where  $\epsilon$  is the depth of the potential well for two molecules at equilibrium separation  $r_0$ . The treatment for rare gases is further characteristically simplified by the sufficiency of finding only the positions of the molecules in the solid, no orientational coordinates being required. It is further known, from the classic work of Born, that conditions of mechanical stability restrict the possible ordering of ideal crystals such as these generally to either cubic (fcc) or hexagonal (hcp) close packing.

There remains, however, some difficulty in treating this problem for rare gases. Until recently the only crystal structure observed for the rare gases was the fcc and in any case all measurements have indicated that fcc is overwhelmingly the most common structure in rare-gas solids. Theoretical investigations on the other hand have invariably concluded, again until recently, that hcp should be the equilibrium structure and that it should therefore be overwhelmingly the most common solid phase for rare gases. The crux of the trouble lies in the small differences of short-range order around a molecule in these two lattices as shown on Table I. Potentials of the form (2) do not adequately discriminate between the two structures.

The situation has been well reviewed by Barron and Domb<sup>49</sup> and by Dobbs and Jones.<sup>1</sup> The Gibbs free energy is most easily computed at  $T=0^{\circ}\text{K}$  and  $P=0$ , for which if zero-point energy is neglected,  $G=U_0$ , the static lattice potential energy. Under these conditions the equilibrium lattice is the one for which  $U_0$  is minimum. From a potential of the form (2), assuming only

<sup>49</sup> T. H. K. Barron and C. Domb, Proc. Roy. Soc. (London) **A227**, 447 (1955).

TABLE I. Comparison of local (microscopic) structure of cubic close packed (fcc) and hexagonal close packed (hcp) lattices.  $R$  is the radius of the close packed spheres. At distance  $2R\sqrt{3}$  the hcp lattice has 18 spheres. Much more complete tables of near neighbor distributions for several lattices may be found in: J. O. Hirschfelder, C. F. Curtiss, and R. B. Bird, *Molecular Theory of Gases and Liquids* (John Wiley & Sons, Inc., New York, 1954), pp. 1037–1039.

	First-nearest neighbors		Second-nearest neighbors		Third-nearest neighbors	
	Number	Distance	Number	Distance	Number	Distance
fcc	12	$2R$	6	$2R\sqrt{2}$	24	$2R(3)^{\frac{1}{2}}$
hcp	12	$2R$	6	$2R\sqrt{2}$	2	$2R(8/3)^{\frac{1}{2}}$

two-body forces, and neglecting zero-point energy, one obtains for  $U_0$  of a large crystal with  $N$  molecules

$$U_0 = \frac{N \epsilon n m}{2(n-m)} \left[ \frac{A_m (r_0)^m}{m (r_0')^m} - \frac{A_n (r_0)^n}{n (r_0')^n} \right], \quad (3)$$

where  $r_0'$  is the nearest neighbor distance and  $A_m$  and  $A_n$  are crystal potential constants which depend on the lattice. For study of the relative stability of cubic and hexagonal close-packed phases the significant quantities are differences in  $A_j$  between the two lattices for different values of  $j$  and a comprehensive statement of these is available.<sup>49</sup> The conclusion of calculations of this kind is that the hcp structure is preferred at 0°K and zero pressure for all values of  $n$  and  $m$  except for unrealistically small ones ( $m=4$ ,  $5 \leq n \leq 8$ ;  $m=5$ ,  $n=6$ ). The relative difference in  $U_0$  between the two lattices has been found to be rather small, the hcp value being only about 0.01% below the fcc value. If the pressure over the solid is increased as the temperature is kept constant at 0°K, the hexagonal structure becomes decreasingly preferred and at sufficiently high pressures cubic structure is indeed preferred. Using a Lennard-Jones (6, 12) potential, Barron and Domb<sup>49</sup> found that the solid–solid phase transition takes place at pressures for which the cell volume is equal to or smaller than one-half the equilibrium cell volume at zero pressure. In Ar this corresponds to pressures of  $10^5$  atm and above.

If the temperature of the solid is increased and the pressure remains constant one must examine the behavior of

$$\left( \frac{\partial G}{\partial T} \right)_P = - \int C_p \frac{dT}{T} \propto - \frac{1}{\Theta_{D0}^3}, \quad (4)$$

where  $\Theta_{D0}$  is the Debye temperature calculated near 0°K. From Eq. (4) it may be seen that if  $\Theta_{D0}$  for the hcp is larger than that of the fcc phase then it is still possible that a transition temperature exists at which the two states have equal  $G$  and above which  $G_{\text{fcc}} < G_{\text{hcp}}$ . Calculation of  $\Theta_D$  requires detailed knowledge of the lattice dynamics of the crystals, in particular of the

frequency distribution of normal modes in the lattices.<sup>50</sup> Barron and Domb<sup>49</sup> have made such a calculation using Born–von Kármán lattice dynamics. The most important contributions in  $\Theta_D$  near 0°K come from the low frequency, long wavelength modes, and the velocity and frequency distribution of long waves in both fcc and hcp lattices were calculated assuming a potential of the form (2). Symmetries of the two structures are quite different, e.g., the fcc is a Bravais lattice but the hcp is not, as are the elastic constants and hence the velocity and frequency distribution of the normal modes. Smaller elastic constants are associated with the hcp lattice since it is more easily deformed under stress<sup>51</sup> than the fcc and this implies generally a lower  $\Theta_{D0}$  for the hcp phase. Fortunately, although the average velocity of long waves in the hexagonal lattice is smaller,  $\Theta_{D0}$  is actually greater since the distribution of the velocities for the cubic lattice is wider. The temperature of transition from the hcp to the fcc phase is found to be approximately equal to the melting-point temperature. Since, however, all the rare-gas solids are known to be cubic close packed even at 4.2°K, it is clear that for agreement with experiments either the lattice dynamics must be modified so that the transition temperature falls lower than this, or  $U_0$  must be calculated in a more refined manner to show that the fcc static lattice potential energy is smaller than the hcp value. This latter approach has been employed almost exclusively and we discuss each of the modifications in calculating  $U_0$  in turn. The possible existence of a stable hcp phase for rare gases at very low temperatures cannot be dismissed but must await further experiments. If such an hcp–fcc phase transition does indeed exist much could be learned from studying problems of nucleation of solid–solid phase transitions, and of solid–solid phase diagrams, in such prototype systems.

<sup>50</sup> Since the publication of Ref. 49, neutron spectrometry techniques have been developed which make possible direct measurement of the normal mode frequencies by inelastic scattering of neutrons from single crystals of rare gases; cf. *Inelastic Scattering of Neutrons in Solids and Liquids* (International Atomic Energy Agency, Vienna, 1961), especially Chap. B. 1.

<sup>51</sup> A. W. Sleeswyk, *Phil. Mag.* **7**, 1597 (1962).

In calculating and comparing  $U_0$  for the fcc and the hcp lattices, two-body sums over the lattices of the form  $A_j = \sum (r)^{-j}$  are found where the summation includes all molecules at distance  $r$  from the molecule at the origin; the principal contributions coming from nearest neighbors. Since the number and distance of nearest and second-nearest neighbors are the same for both lattices (Table I), the difference in  $U_0$  depends upon the distribution of further neighbors and is thus small. The most commonly used form of Eq. (2) for rare-gas molecules is the Lennard-Jones (6, 12) potential where the  $r^{-6}$  term represents two-body induced dipole attractions from second-order perturbation theory and the  $r^{-12}$  term represents conveniently the short-range repulsion between molecules. It is to be emphasized that the *distribution* of nearest neighbors is different in the two lattices so that if the dipole-dipole forces are not strictly additive two-body forces, but instead the force between any two molecules is modified by the position of other molecules, then a difference in the lattice sums even over nearest neighbors may exist.

This correction has been considered in third-order perturbation theory by Axilrod<sup>52</sup> who then computed the effect of the triple-dipole interaction on the static potential-energy difference between the two possible lattices of rare-gas solids.<sup>53</sup> Summing triples of dipoles over a large but finite cylindrical lattice volume it was found that the difference in  $U_0$  due to these three-body forces favors the fcc lattice but not enough to counteract the original 0.01% lower  $U_0$  of the hcp.

Using the same general approach Ayres and Tredgold<sup>54</sup> investigated two more cases of nonadditivity of the two-body dipole-dipole force. They found first that the triple dipole forces interact with the repulsive energy in first order so as to favor the cubic structure, but only by an energy difference of the same order of magnitude as the triple dipole forces themselves. Secondly, higher-order multipole three-body interactions were investigated but the only important contribution of these is in the dipole-dipole-quadrupole case for which the hexagonal structure was found to be heavily favored. Doniach<sup>55</sup> has examined in some detail many-body effects on long-range dipole-dipole forces for ground-state interacting molecules in an undisplaced lattice. Considering the lattice as an array of electron oscillators he found that the effect of the lattice through this mechanism still allowed valid consideration of pairwise  $r^{-6}$  van der Waals attractions at long range for isotropic lattices. For Ar the long-range contribution to cohesive energy thus corrected becomes about 95% of the free-space value. The form and strength of the

long-range interaction depend upon which of the two lattices is considered but no estimate of this effect has been given.

Cuthbert and Linnett<sup>56</sup> have qualitatively examined the effect of angular dependence in the intermolecular force on the relative stability of the two static lattices. Because of electron-spin correlation the 8 electrons in the outer shell of isolated rare-gas atoms tend to pair at the corners of a regular tetrahedron. Since the pattern of neighbors is different in the two lattices the interaction of tetrahedral charge distributions may cause a difference in the static potential energies. Calculation of the interaction energy for several mutual orientations of two rigid tetrahedral-charge distributions shows that the effect of the pattern especially of first, second, and third-nearest neighbors may be to favor the cubic structure although the difference in distances of third nearest and further neighbors in the two lattices favors the hexagonal. Kihara<sup>57,58</sup> has suggested that the pattern of nearest neighbors in hcp structure favors the induction of an octapole moment in the molecules and that the repulsion of these octapoles decreases the stability. In the fcc lattice by comparison the lowest-order induced moments from this model are hexadecapoles, with consequently smaller mutual repulsions.

The possibility that the static potential energy may be properly a sum of two body forces of the form (2) but with constants different from  $m=6$ ,  $n=12$  has been extensively investigated by Kihara and Koba.<sup>59</sup> These workers examined potentials with  $m=6$  and  $n>6$ ; increasing  $n$  corresponds to narrowing the hollow part of the potential. It was found that the hcp structure is always favored under these forces; fcc structure would become more stable if the well were broadened. Although the use of the inverse sixth attraction term is well founded by both theory and experiment, for many calculations an exponential rather than inverse power in the repulsive potential is more realistic. In the usually employed (exp, 6) Buckingham potential,

$$\phi(r) = \frac{-\epsilon}{\alpha-6} \left[ \alpha \left( \frac{r_0}{r} \right)^6 - 6 \exp \alpha \left( 1 - \frac{r}{r_0} \right) \right], \quad (5)$$

$\alpha$  is a parameter controlling the narrowness of the hollow part of the potential. Experimentally realistic values of  $\alpha$  vary<sup>60</sup> from 12.3 for Kr to 14.5 for Ne but Kihara and Koba demonstrated that for  $\alpha > 8.675$ , the hcp has lower energy and that for the wider wells,  $\alpha < 8.675$ , the fcc structure is preferred.

These calculations were further extended to include zero-point energy by Jansen and Dawson<sup>61,62</sup> who

<sup>52</sup> B. M. Axilrod, *J. Chem. Phys.* **19**, 719 (1951).

<sup>53</sup> B. M. Axilrod, *J. Chem. Phys.* **19**, 724 (1951).

<sup>54</sup> R. U. Ayres and R. H. Tredgold, *Proc. Phys. Soc. (London)* **B**, 840 (1956).

<sup>55</sup> S. Doniach, *Phil. Mag.* **8**, 129 (1963).

<sup>56</sup> J. Cuthbert and J. W. Linnett, *Trans. Faraday Soc.* **54**, 617 (1958).

<sup>57</sup> T. Kihara, *J. Phys. Soc. Japan* **15**, 1920 (1960).

<sup>58</sup> T. Kihara, in *Advances in Chemical Physics*, edited by I. Prigogine (John Wiley & Sons, Inc., New York, 1963), Vol. V, pp. 186-188.

<sup>59</sup> T. Kihara and S. Koba, *J. Phys. Soc. Japan* **7**, 348 (1952).

<sup>60</sup> E. A. Mason and W. E. Rice, *J. Chem. Phys.* **22**, 843 (1954).

<sup>61</sup> L. Jansen and J. M. Dawson, *J. Chem. Phys.* **22**, 1619 (1954).

<sup>62</sup> L. Jansen and J. M. Dawson, *J. Chem. Phys.* **23**, 482 (1955).

showed that for Lennard-Jones ( $6, n$ ) potentials with  $n$  between 7 and 16 and for Buckingham (exp, 6) potentials with  $\alpha$  between 10 and 16 the hcp structure is preferred by a relative static potential-energy difference of about 0.01%. The consistency with which this factor arises for all reasonable values of zero-point energy parameter and two-body potential-function parameters led these workers to suggest along with Axilrod<sup>63</sup> and others that theoretical failure to account for the stability of fcc structure for rare-gas solids can only be avoided by due consideration of many-body forces. Wallace,<sup>68</sup> however, has recently calculated the zero-point energies of rare-gas solids including anharmonic corrections and found that the fcc structure is thus made stable for Ne and Ar at 0°K but not for Kr and Xe.

General consideration of three-body forces has shown<sup>64</sup> that their effect on the relative stability of the lattices may be to produce differences in  $U_0$  an order of magnitude larger than those calculated from two-body forces alone. The dipole-dipole and dipole-quadrupole interactions of two nearest-neighbor molecules  $A$  and  $B$  with a molecule  $C$ , considered in second-order perturbation theory with an adjustable Gaussian distribution assumed for the electronic charge around the molecules, yields results of this kind whose magnitudes depend critically on the details of the model. For close approach of  $C$  to  $A$  and  $B$ , e.g.,  $C$  is a nearest or next-nearest neighbor to either  $A$  or  $B$ , the perturbation-theory calculation breaks down since effects on the three-body forces of increased electron exchange among molecules become important. A summation over a large but finite volume of  $C$  excluding nearest and next-nearest neighbors gives a  $U_0$  for fcc 0.1% lower than for hcp. When nearer  $C$ 's are included, however, this effect rapidly reverses sign.

The three-body forces between a central atom and all pairs of its nearest neighbors are principally due to electron exchange. These forces and their effect on the relative stability of fcc and hcp lattices have been analyzed by Jansen<sup>65</sup> in first order and by Jansen and Zimering<sup>66</sup> in second-order perturbation theory. Their net result is to favor the cubic lattice for rare gases at 0°K and when taken in conjunction with the lattice dynamics analysis previously discussed,<sup>49</sup> to favor the cubic lattice at all temperatures in substantial agreement with experiment. In these calculations only the exchange of single electrons among different neighboring molecules need be taken into account and this is conveniently done with a spherically symmetric Gaussian charge distribution for the single electron effective in the exchange interaction. The width of the charge distribution determines which rare-gas atom is considered and the three-body effect depends thus only

on a width parameter and the angles of the triangles formed by the triplets of nearest neighbors. Of the 66 possible triangles so formed in each lattice, 9 are different between the hcp and the fcc structures and their net effect in the first order is to stabilize the hcp structure by an order of magnitude larger than the stabilization due to pair potentials alone. The second-order calculation, however, gives a further important contribution to  $U_0$  composed of two parts: diatomic exchange (favoring hcp structure) and triatomic exchange (favoring fcc structure). The net effect of these, in agreement with experiment, is to decisively favor the cubic structure so that the sum of first and second-order calculations of three-body exchange forces is to give a  $U_0$  for the fcc structure about 1% smaller<sup>67</sup> than that for hcp. Higher order contributions are negligible as are also exchange forces between next-nearest neighbors and beyond.

## II. MELTING AND CRYSTALLIZATION

### A. Melting

#### 1. General and Theoretical

The investigation of melting phenomena in rare gases is a particularly fruitful way of studying melting phenomena in general. A fundamental goal of the theory has been to quantitatively understand the behavior of physical properties upon and near melting and especially to understand the melting curve,  $P$  vs  $T$ , itself. This is a hard problem, of course, and even for the simplest case of rare-gas melting it is not well solved.

The theory of the molecular solid is much further advanced than the theory of the corresponding liquid, so considerable work has been done on calculating the liquid-state properties from those of the solid. The long-standing investigation on Ar of Rice<sup>68</sup> connects the vibration spectrum of the solid with that of the liquid by considering the liquid as a highly disordered solid. From the  $\Theta_D$  of the solid a characteristic temperature for the liquid may thus be constructed and from it some properties of the liquid near the melting point may be calculated, e.g., free energies, entropies, and specific heats. From the more general thermodynamic approach<sup>69,70</sup> it has been possible to discuss fruitfully the rare-gas melting properties qualitatively and to compare these in meaningful quantitative juxtaposition to those of other substances which have seemingly much different melting parameters.

Modern theories of melting have tended to treat the short-range order characteristic of the liquid and the

<sup>63</sup> D. C. Wallace, *Phys. Rev.* **133**, A153 (1964).

<sup>64</sup> L. Jansen and R. T. McGinnies, *Phys. Rev.* **104**, 961 (1956).

<sup>65</sup> L. Jansen, *Phys. Letters* **4**, 91 (1963).

<sup>66</sup> L. Jansen and S. Zimering, *Phys. Letters* **4**, 95 (1963).

<sup>67</sup> L. Jansen and E. Lombardi, *Phys. Rev. Letters* **12**, 11 (1964).

<sup>68</sup> O. K. Rice, in *Phase Transformations in Solids*, edited by R. Smoluchowski (John Wiley & Sons, Inc., New York, 1951).

<sup>69</sup> A. R. Ubbelohde, *Quart. Rev. (London)* **4**, 356 (1950).

<sup>70</sup> A. R. Ubbelohde, *Chem. Ind. (London)* **7**, 186 (1961).

long-range order characteristic of the solid more explicitly. Some success has resulted from the cell-model theory of liquids.<sup>71,72</sup> The fusion process is viewed as involving increased correlation between motions of molecules in different cells. To calculate these "correlation effects" a mathematically convenient, well defined, harmonic intermolecular potential function which acts only between nearest neighbors serves best; these conditions are satisfied best by the potentials between rare-gas molecules. Models of this type have been used to calculate entropy of fusion, vapor pressure of fusion, and melting points for rare gases and other molecular crystals. The results have been in fair agreement with experiment, especially for the melting temperature.<sup>72</sup> These same properties of the rare-gas intermolecular potential have been used with other models of melting. The Einstein model of the solid, which accounts for some thermodynamic properties of rare-gas solids fairly well above about 20°K, has been applied to the melting of solid Xe by Moelwyn-Hughes<sup>73</sup> with special emphasis on quantum effects. Assuming harmonic oscillations and a (6, 11) intermolecular potential (see III.A.) the approximate isotherm at the triple-point temperature could be calculated. Bazarov<sup>74</sup> considered the melting point as the temperature at which the Einstein vibration spectrum of the solid disappears. Assuming especially a well-defined correlation number permitted by the short range of the forces, melting temperatures could be calculated. These are all about three times too high when compared with experiments on rare gases, presumably principally the result of the relative crudeness of the frequency distribution. Approximations of this same kind have also been reported on Ar melting studies of Henkel.<sup>75</sup> The role of pair exchanges in rare-gas melting has been briefly discussed by Nardi *et al.*<sup>76</sup> and a recent calculation<sup>77</sup> of heats of fusion using a rigid-sphere equation of state for the liquid gives results for rare gases within about 15% of experiment.

We have so far discussed theoretical approaches to melting especially of rare gases, at the relatively low pressures near the triple point. The theoretical situation at higher pressures stimulates even more interest. In 1929 Simon and Glatzel<sup>78</sup> proposed on empirical grounds the melting equation

$$\log (P+a) = c \log T+b. \quad (6)$$

This was a vast improvement over the other melting equations of the time some of which, for example,

<sup>71</sup> J. A. Barker, Proc. Roy. Soc. (London) **A240**, 265 (1957).

<sup>72</sup> L. A. Rott, Fiz. Tverd. Tela **4**, 577 (1962) [English transl.: Soviet Phys.-Solid State **4**, 421 (1962)].

<sup>73</sup> E. A. Moelwyn-Hughes, Z. Physik. Chem. **15**, 270 (1958).

<sup>74</sup> I. P. Bazarov, Dokl. Akad. Nauk SSSR **135**, 1351 (1960) [English transl.: Soviet Phys.-Doklady **5**, 1293 (1960)].

<sup>75</sup> J. H. Henkel, Bull. Am. Phys. Soc. **1**, 258 (1956).

<sup>76</sup> V. Nardi, J. P. Auffray, and J. K. Percus, Bull. Am. Phys. Soc. **8**, 323 (1963).

<sup>77</sup> S. J. Yosim and B. B. Owens, J. Chem. Phys. **39**, 2222 (1963).

<sup>78</sup> F. Simon and G. Glatzel, Z. Anorg. u. Allgem. Chem. **178**, 309 (1929).

curved back at high  $P$  to give only a finite region for existence of the solid in the  $(P, T)$  plane. Equation (6) and its equivalent, known as the Simon melting equation:

$$P/a = (T/T_{tp})^c - 1 \quad (7)$$

using the same parameters  $a$  and  $c$ , have been widely fitted<sup>79</sup> to the melting curves of rare gases, metals, and other substances up to very high pressures. The parameters are to be viewed as follows:  $a$  is the internal pressure,  $(\partial E/\partial V)_{T=0}$ , for a van der Waals gas model;  $T_{tp}$  is taken either as the triple-point temperature or some other low-pressure melting temperature; and  $c$  is a constant usually related to Grüneisen's constant. Equations (6) and (7) have not yet been satisfactorily derived theoretically, nor have the parameters been satisfactorily quantitatively discussed in terms of other molecular properties. Some general attempts in this direction have been made, most successfully on the rare gases. An interesting approach to deriving the Simon-melting equations (6) and (7) from a classical statistical, order-disorder model of melting based on some earlier work of Lennard-Jones and Devonshire is due to Domb.<sup>80</sup> Unfortunately not enough is known about melting mechanisms for success of such a model and Domb was unable to get quantitatively close to the equation. Subsequent researchers have therefore bypassed questions of detailed mechanisms and attempted, with more success, to derive the Simon equations from less fundamental postulates. One such attempt is due to Salter<sup>81</sup> whose rather successful derivation uses as a base the Grüneisen equation of state and the Lindemann melting formula, both also of wide range of applicability. A more recent such derivation<sup>82</sup> using a quantum-mechanically corrected version of the Lindemann melting formula and another equation of state also applies in some quantitative approximation to rare-gas melting. Unfortunately, critical tests of these theories frequently rely on accurate experimental values of Grüneisen's constant, and these are only seldom available (see III.C.2 Anharmonicity and Grüneisen's Constant).

The rare-gas melting curves have also been much used following the suggestions of Simon *et al.*,<sup>83,84</sup> to test for the possible existence of a critical point for the solid-liquid transition analogous to the well-known critical point for the liquid-gas transition.<sup>85</sup> The co-

<sup>79</sup> S. E. Babb, Jr., Rev. Mod. Phys. **35**, 400 (1963). This is a review of the Simon-Glatzel melting equation in the form  $(P-P_0)/a = (T/T_0)^c - 1$ , and an exhaustive compilation of the parameters and their precisions for many substances including Ar, Kr, Xe, and Ne.

<sup>80</sup> C. Domb, Phil. Mag. **42**, 1316 (1951).

<sup>81</sup> L. Salter, Phil. Mag. **45**, 369 (1954).

<sup>82</sup> S. E. Babb, Jr., J. Chem. Phys. **38**, 2743 (1963).

<sup>83</sup> F. Simon, M. Ruhemann, and W. A. M. Edwards, Z. Physik. Chem. **B2**, 340 (1929).

<sup>84</sup> F. E. Simon, Res. Council Israel, Spec. Publ. **1**, 37 (1952).

<sup>85</sup> B. J. Alder and G. Jura, J. Chem. Phys. **20**, 1491 (1952).

In this note approximate estimates of the solid-liquid critical points for Ar (250 000 atm, 1840°K) and Ne are calculated under the condition that the solids are harmonic, independent of volume.

TABLE II. Some properties of rare gases at the triple point, boiling point, and critical point.

	Triple point properties					Boiling point $T(\text{b.p.})^{\circ}\text{K}$	Critical temperature $T_c^{\circ}\text{K}$	Critical pressure $P_c(\text{atm})$
	Temperature $T(\text{t.p.})^{\circ}\text{K}$	Pressure $P(\text{t.p.})\text{mm}$	Density of solid $\rho_s(\text{t.p.})$ $\text{g}/\text{cm}^3$	Density of liquid $\rho_L(\text{t.p.})$ $\text{g}/\text{cm}^3$	Initial slope of melting curve $dP/dT$ ( $\text{atm}/^{\circ}\text{K}$ )			
Ne	24.56 <sup>a,b</sup>	323.5 <sup>e,b</sup>	1.444 <sup>d</sup>	1.248 <sup>d</sup>	62.7 <sup>e</sup>	27.07 <sup>a</sup>	44.5 <sup>f</sup>	25.9 <sup>f</sup>
Ar	83.810 <sup>g,h</sup>	516.86 <sup>g,h</sup>	1.623 <sup>i</sup>	1.4100 <sup>i</sup>	39.2 <sup>i</sup>	87.293 <sup>j</sup>	150.9 <sup>k,l</sup>	48.3 <sup>l</sup>
Kr	115.78 <sup>m</sup>	548.7 <sup>m</sup>	2.826 <sup>i</sup>	2.451 <sup>i,s</sup>	31.1 <sup>i</sup>	119.81 <sup>j</sup>	209.4 <sup>n</sup>	54.3 <sup>n</sup>
Xe	161.37 <sup>j</sup>	612.2 <sup>o</sup>	3.399 <sup>p</sup>	3.076 <sup>i</sup>	25.1 <sup>i</sup>	165.04 <sup>j</sup>	289.8 <sup>t</sup>	57.64 <sup>q</sup>
Rn	202 <sup>r</sup>	$\approx 500^r$		$\approx 5.7^r$		211 <sup>r</sup>	377.5 <sup>r</sup>	62.4 <sup>r</sup>

<sup>a</sup> Reference 185.<sup>b</sup> For triple point coordinates ( $P$ ,  $T$ ) of Ne isotopes see caption of Fig. 23.<sup>c</sup> Reference 186.<sup>d</sup> Reference 24.<sup>e</sup> Reference 102.<sup>f</sup> *International Critical Tables* (McGraw-Hill Book Company, Inc., New York, 1928), Vol. III.<sup>g</sup> Reference 171.<sup>h</sup> K. Clusius, K. Schleich, *et al.* (Ref. 191) have recently determined the triple point coordinates ( $P$ ,  $T$ ) for Ar isotopes: <sup>36</sup>Ar (516.52 mm, 83.76°K) and <sup>40</sup>Ar (516.76 mm, 83.82°K).<sup>i</sup> Reference 25.<sup>j</sup> Reference 97.<sup>k</sup> E. Mathias, H. Kamerlingh Onnes, and C. A. Crommelin, *Commun. Kamerlingh Onnes Lab. Univ. Leiden* **12**, 131a (1912).<sup>l</sup> A. Michels, J. M. Levelt, and W. de Graaff, *Physica* **24**, 659 (1958).<sup>m</sup> Reference 99.<sup>n</sup> K. A. Kobe and R. E. Lynn, Jr., *Chem. Revs.* **52**, 117 (1953).<sup>o</sup> Reference 100.<sup>p</sup> Reference 35.<sup>q</sup> H. W. Habgood and W. G. Schneider, *Can. J. Chem.* **32**, 98 (1954).<sup>r</sup> Reference 188.<sup>s</sup> E. Mathias, C. A. Crommelin, and J. J. Meihuizen, *Physica* **4**, 1200 (1937).

ordinates of the liquid-gas critical points ( $P_c$ ,  $T_c$ ) for the rare gases are listed in Table II. Simon pointed out that since the solid-liquid critical point coordinates must be considerably higher than ( $P_c$ ,  $T_c$ ) the use of low-triple point, low-critical point substances such as the rare gases (and especially helium) makes possible investigation of the melting curve at high ratios of  $P/P_c$  and  $T/T_c$  without the great experimental difficulties attending work at high pressures and temperatures. As one approaches the proposed critical point along the melting curve, the discontinuities in physical properties upon transition are expected to become smaller, and above the critical point there should be no discontinuities at all. Bridgman<sup>86</sup> has directly measured the change in volume upon compression of the liquid to solid along the melting curve of Ar with this in view. He found from his data that although the volume change indeed does become smaller along the melting curve, a plot of  $\Delta V$  vs  $T$  shows that  $\Delta V$  will only vanish at infinite  $T$ . Subsequent investigators<sup>87</sup> working at still higher pressures have found that  $\Delta V$  approaches zero even more slowly. The latent heat of melting along the Ar melting curve stays constant

<sup>86</sup> P. W. Bridgman, *Proc. Am. Acad. Arts Sci.* **70**, 1 (1935).<sup>87</sup> P. H. Lahr and W. G. Eversole, *J. Chem. Eng. Data* **7**, 42 (1962).

whereas, for example, for nitrogen it increases. We must therefore conclude with Bridgman<sup>88</sup> that experimental evidence suggests that the melting curve does not terminate in a critical point, but rather that it "rises indefinitely with continually decreasing curvature" for rare gases and other simple substances.

## 2. Experimental

The melting curve of Ar has been studied over the widest range of all the rare gases. The first extensive study was that of Simon, Ruhemann, and Edwards<sup>89</sup> who made measurements of melting pressure  $P$  vs  $T$  from the triple point to 3400 kg/cm<sup>2</sup> and 150°K. To detect the onset of freezing these workers used a blocked capillary method.<sup>90</sup> Pressure is continuously increased by a pump on one side of the cold fluid sample in a capillary tube as it is monitored on both sides. When freezing occurs, the manometer on the pump side of the capillary shows increasing pressure but the manometer, typically a sensitive Bourdon gauge, on the

<sup>88</sup> P. W. Bridgman, in *Solids Under Pressure*, edited by W. Paul and D. M. Warschauer (McGraw-Hill Book Co., Inc., New York, 1963).<sup>89</sup> F. Simon, M. Ruhemann, and W. A. M. Edwards, *Z. Physik. Chem.* **B6**, 331 (1930), also erratum, *ibid.* **B7**, 80 (1930).<sup>90</sup> F. Simon, M. Ruhemann, and W. A. M. Edwards, *Z. Physik. Chem.* **B6**, 62 (1929).

far side of the sample remains stationary. Bridgman<sup>86</sup> extended the experimental range from the triple point to about 5500 kg/cm<sup>2</sup> and 185°K with his piston displacement technique. The fluid sample is compressed by applying pressure on a piston; when the sample freezes the discontinuous change in density causes a discontinuity in the plot of piston displacement vs  $P$  at the melting pressure. Decreasing the pressure over the solid then melts it, again with the corresponding discontinuity in density. This technique avoids a difficulty in interpretation which is inherent in blocked capillary measurements. As Bridgman has pointed out, the melting curve measured from a sample plugging a capillary should be lower than the true-melting curve because the sample is under a shearing stress. Although the curve of Simon *et al.*<sup>89</sup> does indeed lie lower than Bridgman's, later experiments<sup>91</sup> show that the effect of the shearing stress is probably negligible.

Robinson<sup>92</sup> used a unique method for measuring the melting curve, his measurements extend up to 8500 kg/cm<sup>2</sup> and 234°K on Ar. A small magnetic pellet in the freezing chamber was alternately lifted and dropped by an external magnet. The pellet moves freely in the fluid sample but its motion is arrested when freezing occurs and this is indicated by the absence of signals on a built-in microphone. The high pressure was produced in stages and the final intensifying pressure stroke was applied effectively right in the cryostat, thus avoiding low-temperature seals. Michels and Prins<sup>93</sup> recently have reported very accurate blocked capillary measurements on the melting curve up to 1550 kg/cm<sup>2</sup>. To measure absolute pressure, a pressure balance with sensitivity 1 part in 10<sup>5</sup> was used and the melting curve was expressed by a Simon-Glatzel formula of the type Eq. (6) to within about 0.1 kg/cm<sup>2</sup> over the experimental range.

The measurements at highest pressure are due to recent work of Lahr, Eversole, and Williams.<sup>87</sup> They used a piston displacement method very similar to Bridgman's and report data on Ar from about 2500 kg/cm<sup>2</sup> and 137°K to 18 500 kg/cm<sup>2</sup> and 360°K. In their measurements the increase in density upon freezing occurs at a somewhat lower pressure than the decrease on melting for the same sample at the same temperature. This interesting hysteresis may be averaged over conveniently to get a single curve for melting or freezing pressure. The effect is not surprising since other workers<sup>93,94</sup> have indeed reported supercooling of between 3° and 6°K in rare-gas freezing. Representative data of all the above work on Ar has been plotted on Fig. 9.

The melting curve of Ar may be fitted<sup>87</sup> satisfactorily from the triple point to 18 500 kg/cm<sup>2</sup> by the following

<sup>91</sup> C. A. Swenson, *Phys. Rev.* **89**, 538 (1953).

<sup>92</sup> D. W. Robinson, *Proc. Roy. Soc. (London)* **A225**, 393 (1954).

<sup>93</sup> A. Michels and C. Prins, *Physica* **28**, 101 (1962).

<sup>94</sup> H. J. De Nordwall and L. A. K. Staveley, *J. Chem. Soc.* **1954**, 224.

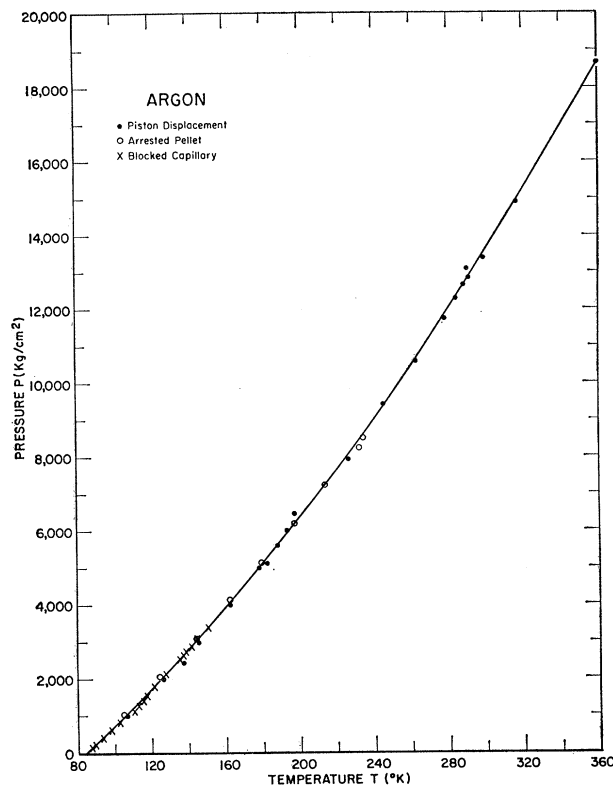


FIG. 9. Melting curve of argon, pressure  $P$  (kg/cm<sup>2</sup>) as function of temperature  $T$  (°K). The piston displacement data are from Bridgman (Ref. 86), and Lahr and Eversole (Ref. 87); the arrested pellet data are from Robinson (Ref. 92); and the blocked capillary data are from Simon *et al.* (Refs. 89, 90), and Michels and Prins (Ref. 93). In addition to the above, measurements have been made on Ar by Clusius and Weigand between 0.7 and 205 kg/cm<sup>2</sup> (Ref. 25).

Simon melting formula of the type Eq. (7):

$$P(\text{kg/cm}^2)/2308 = (T/83.2)^{1.5} - 1, \quad (8)$$

where  $P$  is the melting pressure and  $T$  the melting temperature in °K. For the region below 1500 atm (1550 kg/cm<sup>2</sup>) the equation fitted by Michels and Prins<sup>93</sup> is better:

$$\log [P(\text{atm}) + 2087.00] = 1.5932926 \log T + 0.2553075. \quad (9)$$

Since, as already discussed, grain growth makes x-ray determination of  $a_0$  near the triple point difficult, solid density at the triple point is best obtained from the initial slope of the melting curve and application of the Clausius-Clapeyron equation

$$dP/dT = L_f/T \Delta V, \quad (10)$$

where  $L_f$  is the latent heat of fusion (Table VIII) and  $\Delta V$  is the change in specific volume upon melting. This has been done by Clusius and Weigand<sup>25</sup> from their measurements on the melting curves of Ar, Kr, and Xe,

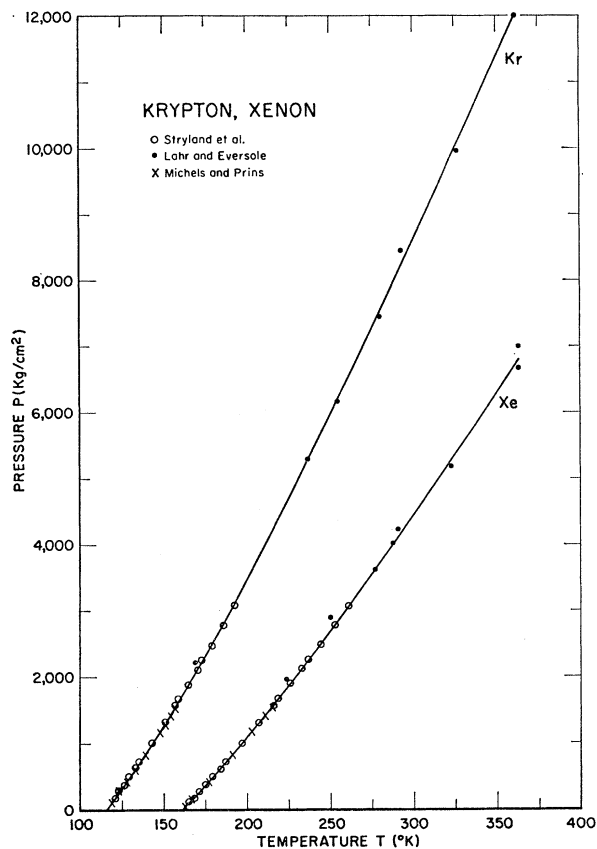


FIG. 10. Melting curves of krypton and xenon, pressure  $P$  ( $\text{kg}/\text{cm}^2$ ) as function of temperature  $T$  ( $^\circ\text{K}$ ). In addition to those shown, measurements have been made by Clusius and Weigand between 0.7 and 112  $\text{kg}/\text{cm}^2$  on Kr, and between 0.8 and 78  $\text{kg}/\text{cm}^2$  on Xe (Ref. 25).

up to about 210  $\text{kg}/\text{cm}^2$ . The initial slopes, as well as the more reliable of the solid densities they found, are entered on Table II. In order to apply Eq. (10) the liquid density near the triple point must be independently determined. This is not as difficult, and reliable values of liquid density are also shown.

The triple points of the rare gases are particularly suitable as low-temperature thermometric fixed points since the pure gases are readily available and consistently high reproducibility has been obtained. The most thorough measurements have been on Ar<sup>95-97</sup> for which a reproducibility of about 0.001 $^\circ\text{K}$  has been reached. Current investigations<sup>97</sup> of rare gases up to 99.999% pure show, however, that Kr and Xe may also be used for the same purpose. Modern, reliable values of the triple point temperature and pressure appear in Table II; the normal boiling points have also been included.

<sup>95</sup> A. Michels, T. Wassenaar, T. Slayters, and W. De Graaff, *Physica* **23**, 89 (1957).

<sup>96</sup> R. A. H. Pool, B. D. C. Shields, and L. A. K. Staveley, *Nature* **181**, 831 (1958).

<sup>97</sup> D. R. Lovejoy, *Nature* **197**, 353 (1963).

The melting curve of Kr has been measured up to 12 000  $\text{kg}/\text{cm}^2$ . Representative data has been plotted on Fig. 10. Stryland *et al.*<sup>98</sup> used an arrested-rod technique, a modification of earlier experiments,<sup>99</sup> from 190  $\text{kg}/\text{cm}^2$  up to 3100  $\text{kg}/\text{cm}^2$ . Lahr, Eversole, and Williams<sup>87</sup> extended the measurements from about 2200  $\text{kg}/\text{cm}^2$  to 12 000  $\text{kg}/\text{cm}^2$  and 362 $^\circ\text{K}$  and give the following equation as a satisfactory fit over the whole range of the Kr melting curve:

$$P (\text{kg}/\text{cm}^2)/3100 = (T/116.1)^{1.4} - 1. \quad (11)$$

For the region below 1500 atm the melting curve has been measured very accurately by Michels and Prins<sup>93</sup> who give for this region the melting formula

$$\begin{aligned} \log [P (\text{atm}) + 2345.00] \\ = 1.616\,984\,1 \log T + 0.033\,615\,4. \quad (12) \end{aligned}$$

Reliable triple-point data for Kr have been obtained by Beaumont *et al.*<sup>99</sup> and their results are included in Table II.

The melting curve of Xe has been measured up to 7000  $\text{kg}/\text{cm}^2$ . Representative data have been plotted along with Kr on Fig. 10. Arrested-rod measurements<sup>93</sup> extend from 130  $\text{kg}/\text{cm}^2$  to 3100  $\text{kg}/\text{cm}^2$  and the highest pressure measurements of Lahr *et al.*<sup>87</sup> go from 2000  $\text{kg}/\text{cm}^2$  to 7000  $\text{kg}/\text{cm}^2$  and 363 $^\circ\text{K}$ . A satisfactory fit over the whole range of the Xe melting curve is given by

$$P (\text{kg}/\text{cm}^2)/3513 = (T/161.5)^{1.31} - 1. \quad (13)$$

For the region below 1500 atm the melting curve has been measured very accurately by Michels and Prins<sup>93</sup> who give for this region the melting formula

$$\begin{aligned} \log [P (\text{atm}) + 2576.00] \\ = 1.589\,165\,0 \log T - 0.097\,818\,8. \quad (14) \end{aligned}$$

A rather old value<sup>100</sup> of the triple point pressure of Xe is apparently still the most reliable but the triple point temperature has been more recently accurately determined.<sup>97,101</sup>

The earliest measurements of the melting curve of Ne are those of Simon *et al.*<sup>89</sup> who took data from the triple point up to 4900  $\text{kg}/\text{cm}^2$  with the blocked capillary method. This work suffered from the relative impurity of the Ne obtainable, resulting in noticeably gradual melting points. On Fig. 11 the data is plotted along with modern determination of the melting curve and the melting-point depression characteristic of impure samples is apparent. A more accurate determination over the limited range below 200  $\text{kg}/\text{cm}^2$  was carried

<sup>98</sup> J. C. Stryland, J. E. Crawford, and M. A. Mastoor, *Can. J. Phys.* **38**, 1546 (1960).

<sup>99</sup> R. H. Beaumont, H. Chihara, and J. A. Morrison, *Proc. Phys. Soc. (London)* **78**, 1462 (1961).

<sup>100</sup> K. Clusius, *Z. Physik. Chem.* **B50**, 403 (1941).

<sup>101</sup> R. Heastie and C. Lefebvre, *Proc. Phys. Soc. (London)* **76**, 180 (1960).

out by Keesom and Lisman<sup>102</sup> at Leiden where the blocked capillary method had been originally developed. The modern work on Ne of Mills and Grilly<sup>103</sup> extends from the triple point to 3500 kg/cm<sup>2</sup>, impurity effects were mitigated by using Ne which was at least 99.8% pure. A satisfactory melting formula for the range of their measurements is:

$$P \text{ (kg/cm}^2\text{)} = -1057.99 + 6.289415T^{1.599916}. \quad (15)$$

### B. Crystallization

Conditions under which rare gases crystallize and their crystallization habits have long been studied<sup>104</sup> but progress has been slow mainly due to difficulty in maintaining and manipulating the solids at the necessary temperatures. Much has been learned, however, about the importance of single crystal samples for accurate measurement of physical properties from studies on other solids; and techniques for growing large single crystals have been developed from the more active interest in metals, semiconductors, etc. From such studies rather detailed knowledge, theoretical and experimental, of crystal growth has come. In this section we describe some measurements that have been made on crystalline rare gases and the limitations imposed by the crystals, then studies of the grain size and crystal growth of rare gases as such are treated.

The earliest difficulties due to lack of suitably large single crystals in measuring solid-state properties of rare gases were rather successfully circumvented by Barker *et al.*<sup>105,106</sup> in their determination of the elastic properties of argon. They measured the velocity of standing waves in a polycrystalline block of grain size about 0.1 mm (as estimated with x rays) which had been deposited from the vapor. By properly choosing the quartz transducers they were able to generate waves of wavelength ( $\lambda$ ) 1 mm or more so that the higher compressibility of the intergrain regions had only a negligible effect on the over-all elastic properties. Grain boundaries were found to attenuate the waves considerably, even at this wavelength, and thus led to lower accuracy in the experiment than could have been obtained with single crystals. It must be emphasized that generally the effect on physical properties of intergranular material may be difficult to assess even qualitatively. Molecules in this region may be viewed as forming a highly defected lattice characterized by both low density and high compressibility, these imply, respectively, lower and higher sound velocities.

Difficulties in measuring the index of refraction<sup>107</sup> may also be worth consideration. Accurate measurements

<sup>102</sup> W. H. Keesom and J. H. C. Lisman, *Commun. Kamerlingh Onnes Lab. Univ. Leiden* **20**, 224b (1933).

<sup>103</sup> R. L. Mills and E. R. Grilly, *Phys. Rev.* **99**, 480 (1955).

<sup>104</sup> W. Wahl, *Proc. Roy. Soc. (London)* **A87**, 371 (1912).

<sup>105</sup> J. R. Barker, E. R. Dobbs, and G. O. Jones, *Phil. Mag.* **44**, 1182 (1953).

<sup>106</sup> J. R. Barker and E. R. Dobbs, *Phil. Mag.* **46**, 1069 (1955).

<sup>107</sup> B. L. Smith, *Rev. Sci. Instr.* **34**, 19 (1963).

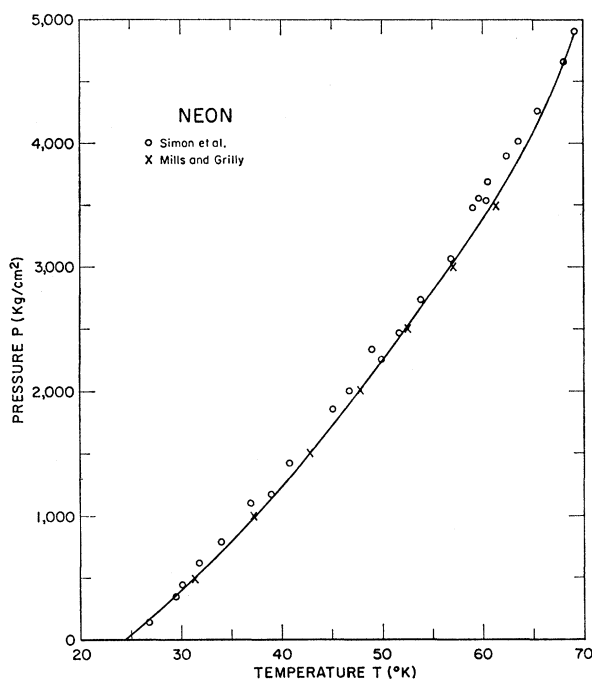


Fig. 11. Melting curve of neon, pressure  $P$  (kg/cm<sup>2</sup>) as function of temperature  $T$  (°K). In addition to those shown, measurements have been made by Keesom and Lisman between 0.4 and 198 kg/cm<sup>2</sup> (Ref. 102).

demand large angles of deviation and thus large solid samples. If the grain diameter in the samples is of the order of  $0.1\lambda$  however, scattering from grain boundaries causes the samples to be almost opaque. This problem may be partially circumvented by using grains that are as large as possible so that the number of boundaries the light crosses, and thus the apparent decrease in refractive index, are minimized. Measurements of thermal properties are also difficult to interpret from molecular properties unless carried out on almost perfect single crystals. Thermal conductivity measurements<sup>108</sup> on Ar have shown that the scattering of lattice waves by grain boundaries and other imperfections is a dominant mechanism increasing thermal resistance in the lattice at very low  $T$ . Thermal conductivity data may then be more characteristic of the crystallization conditions and other past history of the samples than of the lattice itself. The general problem of scattering of low-frequency waves from lattice imperfections has been treated by Klemens.<sup>109</sup>

Rare-gas crystal sizes have been investigated by both x rays and thermal etching. Bolz *et al.*<sup>110</sup> took back-reflection x-ray photographs of polycrystalline solid Ar which had been frozen from the melt near the triple point at growth velocities around 1 mm/min. A rough

<sup>108</sup> G. K. White and S. B. Woods, *Nature* **177**, 851 (1956).

<sup>109</sup> P. G. Klemens, *Proc. Phys. Soc. (London)* **68**, 1113 (1955).

<sup>110</sup> L. H. Bolz, H. P. Broida, and H. S. Peiser, *Acta Cryst.* **15**, 810 (1962).

estimate of grain size  $\approx 4$  mm was possible and by comparing the patterns on photographs taken from quickly grown Ar crystals with that of slowly grown Ar they concluded that the latter had the larger grain size.

Observations on thermal etching have provided most of the knowledge about grain size and crystallization habits of rare gases. The essentials of the process are these: (a) Since surface molecules which are on highly defected sites, e.g., those near a crystal boundary, are more loosely bound than those on true crystal faces, they are more rapidly evaporated from a free solid surface. This *preferential evaporation* results in the appearance of indented etched lines along the boundaries of grains. (b) Since surfaces formed by molecules which are on highly defected sites have higher surface free energies than those of true crystal faces, the molecules migrate along a polycrystalline surface from the grain boundaries onto the crystal faces as the surface energy of the crystal tends to a minimum. Thus *surface migration* away from grain boundaries also causes grain boundaries to be etched on polycrystal faces. Thermal etching has been most extensively studied in metals but it is not yet clear which of these mechanisms predominates.<sup>111,112</sup> Etching in rare-gas solids is expected to take place more rapidly in general than in metals since the weak intermolecular forces lead to more rapid surface migration and higher triple-point pressures; experiments on Ar have borne this out.

Polycrystalline Ar is most conveniently grown by progressive freezing from the melt, a modified Bridgman's method. The Ar liquid is contained in a glass growing chamber which is lowered into a cold bath at a rate which determines the crystal-growth rate. The pressure over the liquid is usually maintained somewhat above the triple-point pressure and the bath may be held at any temperature below the triple-point temperature, normally boiling liquid nitrogen (77°K), or liquid oxygen boiling under reduced pressure (90°–55°K) are convenient coolants. In this manner transparent samples of solid Ar may be grown large enough for experimental purposes. These solids are generally polycrystalline, partly because the probability of nucleating a new crystal is higher on the normally colder chamber walls than on the warmer crystal. This difficulty may be partially obviated by warming the walls with a heater or by keeping the coolant level sufficiently far below the growing interface so that the solid surface is convex toward the melt. In practice largest grain sizes are obtained from slowest growth rates. It is expected that the other rare gases would crystallize in an analogous way if solidified in appropriate coolants.

If the flow of warm gas to the growing chamber is cut off and at the same time the coolant level is raised so as to bring the upper surface of the melt below the triple

point, a crust freezes on the melt and the very interesting phenomenon of vapor snakes<sup>113,114</sup> may be observed. The melt in the closed volume between the crust above and the crystalline solid below is effectively sealed off and as this enclosed melt solidifies, with attendant density increase, a vapor filled bubble appears just below the crust. The rare gases in common with some other substances, especially those with globular molecules, have large heats of vaporization compared to their heats of fusion so that as the liquid evaporates to fill the vapor bubble a thin solid shell freezes around it. Further solidification of the liquid leads to more free volume and the bubble propagates into the melt as a vapor filled *tube* with a transparent thin-walled solid sheath and an apparently closed tip. The velocity with which this snake propagates, from about 0.1 cm/sec to 10 cm/sec, is determined by the rate at which the melt solidifies and the ratio of sheath thickness to tube radius is determined from conservation of thermal energy during evaporation and freezing.<sup>114,115</sup> The phenomenon has been observed in both Ar and Kr and presents many interesting problems especially concerning the nature of the sheath and its rapid growth, and the radius of the snake and its wall thickness.

The application of Bridgman's method to rare-gas crystal growth was developed by Stansfield<sup>116</sup> and extended by Followell<sup>117</sup> who studied polycrystalline Ar samples grown from the melt, and observed thermal-etch patterns on the free surface which was exposed when the solid contracted and separated from the growing-chamber walls upon cooling. Grain boundary grooves indicating grains of about 4 mm diameter and 2 mm thickness were observed similar in appearance and properties to those observed on thermally etched metals. The grain boundaries are to be interpreted as enclosing single-crystal faces, i.e., the lattice orientation is essentially constant within a grain.

Beltrami<sup>118</sup> has extended Bridgman's method to produce grain-boundary-free Ar specimens of volumes up to 1.5 cm<sup>3</sup>; in general, however, the samples were polycrystalline and exhibited grain boundaries and surface striations. The crystals were grown at rates from 1–5 mm/h with solid interfaces either flat or convex toward the melt. In this work the free surface examined was the upper one and the depth of the crystals could be determined by successively pumping and sublimating off the top surface of the crystal. Surface striations and other surface structure, less pronounced than grain boundaries, also appear on grain faces. Their interpreta-

<sup>113</sup> D. Stansfield, Ph.D. thesis, University of Bristol, 1954.

<sup>114</sup> G. L. Pollack and H. P. Broida, *J. Chem. Phys.* **38**, 968 (1963).

<sup>115</sup> R. Verschigel and H. I. Schiff, *J. Chem. Phys.* **22**, 723 (1956).

<sup>116</sup> D. Stansfield, *Phil. Mag.* **1**, 934 (1956).

<sup>117</sup> R. F. Followell, Ph.D. thesis, University of Bristol, 1957.

<sup>118</sup> M. Beltrami, *J. Appl. Phys.* **33**, 975 (1962).

<sup>111</sup> E. D. Hondros and A. J. W. Moore, *Acta Met.* **8**, 647 (1960).

<sup>112</sup> G. E. Rhead and H. Mykura, *Acta Met.* **10**, 578 (1962).

tion is less definite but they may indicate coherent or noncoherent twin boundaries, growth steps, or slip planes. It has been suggested that some of the finer striations are due to intersections of (111) planes with the crystal surface, this may allow tentative determination of the crystal orientation without x-ray examination. A photograph of a typical thermally etched Ar surface is shown in Fig. 12.

The surface configuration and energy<sup>119</sup> of rare-gas type solids has been considered in theoretical work of Schmidt and Jura.<sup>120,121</sup> Their results indicate that for the lattice at 0°K the surface layer of molecules may be slightly displaced in the normal direction to the crystal surface. Using the same techniques they were able to calculate surface energies for Ar at grain-boundary interfaces separating two perfect half crystals at low-index planes misfitted in a simple way. They found energies from 16.0 ergs/cm<sup>2</sup> at (111)-(111) interfaces to 41.7 ergs/cm<sup>2</sup> at (100)-(110) interfaces. No direct measurements have been reported of surface energies of rare-gas crystals although they may be estimated from surface tensions of the liquid near the triple point. The surface energy of solid Ar estimated in this manner<sup>122</sup> is about 35 ergs/cm<sup>2</sup>, the corresponding value<sup>123</sup> for solid Ne at its triple point is about 15 ergs/cm<sup>2</sup>. For comparison the surface energy of Cu at its melting point is 1400 ergs/cm<sup>2</sup>.

Rare gases also offer opportunity to study quantum effects on surface processes,<sup>124</sup> ranging from Xe whose zero-point energy has only a negligible effect on its properties to Ne and He where it has important effects. These solids are also especially interesting as models for crystal growth. The van der Waals forces bond molecules to the surface and to the lattice extremely weakly and this is expected to have far reaching consequences in the production and study of defects, e.g., from radiation damage.

Canonical crystal growth properties of Ar have recently been systematically investigated.<sup>125</sup> Crystalline solids were grown under varying values of conventional growth parameters: rate, temperature gradient at the interface, substrate temperature, chamber geometry, and supersaturation; and the grain size was determined as a function of these. The experiments are still relatively unsophisticated but qualitative agreement with current theory has been obtained. In general, if all

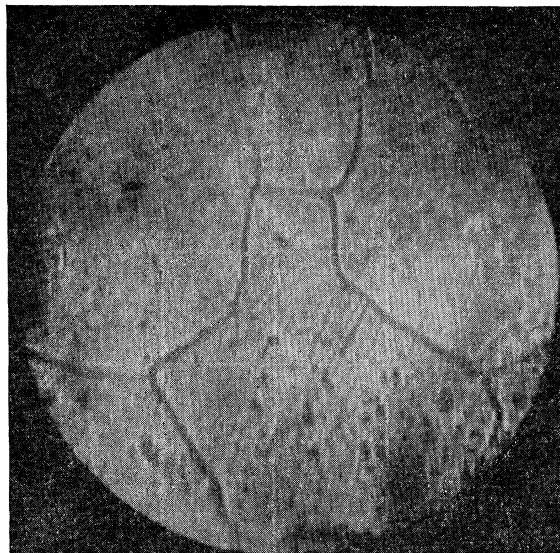


FIG. 12. Thermally etched surface of polycrystalline Ar grown from the melt. The heavy lines are grain boundaries. Notice also the striations on grain faces; these are probably twin boundaries or slip planes. Field diameter is 2 mm.

other parameters are fixed, grain area decreases linearly with increasing growth rate.

Attempts at growing crystals of rare gases other than Ar have been few. Pollack and Broida<sup>126</sup> have investigated spectroscopically the mechanism by which impurities are grown into crystals using NO in Kr as a model. Pure crystalline Kr and Kr-NO solid solutions were grown from the melt and the vapor at the temperature of boiling methane (112°K). The ultraviolet absorption spectrum of NO was followed as the Kr-NO solution was successively liquefied and then solidified. An interesting corollary of this work is that Kr, and probably all the other rare gases, may be purified by zone refining. This is especially important for impurity content frequently controls the upper limit in growing large single crystals.

### III. THERMODYNAMIC PROPERTIES

#### A. Intermolecular Potentials

All thermodynamic properties of a molecular solid in a broad temperature and pressure range could be calculated, in principle at least, from a sufficiently accurate intermolecular potential function and a very few other molecular structure properties. For rare-gas molecules the intermolecular forces may be assumed to be central and the intermolecular potential  $\phi(r)$  is thus particularly simple. Although as we have seen (I.C), noncentral corrections may be decisive in determining the stable crystal structure of the rare

<sup>119</sup> R. Shuttleworth, Proc. Phys. Soc. (London) **63A**, 444 (1950).

<sup>120</sup> H. H. Schmidt and G. Jura, J. Phys. Chem. Solids **16**, 60 (1960).

<sup>121</sup> H. H. Schmidt and G. Jura, J. Phys. Chem. Solids **16**, 67 (1960).

<sup>122</sup> D. Stansfield, Proc. Phys. Soc. (London) **72**, 854 (1958).

<sup>123</sup> A. T. Van Urk, W. H. Keesom, and G. P. Nijhoff, Commun. Kamerlingh Onnes Lab. Univ. Leiden **17**, 182b (1926).

<sup>124</sup> A. Harasima and Y. Shimura, J. Phys. Soc. Japan **11**, 14 (1956).

<sup>125</sup> E. N. Farabaugh and G. L. Pollack, Bull. Am. Phys. Soc. **8**, 227 (1963). Further work is to be published.

<sup>126</sup> G. L. Pollack and H. P. Broida, J. Chem. Phys. **38**, 2012 (1963).

gases, they only account for relative lattice energy differences of the order of 0.01%. This is much less than the experimental uncertainty in measuring thermodynamic properties so little is lost and much is gained in ease of calculation by considering only central forces between rare-gas atoms.

The general procedure in finding an intermolecular potential is to construct, usually on both theoretical and empirical grounds, a sample function containing several parameters, use some experimental data on thermodynamic properties to fix the parameters, and test the resultant  $\phi(r)$  by calculating other experimentally known properties from it. In order to use a property in this manner there must be available accurate experimental data and theoretically well-grounded, preferably simple, equations connecting the property with the intermolecular potential. Properties which have been most frequently used in these roles are the crystal-lattice spacing  $a_{00}$  and heat of sublimation  $L_0$  both at 0°K, and the temperature dependence of the second virial coefficient for the gas,  $B(T)$ . Liquid properties are generally not sufficiently well understood theoretically to be useful for determining potential parameters; recently, however, shock waves in liquids have been so used.<sup>127</sup>

From these few properties only two or three parameter potential functions may be determined and tested and these are of limited use for examining theories and experiments by calculating still other properties. More detailed potential functions can be derived and tested with additional assumptions, from enthalpy, entropy, and equation of state data for the solid, and from Joule-Thomson coefficients, viscosity coefficients, and transport properties in the gas. We here describe and compare the different proposed potential functions between rare-gas molecules and discuss ways of deriving and testing them, especially from solid-state theories and experiments but also where necessary from gas properties.

The simplest commonly used form for  $\phi(r)$  is the Lennard-Jones (6,  $n$ ) potential written

$$\phi(r) = \frac{-\epsilon}{n-6} \left[ n \left( \frac{r_0}{r} \right)^6 - 6 \left( \frac{r_0}{r} \right)^n \right], \quad (n > 6) \quad (16)$$

[cf. Eq. (2)] where  $\epsilon$  and  $r_0$  have the same meaning as earlier. In the most useful special case,  $n=12$ , this takes the form

$$\phi(r) = -4\epsilon \left[ (\sigma/r)^6 - (\sigma/r)^{12} \right], \quad (17)$$

where  $\epsilon$  is again the depth of the well at the minimum,  $r_0 = 2^{1/6}\sigma$ , and  $\phi(\sigma) = 0$ .

Corner<sup>128</sup> investigated potentials of the type (16) for Ar and Ne, determining the three parameters  $\epsilon$ ,  $r_0$ , and  $n$ , so that the lattice parameter  $a_{00}$  and the heat of

sublimation  $L_0$  at 0°K were given correctly, and using second virial and Joule-Thomson coefficient data to determine  $n$  and test the resultant  $\phi$ . The comparison with second-virial data is easily done but in order to connect the parameters with the crystal properties a simple, approximate model must be assumed. He found from a comparison of different potentials that the Lennard-Jones (6, 12) potentials gave almost as accurate predictions as the best potentials with exponential repulsion and the former are much more convenient for many applications. The values of his parameters for Ne and Ar are shown on Table III. Zucker<sup>129</sup> has determined the parameters in the (6,  $n$ ) potential Eq. (16) entirely from solid-state data and used the potential in an appropriate equation of state to compute isotherms for Ne, Ar, and Kr. He obtained reasonable agreement with experiment with values of  $n$ , respectively, 14, 12, and 12. His (6, 12) potential for Ar is shown on Fig. 13.

Some knowledge of the allowable repulsion exponents  $n$  in Eq. (16) may be obtained from a thermodynamic discriminant recently investigated by Brown and Rowlinson.<sup>130</sup> The discriminant, an explicit function of  $P$ ,  $T$ , and several thermodynamic properties as well as  $n$ , can be shown from classical statistical mechanics to satisfy a Schwarz inequality of the form  $D(n) \geq 0$ , at all  $P$  and  $T$ , for all permissible values of  $n$ , and thus sets a lower bound on  $n$ . Although a meaningful lower bound could not be determined from solid-state data for Ar due to the importance of quantum effects, the inequality  $n \geq 13.3$  was obtained for the liquid near the triple point. In order to apply the analogous quantum mechanical discriminant, more must be known about the thermodynamic behavior of the crystal, especially relating to Grüneisen's law.

Most recently Horton and Leech<sup>131</sup> have carried through systematic and thorough machine calculations of the potential parameters  $\epsilon$  and  $r_0$  in Eq. (16), from  $L_0$  and  $a_{00}$ , investigating the effects of: (a) variation of the repulsive exponent  $n$  from  $10 \leq n \leq 14$ ; (b) variation of the order of near neighbors (*viz.*, first only, first and second, and all neighbors) to be considered as contributing nonnegligibly according to Eq. (16); (c) variation of  $L_0$  and  $a_{00}$ ; and (d), respectively, including and excluding zero-point energy. The many quantitative conclusions<sup>131</sup> are difficult to summarize. In general, however, the calculations emphasize the importance of careful determination of  $\epsilon$  and  $r_0$  and in particular of using only assumptions in the further derivation of thermodynamic properties from Eq. (16) which are consistent with the assumptions used in determining  $\epsilon$  and  $r_0$  from the original data. The inclusion of zero-point energy in calculating the parameters, especially  $\epsilon$ , is important particularly and not surprisingly for Ne.

<sup>129</sup> I. J. Zucker, *J. Chem. Phys.* **25**, 915 (1956).

<sup>130</sup> W. B. Brown and J. S. Rowlinson, *Mol. Phys.* **3**, 35 (1960).

<sup>131</sup> G. K. Horton and J. W. Leech, *Proc. Phys. Soc. (London)* **82**, 816 (1963).

<sup>127</sup> W. Fickett and W. W. Wood, *Phys. Fluids* **3**, 204 (1960).

<sup>128</sup> J. Corner, *Trans. Faraday Soc.* **44**, 914 (1948).

TABLE III. Lennard-Jones (6,  $n$ ) and Buckingham (exp, 6) potential parameters for rare-gas molecules.

	Lennard-Jones $\epsilon/k(^{\circ}\text{K})$	(6, $n$ ) $r_0(\text{\AA})$	Potential $n$	Buckingham $\epsilon/k(^{\circ}\text{K})$	(exp, 6) $r_0(\text{\AA})$	Potential <sup>a</sup> $\alpha$
Ne	36.3 <sup>b</sup>	3.16	12.0	38.0	3.147	14.5
Ar	119.3 <sup>b</sup>	3.87	12	123.2	3.866	14.0
Kr	159 <sup>a</sup>	4.04	12	158.3	4.056	12.3
Xe	228 <sup>a</sup>	4.46	12	231.2	4.450	13.0
Rn	290 <sup>c</sup>	4.87	12			

<sup>a</sup> Reference 60.<sup>b</sup> Reference 128.<sup>c</sup> G. A. Miller, *J. Phys. Chem.* **64**, 163 (1960).

Although the  $r^{-6}$  attractive term in Eq. (16) is well founded theoretically from quantum mechanics the  $r^{-n}$  repulsion is not, as noted earlier. A more realistic repulsion, although mathematically less convenient, is an exponential one. Mason and Rice<sup>60</sup> have determined the parameters  $\epsilon$ ,  $r_0$ , and  $\alpha$  of Ne, Ar, Kr, Xe, and some other nonpolar molecules for the (exp, 6) Buckingham

potential (cf. I.C):

$$\phi(r) = \frac{-\epsilon}{\alpha-6} \left[ \alpha \left( \frac{r_0}{r} \right)^6 - 6 \exp \alpha \left( 1 - \frac{r}{r_0} \right) \right]; \quad (5)$$

$\epsilon$  and  $r_0$  have the same meaning as in Eq. (16) and  $\alpha$  determines the steepness of the repulsion at small intermolecular separations.<sup>132</sup> These workers followed Corner in first fitting the parameters to the crystal properties at 0°K but extended the method by using the more sensitive gas viscosity data besides second-virial coefficients to determine the remaining unspecified parameter  $\alpha$  and test the potential. In addition the potentials were tested on other available gas transport properties: thermal conductivity, self-diffusion coefficients, and the isotopic thermal-diffusion ratios. The (exp, 6) potential functions determined in this manner are somewhat superior to the (6, 12) potentials but although they fit the crystal data well they are in only fair agreement with the transport properties. The (exp, 6) parameters of these authors for Ne, Ar, Kr, and Xe are shown on Table III, along with parameters for the (6, 12) potential they calculated by applying an earlier procedure of Corner to Kr and Xe. The Ar (exp, 6) potential they obtained is shown on Fig. 13 in comparison with some other potentials. On Fig. 14 is shown the (6, 12) potential obtained for Kr.

In general, potentials derived from one set of properties predict other sets of properties only fairly. It is useful,<sup>133</sup> for example, to separate potentials derived from equilibrium properties ( $L_0$  and  $a_{00}$  for the crystal, second- and third-virial-coefficient data, Joule-Thomson coefficients) from potentials derived from non-equilibrium properties (thermal conductivity, diffusion). Better theoretical understanding and more accurate experimental data are usually available for equilibrium properties than for nonequilibrium properties. The problem of finding reliable potentials is also

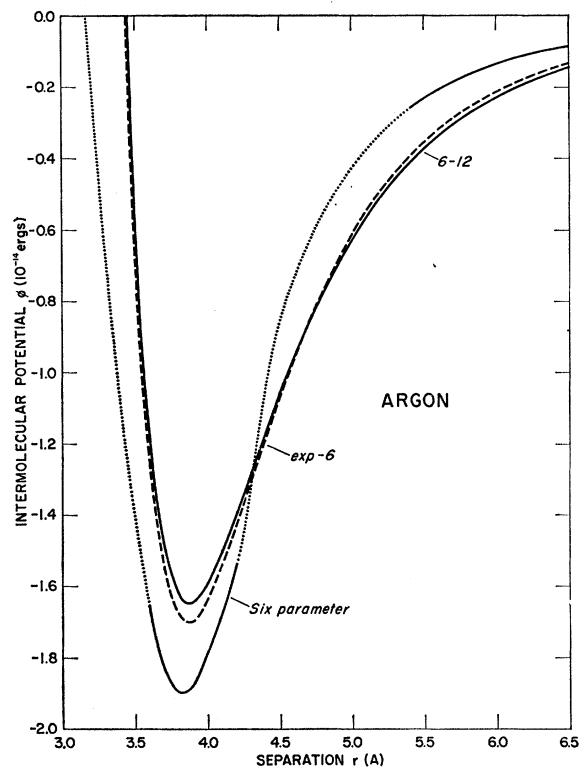


FIG. 13. Comparison of intermolecular potential functions for Ar determined from crystal properties. The dashed curve is the Buckingham (exp, 6) potential obtained by Mason and Rice (Ref. 60), the parameters are given on Table III. The solid curve is the Lennard-Jones (6, 12) potential obtained by Zucker (Ref. 129), the parameters are  $\epsilon=1.644 \times 10^{-14}$  ergs and  $r_0=3.874$  Å. The curve labeled Six parameter is the two-piece potential of Guggenheim and McGlashan (Ref. 147), the parameters are given on Table IV with  $\beta=0$ . Regions between the experimentally determined parts of the six parameter potential are shown by the dotted curve.

<sup>132</sup> This function has a physically unmeaningful maximum at small  $r$ . For a typical value of  $\alpha=13.5$ , the maximum occurs at  $r/r_0 \approx 0.2$  however, and this represents a solid density obtainable only at pressures far beyond present limits. The whole subject of short range repulsions is a very interesting one but unfortunately cannot be treated here.

<sup>133</sup> J. Bahadur and M. P. Madan, *Proc. Natl. Inst. Sci. India* **A26**, 64 (1960).

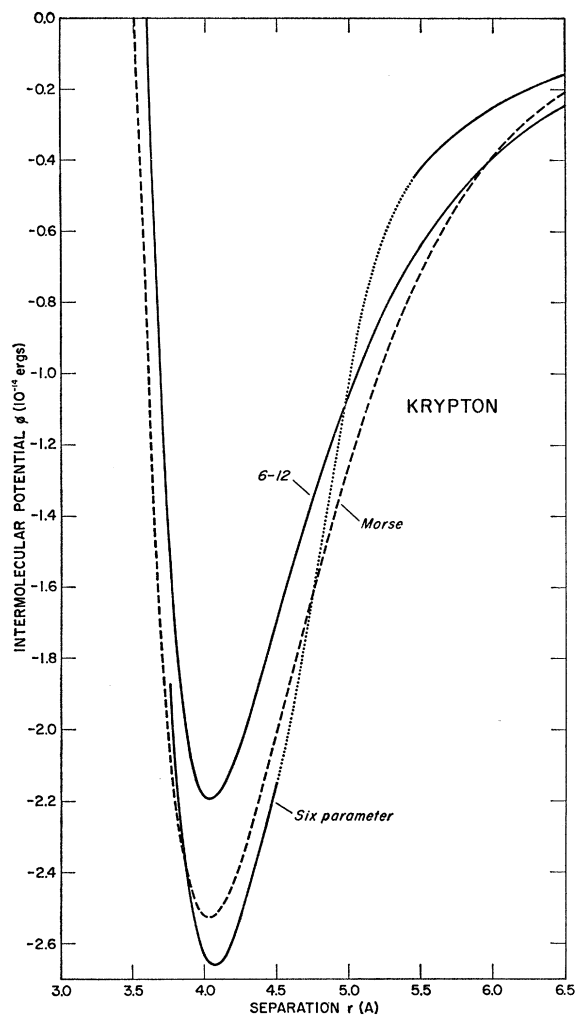


FIG. 14. Comparison of intermolecular potential functions for Kr determined from crystal properties. The dashed curve is the Morse potential obtained by Konowalow and Hirschfelder (Ref. 145), the parameters are  $\epsilon=2.521 \times 10^{-14}$  ergs,  $r_0=4.038$  Å,  $\sigma=3.510$  Å, and  $c=4.5$ . The solid curve is the Lennard-Jones (6, 12) potential obtained by Mason and Rice (Ref. 60) using Corner's method, the parameters are given on Table III. The curve labeled Six parameter is the two-piece potential of Barua and Chakraborti (Ref. 153), the parameters are given on Table IV. The region between the experimentally determined parts of the six parameter potential is shown by the dotted curve.

complicated by unevenness in the experimental uncertainty with which different properties have been measured and unevenness in the sensitivity of different potential parameters to different properties. For example: Accurate second-virial coefficients for rare gases are available, but surprisingly wide ranges in intermolecular potential parameters fit the data; third-virial coefficients are more sensitive to variations in potential parameters but they have not been accurately measured. These coefficients as well as most gas data, especially at high  $T$ , depend largely on the details of

molecular collision, i.e., of the repulsive portion of the potentials. Solid-state properties such as  $a_0$ , enthalpy, entropy, and specific heat are sensitive to the detailed form near the minimum in the potential since this is what controls lattice vibrations;  $L_0$  depends on the form of  $\phi$  from the minimum out to large separations.

Limitations on the applicability of the simple potentials Eqs. (16) and (5) have been especially pointed up for Kr. Second-virial coefficients for Kr have been accurately measured over a broad range of temperature<sup>134,135</sup> and can be used to determine potential parameters. The potential parameters obtained from the high-temperature virial coefficients do not agree well with the low-temperature data. Surprisingly, for Ne the entire range of second-virial data from about 120° to 1000°K and up to 80 atm can be fitted excellently by either an (exp, 6) or a (6, 12) potential.<sup>136</sup> Parameters which have been determined from second-virial data for Kr and some crystal properties do not fit other crystal properties satisfactorily.<sup>137</sup> Potentials on both models for Kr have also been determined from transport property data, especially thermal diffusion and thermal conductivity.<sup>138,139</sup> Both potentials can be used to give good agreement with experiment for the self-diffusion and viscosity but no amount of parameter adjustment makes possible acceptable agreement with experimental crystal properties and low-temperature virial data. For the other rare gases the agreement between virial data and potentials determined from transport properties is uniformly better than for Kr and there has been some discussion<sup>140</sup> on the apparently unique properties of Kr potentials. The difficulty lies in the lack of good experimental and theoretical values for the thermal diffusion factor<sup>141</sup>—by far the most sensitive of the transport properties to small changes in potential.

Recently, however, accurate measurements of viscosity<sup>142</sup> have been reported on Kr gas in the range from 300–660°K and potential parameters obtained on the (6, 12) model from these data are in good agreement with almost all of the equilibrium and nonequilibrium properties of both the solid and the gas. We wish to emphasize that for potentials with few parameters, such as so far considered, the values of the parameters are not unique, i.e., sets of parameters which differ rather widely can still give very similar fits to experimental data.

<sup>134</sup> B. E. F. Fender and G. D. Halsey, Jr., *J. Chem. Phys.* **36**, 1881 (1962).

<sup>135</sup> G. Thomaes and R. van Steenwinkel, *Nature* **193**, 160 (1962).

<sup>136</sup> G. A. Nicholson and W. G. Schneider, *Can. J. Chem.* **33**, 589 (1955).

<sup>137</sup> E. Whalley and W. G. Schneider, *J. Chem. Phys.* **23**, 1644 (1955).

<sup>138</sup> M. P. Madan, *J. Chem. Phys.* **27**, 113 (1957).

<sup>139</sup> E. A. Mason, *J. Chem. Phys.* **32**, 1832 (1960).

<sup>140</sup> B. E. F. Fender, *J. Chem. Phys.* **35**, 2243 (1961).

<sup>141</sup> E. A. Mason, *J. Chem. Phys.* **35**, 2245 (1961).

<sup>142</sup> D. G. Clifton, *J. Chem. Phys.* **38**, 1123 (1963).

To some extent solid-state data have been fitted to the four parameter Buckingham-Corner (exp, 6, 8) potential.<sup>128,143</sup> This potential is a variation of Eq. (5) and is usually considered separately in the two regions  $r \geq r_0$  and  $r \leq r_0$  and suitably matched at  $r_0$ . The essential improvement in the (exp, 6, 8) potential over Eq. (5) is the inclusion of a parametrically variable, additive, dipole-quadrupole ( $r^{-8}$ ) correction to the attractive dipole-dipole ( $r^{-6}$ ) term. The extra parameter  $\beta$  is the dimensionless ratio of the coefficients of these two terms and can be determined from quantum mechanics or from experimental data; in either case its magnitude is about  $\frac{1}{6}$ . The connection between the parameters and data for this potential is through rather complicated transcendental equations; the necessary coefficients and integrals have very largely been worked out and tabulated, however. No significant improvements over the simpler potentials in fitting properties have been reported. Coefficients of the  $r^{-6}$  attractive van der Waals potential term have been calculated<sup>144</sup> to within 10% for Ne and Ar from quantum-mechanical first principles applied to refractive index data. Such fundamental calculations are of great value in uniquely specifying the parameters since, as has been remarked, data fitting usually does not do this.

Konowalow and Hirschfelder<sup>145</sup> have determined from solid-state and virial data the parameters for Ne, Ar, Kr, and Xe in the Morse potential:

$$\phi(r) = \epsilon \left\{ \exp \left[ -2c(r/\sigma - r_0/\sigma) \right] - 2 \exp \left[ -c(r/\sigma - r_0/\sigma) \right] \right\}, \quad (18)$$

in which  $c$  is a new parameter and the other symbols are the same as in Eqs. (16) and (5). At large distances the Morse potential does not have the correct  $r^{-6}$  attraction but for solid-state applications this is relatively unimportant. The agreement this potential gives with experimental virial coefficients is comparably as good as Eqs. (16) and (5), although the more stringent tests of how well Eq. (18) gives transport properties cannot yet be carried through for lack of the necessary collision integrals. One of the major advantages of Eq. (18) is that the Schrödinger equation with a Morse potential may be accurately solved. The other potentials we have discussed do not share this property. This means that the interactions among rare-gas atoms may be studied from first-quantum mechanical principles; calculations of this kind have been carried out for the gas<sup>146</sup> but not the solid phase. The Morse potential obtained for Kr is plotted on Fig. 14.

In the last few years much attention has been paid to finding and investigating potentials which fit all of

<sup>143</sup> A. K. Barua, *J. Chem. Phys.* **31**, 957 (1959).

<sup>144</sup> A. Dalgarno and A. E. Kingston, *Proc. Phys. Soc. (London)* **78**, 607 (1961).

<sup>145</sup> D. D. Konowalow and J. O. Hirschfelder, *Phys. Fluids* **4**, 629 (1961).

<sup>146</sup> N. Bernardes and H. Primakoff, *J. Chem. Phys.* **30**, 691 (1959).

the experimental equilibrium crystal properties for rare gases from 0°K to the melting points. Until recently these properties, especially the density and compressibility, had not been extensively measured, so not much understanding of solids could be gained by increasing the complexity of  $\phi(r)$ . It is now worthwhile to investigate whether a potential can be found which correlates all these solid-state properties as functions of  $T$  and  $P$  over a broad range. Guggenheim and McGlashan<sup>147</sup> have investigated for Ar the two-piece intermolecular potential

$$\phi(r) = -\epsilon + \kappa \left[ (r-r_0)/r_0 \right]^2 - \alpha \left[ (r-r_0)/r_0 \right]^3 + \beta \left[ (r-r_0)/r_0 \right]^4 \quad (19a)$$

for  $r$  in the neighborhood of  $r_0$ , and

$$\phi(r) = -\lambda r^6/r^6 \quad \text{for} \quad r \geq 1.4r_0. \quad (19b)$$

The parameters  $\epsilon$  and  $r_0$  are as before the energy and separation, respectively, at the minimum of  $\phi$ ,  $\kappa$  describes the curvature of the potential at the minimum, and  $\alpha$  describes the rate of change of curvature there. The parameter  $\beta$  in the last term of Eq. (19a) is related to anharmonicity in the lattice vibrations. It has been suggested that the effects of anharmonicity in the experimental data are small and no significant decrease in validity of  $\phi$  results from ignoring it, i.e., taking  $\beta=0$ . An alternate assumption,  $\beta=\alpha$ , which makes anharmonicity in the potential negligible, is equally effective. The principal forces between molecules further apart in the crystal than nearest neighbors are van der Waals  $r^{-6}$  attractions. The factor  $\lambda$  in Eq. (19b) may therefore be either determined a priori from theory or treated as a free parameter. In practice the quantum mechanical value usually gives the best fit to experimental data. Solid state equilibrium data cannot quite specify the parameters in Eq. (19) uniquely and so recourse must be made once again to gas data. For these purposes an extra parameter must be introduced,  $\sigma$ , the crossover separation at which  $\phi(\sigma)=0$ . The six parameters to be fitted to the data are then  $\lambda$ ,  $r_0$ ,  $\epsilon$ ,  $\kappa$ ,  $\alpha$ , and  $\sigma$ , with  $\beta$  generally taken as zero. Table IV contains the best values of these parameters for rare-gas molecules and the resultant potential with  $\beta=0$  is plotted for Ar on Fig. 13 along with simpler potentials which have been discussed above. The behavior of  $\phi$  for  $r$  within the crossover does not affect any of the properties tested and the most convenient, albeit arbitrary, assumption is: for  $r < \sigma$ ,  $\phi$  is infinite. The hard sphere radius  $\sigma$  of the molecule may be straightforwardly estimated from gas viscosities. The form of  $\phi$  in the region between Eqs. (19a) and (19b) is also not critical and this has been drawn in following the example of the original authors.

The potential of Eq. (19a) has been long used in the theory of band spectra and was applied to the study of

<sup>147</sup> E. A. Guggenheim and M. L. McGlashan, *Proc. Roy. Soc. (London)* **A255**, 456 (1960).

TABLE IV. Parameters for rare-gas molecules in the potential.

$$\phi(r) = -\epsilon + \kappa[(r-r_0)/r_0]^2 - \alpha[(r-r_0)/r_0]^3 + \beta[(r-r_0)/r_0]^4 \text{ for } r \text{ near } r_0, \phi(r) = -\lambda r_0^6/r^6 \text{ for } r \geq 1.4r_0, \phi(\sigma) = 0.$$

	$\epsilon/k$ (°K)	$r_0$ (Å)	$10^{-2}\kappa/k$ (°K)	$10^{-3}\alpha/k$ (°K)	$10^{-4}\beta/k$ (°K)	$\lambda/k$ (°K)	$\sigma$ (Å)
Ne <sup>a</sup>	40.6	3.130	13.26	5.78	0.578	44.3	
Ar <sup>b</sup>	137.5	3.818	44.3	18.3	0	150	3.165
Ar <sup>b</sup>	137.5	3.812	44.9	19.6	1.96	150	3.165
Kr <sup>c</sup>	192.8	4.074	65.95	30.74	0	185	<3.67
Xe <sup>d</sup>	267.0	4.435	85.10	39.24	0	300	3.960

<sup>a</sup> Reference 152.<sup>b</sup> Reference 147.<sup>c</sup> Reference 153.<sup>d</sup> Reference 154.

crystal properties of Ar by Rice<sup>148-150</sup> who in fact assumed a Debye frequency spectrum for the solid in contrast to the simpler Einstein model. On the Debye model<sup>148</sup> the parameter  $\kappa \propto \Theta_D^2$ , and  $\alpha$  and  $\beta$  control the thermal expansivity of the lattice. If  $\alpha$  and  $\beta$  are zero the simple case  $\Theta_D = \text{const}$  results. Unfortunately difficulties arose in the theory due to the lack of adequate experimental data at the time. We here describe in outline the procedures and results of the more recent work on Eq. (19) as an elegant example in the use of an intermolecular potential to predict solid-state equilibrium properties. Agreement with experiment has proved to be markedly superior to that of other potentials.

If all the molecules are on their lattice sites and interact according to the force law of Eq. (19) then the static lattice energy per mole is<sup>147</sup>

$$U_0 = 6N[-\epsilon + \kappa \Delta^2 - \alpha \Delta^3 + \beta \Delta^4 - \frac{1}{12}(C_6 - 12)\lambda(1 + \Delta)^{-6}], \quad (20)$$

where  $\Delta = (a_0 - r_0)/r_0$ , and  $C_n$  is the crystal potential constant for an fcc lattice and an  $r^{-n}$  force law [cf. Eq. (3)]. Crystal potential constants have been tabulated by Lennard-Jones and Ingham<sup>151</sup> for many  $n$  and several lattices.

If a molecule is displaced slightly from its static lattice site then to a first approximation it executes harmonic vibrations about its equilibrium position with frequency  $\nu$ , the characteristic Einstein frequency of the lattice. This frequency may be found from a geometric analysis and satisfies the equation

$$2\pi^2 m \nu^2 r_0^2 / 12 = \frac{1}{3} \kappa (1 + \Delta)^{-1} (1 + 3 \Delta) - \alpha \Delta (1 + \Delta)^{-1} (1 + 2 \Delta) + 2\beta \Delta^2 (1 + \Delta)^{-1} (1 + \frac{5}{3} \Delta) - \frac{5}{12} (C_8 - 12) \lambda (1 + \Delta)^{-8}. \quad (21)$$

<sup>148</sup> O. K. Rice, J. Am. Chem. Soc. **63**, 3 (1941).<sup>149</sup> O. K. Rice, J. Chem. Phys. **12**, 289 (1944).<sup>150</sup> O. K. Rice, J. Chem. Phys. **14**, 321 (1946).<sup>151</sup> J. E. Jones and A. E. Ingham, Proc. Roy. Soc. (London) **A107**, 636 (1925).

The partition function  $Q$  is then simply

$$Q = [\frac{1}{2} \text{csch}(h\nu/2kT)]^3, \quad (22)$$

and from the partition function the crystal properties may be calculated in the canonical manner. The free energy ( $F = E - TS$ ) is

$$F = U_0 - RT \ln Q = U_0 + 3RT \ln (2 \sinh h\nu/2kT). \quad (23)$$

The total energy  $U$  is given by

$$U = U_0 + RT^2 \left( \frac{\partial \ln Q}{\partial T} \right)_V = U_0 + 3RT \left( \frac{h\nu}{2kT} \right) \coth \left( \frac{h\nu}{2kT} \right). \quad (24)$$

and the entropy  $S$  is given by

$$S = 3R(h\nu/2kT) \coth(h\nu/2kT) - 3R \ln [2 \sinh(h\nu/2kT)]. \quad (25)$$

The equation of state of the solid Ar comes straightforwardly from

$$P = - \left( \frac{\partial F}{\partial V} \right)_T = \frac{-4}{3N a_0^2} \frac{\partial F}{\partial a_0}. \quad (26)$$

The parameters may be conveniently evaluated and made sensitive to the temperature and pressure dependence of the equilibrium crystal data  $U(T)$ ,  $S(T)$ , and  $\rho(P, T)$  by use of Eqs. (21), (24), and (26) applied at two different temperatures spaced as widely as possible but both sufficiently high so that the Einstein approximation holds, viz.  $T_{\text{tp}}$  and  $T_{\text{tp}}/2$ . The frequency  $\nu$  may be determined from  $S(T)$  which in turn is obtained from integration of experimental specific heat data. At ordinary pressures  $U$  in Eq. (24) is essentially equal to the enthalpy, also obtainable from integration of specific heat. The critical test of the chosen potentials and parameters is how well they give back experimental crystal data in the  $P$  and  $T$  regions between and beyond the points at which they were fitted. These tests have been carried through in detail.<sup>147</sup> The potential of Eq. (19) for Ar with appropriate parameters (see Table IV) was found to fit  $S(T)$  and

$U(T)$  within experimental error and give a passably good fit to  $\rho(P, T)$  data at not too high pressures nor too low temperatures. The fit of the theoretical equation of state to  $\rho(P, T)$  is an especially sensitive test for anharmonicity. As expected, experimental agreement is better than with simpler potentials.

The experimental data on the other rare gases is not as complete as for Ar but their respective potential parameters in Eq. (19) may be obtained from applying the law of corresponding states (see III.B) to the Ar results. This has been done<sup>152</sup> for Kr, Xe, and Ne and the results tested on experimental curves of  $U(T)$ ,  $S(T)$ , and  $\rho(T)$ . The results for Kr and Xe are well within experimental accuracy but for Ne use of the potential can only be made in a narrow-temperature range around 20°K and sufficient experimental data is lacking. The potential parameters obtained in this manner for Ne are the best available for Eq. (19) and they have been included on Table IV.

Barua and Chakraborti<sup>153</sup> have derived the potential for Kr on the six-parameter model of Eq. (19) directly from the available experimental data using the procedure described. Their potential correlates satisfactorily with the solid-state equilibrium properties and the best values are shown on Table IV and plotted on Fig. 14 in comparison with other potentials. From these parameters a closely related (6, 12) potential was derived and this enabled convenient satisfactory correlation with both equilibrium and transport properties of the gas. A potential energy curve for Xe on the model of Eq. (19) has also been recently determined by Chakraborti<sup>154</sup> using essentially the same procedure. The agreement with experiment is again satisfactory for the solid-state and second-virial data and the best fitting parameters for Xe are shown on Table IV.

## B. Law of Corresponding States and Applications

### 1. Law of Corresponding States

The law or principle of corresponding states may be used much as formally derived equations of state, for example, to predict some properties from others, to define ideal behavior and investigate departures from it, and in particular to investigate the effects of quantum mechanics in solids and liquids. Historically, laws of this kind have been investigated and proven mainly for gases and liquids but they are also valid for many solid-state properties especially of argon, krypton, xenon, and to a lesser extent neon. We here describe the modern forms of the law of corresponding states, its general application to the solid state of rare gases, and then briefly investigate some specific properties with it, viz. zero-point properties, melting properties,

and in more detail vapor pressure and thermal conductivity.

The law of corresponding states may be written thus: The equations of state of certain simple substances are identical when expressed in terms of suitable reduced variables. Sufficient conditions under which the law may be shown to hold have been carefully elucidated.<sup>155,156</sup> First, some assumption must be made on the statistical mechanics of the system. If classical statistics apply, i.e. there is no meaningful distinction between the results of Fermi-Dirac or Bose-Einstein statistics, then the universal equation of state in the reduced variables can be shown to read  $P_r = P_r(V_r, T_r)$  if the further assumptions to be discussed below also obtain. In this older form of the law, applied first to van der Waals gases, the variables were reduced or non-dimensionalized by dividing them with the appropriate critical constants:  $P_r = P/P_c$ ,  $V_r = V/V_c$ , and  $T_r = T/T_c$ . The law in this form also holds for liquids and solids so long as quantum effects are negligible as at not too low  $T_r$  and for molecules whose masses are not too small.

Second, the molecules must be either actually spherically symmetric, as the rare-gas molecules, or else be freely rotating so that they are effectively spherically symmetric. Simple diatomic molecules sometimes satisfy this latter condition in the liquid state and less frequently in the solid state. Third, intramolecular vibrations must be the same in the condensed state as they are in the gas, i.e., independent of molecular volume. This means that in order for diatomic and polyatomic molecules to follow the law, the intermolecular forces must be weak and short range. Fourth, the potential energy must be a function only of the intermolecular distances. This is nearly exactly true for rare-gas molecules in the solid state as we have seen from the potential functions in III.A and even holds to a surprisingly good approximation for diatomic molecules. Fifth, the intermolecular potential for two molecules can be written  $\phi = \epsilon f(r/\sigma)$  where  $\epsilon$  is some energy scaling factor,  $\sigma$  is some characteristic distance, and  $f$  is a universal function. In the older forms of the law  $\epsilon$  was taken proportional to  $T_c$  and  $\sigma$  proportional to  $V_c^{1/3}$ . This allows only limited application of the principle to solid-state properties of rare gases although liquid and gas properties can still be given accurately.

In the more flexible, modern, form of the law the reduced variables are  $P^*$ ,  $V^*$ , and  $T^*$ , defined as follows:  $P^* = P\sigma^3/\epsilon$ ,  $V^* = V/N\sigma^3$ , and  $T^* = kT/\epsilon$ , where  $\epsilon$  is the depth of the well and  $\sigma$  is the value of  $r$  for which the potential vanishes. These are of course exactly the parameters used to describe the potentials in III.A and the (6, 12) potential function as we have seen serves adequately as the universal function  $f(r/\sigma)$  which gives quite accurate representation for calcu-

<sup>152</sup> E. A. Guggenheim and M. L. McGlashan, *Mol. Phys.* **3**, 563 (1960).

<sup>153</sup> A. K. Barua and P. K. Chakraborti, *Physica* **27**, 753 (1961).

<sup>154</sup> P. K. Chakraborti, *Physica* **29**, 227 (1963).

<sup>155</sup> K. S. Pitzer, *J. Chem. Phys.* **7**, 583 (1939).

<sup>156</sup> E. A. Guggenheim, *J. Chem. Phys.* **13**, 253 (1945).

lating solid-state properties of rare gases. In these variables the reduced equation of state in the classical approximation is:  $P^* = P^*(V^*, T^*)$ . Compared to  $P_r$ ,  $V_r$ , and  $T_r$ , the starred variables have the advantage that they may be used to investigate quantum effects since  $\epsilon$  and  $\sigma$  are not affected by quantum mechanics as are the critical constants. Guggenheim has pointed out that the value of  $P_c V_c / T_c$  for Ne, for example, is 4% higher than that of the average of the heavier rare gases, presumably a quantum effect.<sup>156</sup> The same effect is apparent in investigation of correspondence in triple-point temperature, pressure, and entropy of fusion. As is expected the reduced constants for Ar, Kr, and Xe are very close but quantum effects tend to keep the Ne lattice more loosely bound so that its reduced triple-point temperature and entropy of fusion are lower, and its reduced triple-point pressure is higher than for the heavier rare gases. In the past, values of the critical constants were much more accurately known than values of the potential parameters but this is no longer true for rare gases. It is worth remembering, however, that for many diatomic molecules, especially heteronuclear ones,  $\epsilon$  and  $\sigma$  cannot be easily determined whereas critical constants are accurately known. Such molecules as N<sub>2</sub>, CO, and CH<sub>4</sub> can be shown to follow the law of corresponding states fairly well as gases and liquids.

De Boer and Blaisse<sup>157,158</sup> have extended the principle of corresponding states to account both qualitatively and quantitatively for quantum effects. Using quantum statistics the sum over states  $Z$  is given as

$$Z = Z^0 \sum_n \exp(-E_n/kT), \quad (27)$$

where  $E_n$  are the eigenvalues of the Schrödinger equation for a system of  $N$  interacting molecules:

$$\left[ -(\hbar^2/2m) \sum_i \nabla_i^2 + \sum_{i>k} \phi(r_{ik}) - E_n \right] \Psi_n(\mathbf{r}_1, \dots, \mathbf{r}_N) = 0. \quad (28)$$

Written in reduced variables with  $E_n^* = E_n/N\epsilon$ ,  $\phi = \epsilon f(r^*)$ , and  $\sigma^2 \nabla_i^2 = \nabla_i^{*2}$  the equation becomes

$$\left[ -\Lambda^{*2} \sum_i (1/8\pi^2) \nabla_i^{*2} + \sum_{i>k} f(r_{ik}^*) - N E_n^* \right] \times \Psi_n(\mathbf{r}_1^*, \dots, \mathbf{r}_N^*) = 0, \quad (29)$$

where  $\Lambda^*$ , a nondimensionalized de Broglie wavelength, is the new variable defined as (see Table VIII in III.D)

$$\Lambda^* = h/\sigma(m\epsilon)^{1/2}. \quad (30)$$

The eigenvalues  $E_n^*$  depend then on  $V^*$  and  $\Lambda^*$  and Eq. (27) may be written

$$Z = Z^0 Q(V^*, T^*, \Lambda^*). \quad (31)$$

The equation of state in De Boer's formulation is then

$$P^* = (T^*/N) (\partial/\partial V^*) \ln Q(V^*, T^*, \Lambda^*) \\ = P^*(V^*, T^*, \Lambda^*). \quad (32)$$

Quantum effects are largest near 0°K where ordinary thermal effects are small and these have been much investigated especially by examining the reduced static-lattice energy (see Fig. 16)  $U_0^* = U_0/N\epsilon$ , and the reduced molar volume  $V_0^* = V_0/N\sigma^3$  for Xe, Kr, Ar, and Ne at 0°K as functions of their respective  $\Lambda^*$ . Quantum deviations are apparent<sup>159</sup> for all the rare-gas solids and are most pronounced for Ne. Deviations increase as the molecular masses decrease further, for example when the solid states of the hydrogens, <sup>4</sup>He, and <sup>3</sup>He are considered. De Boer and Blaisse<sup>158</sup> have examined the quantum law of corresponding states quantitatively giving  $U_0^*$ ,  $V_0^*$ , and  $\Theta_D^* = k\Theta_D/\epsilon$  as explicit functions of  $\Lambda^*$ . This theory applies only for molecules for which  $\Lambda^* \leq \Lambda_{Ne}^*$  since if  $V_0^*$  is too large difficulties arise in averaging the velocity of sound over direction, due ultimately to breakdown of the harmonic approximation. The results are in good quantitative agreement with experiment in this region. In the limit  $\Lambda^* \rightarrow 0$  the results are:  $V_0^* = 0.916$ ,  $U_0^* = -8.610$ , and  $\Theta_D^* = 9.45\Lambda^*$ .

Corrections to the zero-point properties of rare-gas solids due to increasing  $\Lambda^*$  have been calculated from quantum mechanical first principles by Bernardes<sup>160</sup> (see III.D. Zero-Point Properties). In his formulation the reduced molar volume, static lattice potential energy, bulk modulus, sound velocity, Debye temperature, and Grüneisen constant, are calculated at 0°K in the limit  $\Lambda^* \rightarrow 0$  from classical principles applied to a Lennard-Jones potential. The quantum corrections result from a variational principle applied to a Heitler-London wavefunction and are expressed as power series in  $h$  of the form  $(1 + a\Lambda^* + b\Lambda^{*2} + \dots)$  multiplying the classical values. The  $\Lambda^* = 0$  limit as well as the  $\Lambda^*$  dependence of the derived properties are in generally excellent agreement with experiment for the rare gases including Ne. Figure 15 shows as an example the theoretically calculated ratio of reduced bulk modulus  $K^*(\Lambda^*) = -V^*(dP^*/dV^*)$  including quantum effects to bulk modulus in the limit  $\Lambda^* = 0$ , both at 0°K in comparison with experimental data. Zucker<sup>161</sup> has considered corrections in the zero-point properties  $V_0^*$ , and  $U_0^*$  due to large  $\Lambda^*$  as the result of anharmonic effects in an Einstein lattice. These effects become important at large mean excursions of molecules from their static lattice positions such as result from large zero-point energy. His results are also in excellent agreement with experiment for not too large  $\Lambda^*$  and we have shown on Fig. 16 the plot of  $F_0^*$  (or  $E_0^*$ ) vs  $\Lambda^*$ .

<sup>157</sup> J. De Boer, *Physica* **14**, 139 (1948).

<sup>158</sup> J. De Boer and B. S. Blaisse, *Physica* **14**, 149 (1948).

<sup>159</sup> R. Gopal, *Z. Anorg. U. Allgem. Chem.* **281**, 217 (1955).

<sup>160</sup> N. Bernardes, *Phys. Rev.* **120**, 807 (1960).

<sup>161</sup> I. J. Zucker, *Proc. Phys. Soc. (London)* **77**, 889 (1961).

De Boer and Blaisse<sup>158,162</sup> have also derived explicit model equations of state of the form (32). The reduced free energy  $F^* = F/N\epsilon$  at  $T > 0^\circ\text{K}$  may be written as the sum of three terms, respectively: the reduced potential energy  $U_0^*$ , the reduced zero-point energy  $9\Theta_D^*/8$ , and in the Debye approximation a term for thermally excited lattice vibrations,

$$F^* = U_0^* + \frac{9}{8}\Theta_D^* + 3T^* \left[ \ln \left( \exp \frac{\Theta_D^*}{T^*} - 1 \right) - \frac{\Theta_D^*}{T^*} - \left( \frac{T^*}{\Theta_D^*} \right)^3 \int_0^{\Theta_D^*/T^*} \frac{\xi^3 d\xi}{\exp \xi - 1} \right]. \quad (33)$$

All of these terms may be expressed as explicit functions of  $V^*$  and  $T^*$  so that the reduced equation of state

$$P^* = P_{\text{pot.}}^* + P_{\text{z.}}^* + P_{\text{th.}}^* = -(\partial F^*/\partial V^*)_{T^*} \quad (34)$$

may be used to give theoretical reduced isotherms,  $P^*$  vs  $V^*$  at constant  $T^*$ . From theory thus it is expected that correspondence in compression isotherms obtains for the condensed rare gases in the limit  $\Lambda^* = 0$  and that the reduced experimental curves deviate from each

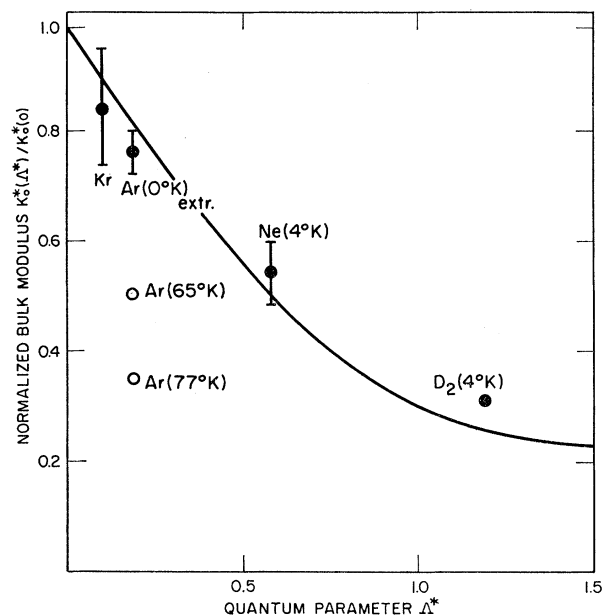


FIG. 15. Comparison of theoretical and experimental variation of reduced bulk modulus  $K^* = -V^*(dP^*/dV^*)$  at  $0^\circ\text{K}$  with quantum parameter  $\Lambda^* = h/\sigma(m\epsilon)^{1/2}$ . The ordinate is the ratio of the quantum mechanically calculated reduced bulk modulus at  $0^\circ\text{K}$ ,  $K_0^*(\Lambda^*)$  to the reduced bulk modulus  $K_0^*(0)$  in the classical limit  $\Lambda^* = 0$ . Experimental values for Ar and Kr have been extrapolated to  $0^\circ\text{K}$ . Measurements of bulk modulus of Ar at higher temperatures are indicated with open circles. The solid curve is theoretically predicted in the form:  $K_0^*(\Lambda^*)/K_0^*(0) = 1 + a\Lambda^* + b\Lambda^{*2}$ . (After Bernardes Ref. 160.)

<sup>162</sup> B. S. Blaisse, *Ned. Tijdschr. Natuurk.* **19**, 267 (1953) (in Dutch).

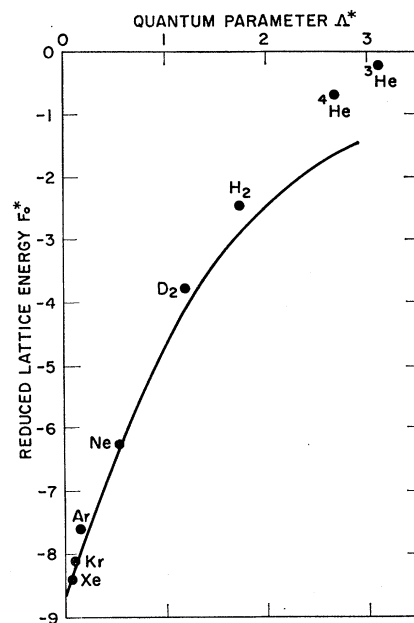


FIG. 16. Comparison of theoretical and experimental variation of reduced lattice free energy  $F^* = F/N\epsilon$  at  $0^\circ\text{K}$  with quantum parameter  $\Lambda^* = h/\sigma(m\epsilon)^{1/2}$ . For this temperature  $F_0^* = E_0^* = U_0^* + E_z^*$ , the reduced static-lattice cohesive energy + reduced zero-point energy. The solid curve is theoretically predicted. (After Zucker Ref. 161.) (Courtesy of The Institute of Physics and The Physical Society.)

other to the extent that quantum effects are important, e.g., at low  $T^*$ . These curves have been tabulated and examined<sup>158</sup> for Kr, Ar,  $\text{N}_2$ , Ne,  $\text{H}_2$ , and He in order of increasing  $\Lambda^*$  ( $\Lambda^*$  from 0.1 to 2.7) and give general qualitative agreement with experimental curves although quantitative agreement is poor. The experimental compressibility isotherms show the expected correspondence for the heavier rare gases near  $\rho_c$ .<sup>163</sup> However, even at  $T_c$  deviations from correspondence at pressures only a few times higher than  $P_c$  have been observed. Correspondence in the compressibility of the solids at low  $T$  has not been extensively investigated and would be of much interest although the same problem for liquids and gases has been treated.<sup>164</sup>

Correspondence in the melting lines of substances following the assumptions may also be straightforwardly demonstrated.  $G^*$ , the reduced Gibbs free energy may be written in general from Eq. (31)

$$G^* = (T^*/N) (\partial \ln Z / \partial \ln V^* - \ln Z), \quad (35)$$

so that the reduced melting curve along which the liquid and solid  $G^*$  are equal becomes

$$(\partial \ln / \partial \ln V^*) [Q_L(V^*, T^*, \Lambda^*) / Q_S(V^*, T^*, \Lambda^*)] = \ln [Q_L(V^*, T^*, \Lambda^*) / Q_S(V^*, T^*, \Lambda^*)]. \quad (36)$$

<sup>163</sup> F. Danon and K. S. Pitzer, *J. Phys. Chem.* **66**, 583 (1962).

<sup>164</sup> J. M. H. Levelt, *Physica* **26**, 361 (1960).

Application of the law of corresponding states to the theory of melting and to melting parameters has been of much use in generalizing and understanding the Simon melting formula.<sup>84</sup> Domb<sup>165</sup> has discussed and derived the Lindemann melting formula in terms of the law of corresponding states and has extended the formula taking into account quantum effects and other melting parameters. Theoretical reduced melting curves for rare gases may be derived in principle from Eq. (36) and in practice<sup>158</sup> from Eqs. (33) and (34). It is expected from theory that in the classical limit  $\Lambda^*=0$  and high  $T^*$  the melting curves  $P^*$  vs  $T^*$  of all substances satisfying the five conditions described above be identical. At lower  $T^*$ , and for larger  $\Lambda^*$  where quantum effects become important, the universal melting curve splits into individual curves for each substance. These results are in qualitative agreement with the experimental curves. Michels and Prins<sup>98</sup> have measured the melting curves of Ar, Kr, and Xe, up to 1500 atm and compared the reduced melting curves for all the rare gases. The variations from a universal melting curve are of the order of a few percent, probably the result of assuming the Lennard-Jones two-body intermolecular potential. However, the introduction of arbitrary scale parameters on  $P^*$  and  $T^*$  brought the results to a universal melting line. This means that for some set of  $\sigma$  and  $\epsilon$  the law of corresponding states holds more rigorously for the experimental melting curves.

Boato and Casanova<sup>166</sup> have found a self-consistent set of  $\epsilon$  and  $\sigma$  for all the rare gases by assuming that the law of corresponding states holds and adjusting the parameters to give universal reduced vapor-pressure curves over a wide range of temperature. The parameters obtained in this manner are usually somewhat different from the  $\epsilon$  and  $\sigma$  determined by the methods described in III.A, and can be used to predict rather well the variation with  $\Lambda^*$  of  $P_{tp}^*$ ,  $V_{tp}^*$ ,  $T_{tp}^*$ ,  $V_0^*$ , and  $U_0^*$ . It is interesting to note that the values of  $\epsilon$  and  $\sigma$  obtained in this manner are independent of the particular potential assumed so long as  $\phi(r) = \epsilon f(r/\sigma)$  whereas the values of the parameters shown, for example, on Tables III and IV are obtained from and depend on specific postulated potentials. Another interesting point is that measurements of isotopic effects in a property provide information on the local variation with  $\Lambda^*$  since for isotopes of the same monatomic molecule both  $\epsilon$  and  $\sigma$  are the same and  $\Lambda^*$  changes only due to the change in mass. Unfortunately isotope effects in solids are difficult to measure although in recent years continuing excellent work has been reported along these lines.<sup>167</sup>

In applying the law of corresponding states to the molecular parameters  $\epsilon$  and  $\sigma$  and calculating crystal density, energy, and entropy for the rare gases from

<sup>165</sup> C. Domb, Suppl. Nuovo Cimento **9**, 9 (1958).

<sup>166</sup> G. Boato and G. Casanova, Physica **27**, 571 (1961).

<sup>167</sup> G. Boato, J. Chim. Phys. **60**, 44 (1963).

20°K up to the triple points, Guggenheim and McGlashan<sup>152</sup> have introduced the principle of corresponding interactions, a natural extension of corresponding states. This is an effective way to use correspondence to predict crystal properties which are sensitive to molecular mass and hence cannot be found from a straightforward application of the law of corresponding states. For example, the absolute entropies of rare-gas crystals when plotted as functions of  $T_r$  follow distinctly separate curves.<sup>152</sup> However, when the values of  $\epsilon$  and  $\sigma$  for Kr and Xe obtained from applying corresponding interactions to the potential curve of Ar, for example, are used to calculate characteristic frequencies and hence densities, entropies, and energies for the crystals, agreement is obtained almost to within experimental error from about 20°K to the triple points. The deviations from experiment increase toward lower temperatures, probably the result of breakdown of the Einstein approximation.

## 2. Vapor Pressure

For a monatomic solid the statistical mechanical expression for vapor pressure is

$$\ln P = -\frac{L_0}{RT} + \frac{5}{2} \ln T - \int_0^T \frac{dT'}{T'^2} \int_0^{T'} C_p(T'') dT'' + \ln \left[ \left( \frac{m}{2\pi} \right)^{\frac{3}{2}} \frac{k^{\frac{3}{2}}}{\hbar^3} \right], \quad (37)$$

where  $L_0$  is the heat of sublimation at 0°K. This relation may be applied, at least in principle, to estimate  $P(T)$ ,  $C_p(T)$ , or  $L_0$  from the other two. In practice, the vapor-pressure curve may usually be described as

$$\ln P = -\frac{1}{2} \ln T + a/T + b. \quad (38)$$

Salter<sup>168</sup> has derived Eq. (38) from first principles assuming perfect crystal structure, quasi-harmonic lattice vibrations, and an almost ideal vapor, and has shown that for  $T \gtrsim \Theta_D/2$

$$a = U_0/Nk; \quad b = 3 \ln \omega_g + \frac{1}{2} \ln [(m/2\pi)^3(1/k)], \quad (39)$$

in which if the zero-point energy is called  $E_z$ ,  $U_0 = -L_0 - E_z$  is the static lattice energy and

$$\omega_g = \left( \prod_{i=1}^{3N} \omega_i \right)^{1/3N}$$

is the geometric mean frequency of the lattice vibrational spectrum. The theory may be refined by taking into account anharmonicity: on an Einstein model at moderate temperatures this results in the addition of a term  $cT$  to the right side of Eq. (38). No experimental evidence for the existence of such a term has yet been reported. This is, however, not an argument against the importance of anharmonic effects in rare-gas solids,

<sup>168</sup> L. S. Salter, Trans. Faraday Soc. **59**, 657 (1963).

as Salter has noted, since more sophisticated theories would make clear anharmonic contributions to  $a$  and  $b$ .

The  $\ln$  term in Eq. (38) is usually negligible in comparison with the  $aT^{-1}$  dependence and is customarily omitted from empirical vapor pressure curves for convenience. Recent thermodynamic measurements on solid Ar and Kr (see III.C. Specific Heat) indicate that at higher  $T$  the crystal properties may be influenced by the presence of lattice vacancies. If the Gibbs free energy for creation of such an imperfection is  $g_s$  then the vapor-pressure curve becomes instead of Eq. (38)

$$\ln P = -\frac{1}{2} \ln T + a/T + b - \exp(-g_s/kT). \quad (40)$$

From this improved curve and accurate vapor-pressure measurements on Ar and Kr, Salter finds

	$U_0$ (cal/mole)	$\omega_0$ (sec <sup>-1</sup> )	$E_z$ (cal/mole)
Ar	-1991±16	(6.99±0.15)×10 <sup>12</sup>	185±26
Kr	-2747±18	(5.14±0.21)×10 <sup>12</sup>	146±28.

These theoretical values of  $\omega_0$  and  $E_z$  are in good agreement with independent determinations.

Vapor pressures for the rare-gas solids have been experimentally determined over broad ranges of pressure and temperature although much of interest at the lower  $P$  and  $T$  remains to be done. The experimental techniques need not be described in any detail here, the central experimental problems have been: measuring low pressures and low temperatures accurately on standardized scales, controlling the temperature, and in dynamic experiments, the slow temperature rise over the whole volume of solid and vapor so that measurements at equilibrium can be made, and obtaining sufficiently pure samples. Smoothed data and references to the earlier literature on sublimation pressures for rare-gas solids and vapor pressures for the liquids including helium have been well tabulated.<sup>8</sup> In the region of  $P$  and  $T$  below present experiments, approximate vapor-pressure curves have been given by Honig and Hook<sup>169</sup> who fitted high temperature sublimation pressure data to equations of the form

$$\log_{10} P = AT^{-1} + B \log_{10} T + CT + DT^2 + E,$$

in which  $A$ ,  $B$ ,  $C$ ,  $D$ , and  $E$  are constant for each substance, and extrapolated down to very low  $P$  (10<sup>-13</sup> mm). Although their data in some cases were over narrow regions the equation is a reasonable one and their estimations are the only ones in this region. Some of their results are shown on Table V.

*Argon* The vapor pressure of solid Ar from about (66°K, 24.7 mm) to the triple point has been determined most recently in a thorough investigation of

<sup>169</sup> R. E. Honig and H. O. Hook, RCA Rev. **21**, 360 (1960).

TABLE V. Vapor pressures and temperatures of rare-gas solids for low ( $P$ ,  $T$ ). These results have been obtained (Honig and Hook, Ref. 169) by extrapolation of experimental sublimation pressures for Ne from 15°–45°K, for Ar from 82°–88°K, for Kr from 63°–121°K, and for Xe from 110°–166°K. Errors in  $T$  increase at lower  $P$  but are probably never worse than ±1°K.

Pressure	Ne	Ar	Kr	Xe
10 mm	18.45°K	62.5°K	85.9°K	118.5°K
10 <sup>-1</sup>	13.85	48.2	66.3	91.5
10 <sup>-3</sup>	11.05	39.2	53.9	74.4
10 <sup>-6</sup>	8.48	30.6	42.2	58.2
10 <sup>-9</sup>	6.88	25.2	34.6	47.7
10 <sup>-13</sup>	5.50	20.3	27.9	38.5

thermodynamic properties of Ar by Flubacher *et al.*<sup>170,171</sup> Over the measured range the vapor pressure of the solid was fitted to the equation

$$\log_{10} P(\text{mm}) = A - B/T \quad (41)$$

with constants  $A = 7.65590$ ,  $B = 414.272$  to about 0.05 mm. Pressure was measured on a differential mercury manometer, the general rule for these experiments, and temperature was measured on a Pt resistance thermometer. Freeman and Halsey<sup>172,173</sup> using the same general technique fitted a curve of the form Eq. (41) to their data between 82°K and the t.p. in good agreement with other data. The vapor pressure results of simultaneous independent experiments from groups in England and Holland on solid Ar between 70°K and the t.p. have been reported by Clark *et al.*<sup>174</sup> Results of all these investigations are shown on Fig. 17 and they are all in good agreement.

Some earlier work reflects difficulties in obtaining pure samples. Born<sup>175,176</sup> for example, measured the sublimation pressure of Ar from 65°K to the t.p. but his pressures are consistently lower than modern pressures for  $T \gtrsim 72^\circ\text{K}$  and higher for temperatures below this, apparently the result of oxygen impurities. The most important impurities in modern rare-gas samples are other rare gases.

*Krypton* The vapor pressure of solid Kr from about (83°K, 6.1 mm) to the triple point has been determined by Beaumont *et al.*<sup>99</sup> in a thorough investigation of thermodynamic properties of Kr, a continuation of the Ar study by Flubacher *et al.*<sup>170,171</sup> A least-squares fit to their data to approximately 0.05 mm is given by Eq.

<sup>170</sup> P. Flubacher, A. J. Leadbetter, and J. A. Morrison, Proc. Seventh Intl. Conf. Low Temp. Phys., Toronto, Canada, 1960, pp. 695–7.

<sup>171</sup> P. Flubacher, A. J. Leadbetter, and J. A. Morrison, Proc. Phys. Soc. (London) **78**, 1449 (1961).

<sup>172</sup> M. P. Freeman, Ph.D. thesis, University of Washington, 1956, pp. 103–6.

<sup>173</sup> M. P. Freeman and G. D. Halsey, Jr., J. Phys. Chem. **60**, 1119 (1956).

<sup>174</sup> A. M. Clark, F. Din, J. Robb, A. Michels, T. Wassenaar, and Th. Zwietering, Physica **17**, 876 (1951).

<sup>175</sup> F. Born, Ann. Physik **69**, 473 (1922).

<sup>176</sup> T. Batuecas and E. Garcia-Rodeja, Anales Real Soc. Españ. Fis. y Quím. (Madrid) **52B**, 485 (1956).

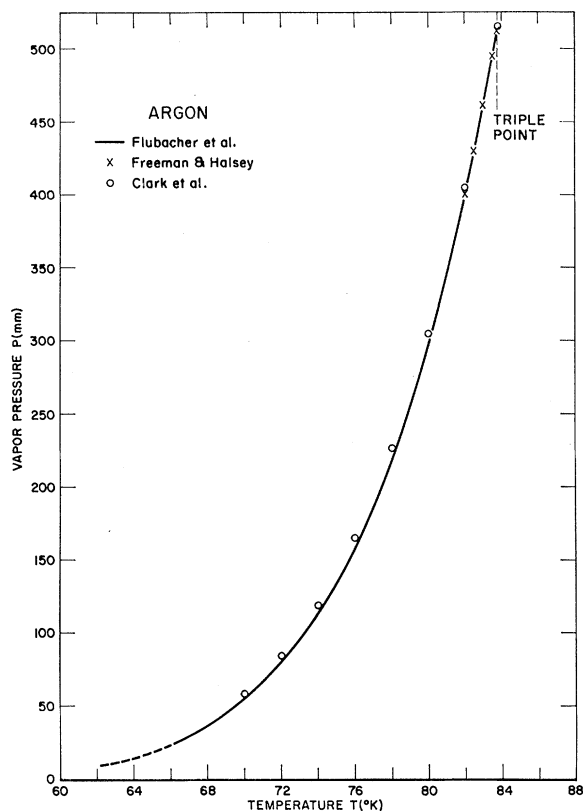


FIG. 17. Vapor pressure of solid Ar as function of temperature. The solid curve is drawn from the equation  $\log_{10} P (\text{mm}) = A - B/T$  with  $A$  and  $B$  experimentally determined by Flubacher *et al.* (Ref. 171). The dotted curve is part of the extrapolation of Honig and Hook (Ref. 169). For lower  $P$  and  $T$  see Table V.

(41) with  $A=7.0741$ ,  $B=575.267$ . Part of this same region has also been covered, with reasonable agreement, in work of Freeman and Halsey<sup>172,173</sup> between about 87°K and the t.p. on studies of Kr-Xe solid solutions. The constants found over this narrow range for Eq. (41) are however, somewhat larger than those of Beaumont *et al.* In the lower temperature region 63°–80°K sublimation pressure measurements have been reported by Fisher and McMillan<sup>177</sup> whose experimental results below 70°K differ significantly from the theoretically expected curve, probably due to trace quantities of nitrogen impurities. Selected data of all the above work have been plotted on Fig. 18 and connected with a smooth curve. In the region below 70°K the dashed curve follows theoretically corrected data.<sup>177</sup>

Ramsay and Travers, the discoverers (1898) of Kr, Ne, and Xe,<sup>178</sup> reported low-temperature vapor-pressure data only three years later<sup>179</sup> on Ar, Kr, and Xe. Their

<sup>177</sup> B. B. Fisher and W. G. McMillan, *J. Phys. Chem.* **62**, 494 (1958).

<sup>178</sup> Ar was discovered in 1895 by Rayleigh and Ramsay.

<sup>179</sup> W. Ramsay and M. W. Travers, *Phil. Trans. Roy. Soc. (London)* **A197**, 47 (1901), W. Ramsay and M. W. Travers, *Z. Physik. Chem.* **38**, 641 (1901).

results for Kr solid extended from about 84°K almost up to the t.p. and fall gratifyingly near modern determinations.

Xenon Freeman and Halsey<sup>172,173</sup> have measured the vapor pressure of solid Xe from 110°K to the triple point and fitted their data to Eq. (41) with  $A=7.371$ ,  $B=799.1$ . Recently Podgurski and Davis<sup>180</sup> have reported vapor-pressure data on Xe between 83°–90°K and have extrapolated an equation of the form (41) down to 70°K. In this region the data show a scatter of about 2% and were corrected for thermal transpiration and other related effects. The region between 90° and 110°K has not been well covered except for the measurements of Peters and Weil<sup>181</sup> which are not in good agreement with data of others in overlapping regions. On Fig. 18 some of the data of Peters and Weil have been plotted along with vapor pressures calculated from Eq. (41) with appropriate constants.<sup>173,180</sup>

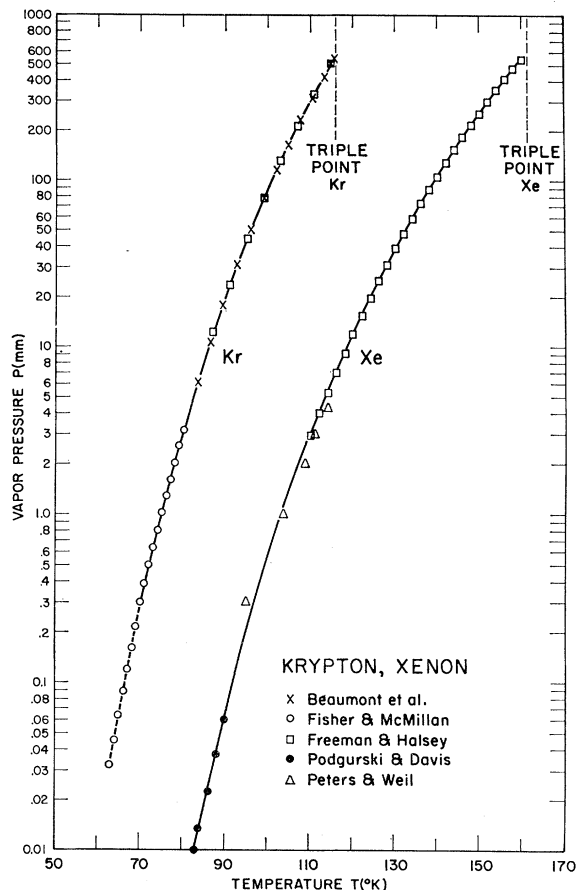


FIG. 18. Vapor pressures of solid Kr and Xe as functions of temperature.

<sup>180</sup> H. H. Podgurski and F. N. Davis, *J. Phys. Chem.* **65**, 1343 (1961).

<sup>181</sup> K. Peters and K. Weil, *Z. Physik. Chem. (Leipzig)* **148A**, 27 (1930).

*Neon* The vapor pressures of solid  $^n\text{Ne}$  and its principal isotopes  $^{20}\text{Ne}$  and  $^{22}\text{Ne}$  from about 16.4°K to the triple point have been determined in a recent thorough investigation of isotopic effects on vapor pressure by Bigeleisen and Roth.<sup>182,183</sup> In these experiments the vapor pressure of  $^n\text{Ne}$  and also the vapor pressure difference between solids enriched, respectively, with  $^{20}\text{Ne}$  and  $^{22}\text{Ne}$  are measured directly. The vapor pressures of pure  $^{20}\text{Ne}$  and  $^{22}\text{Ne}$  are calculated from the data by Raoult's law for solid solutions. On Fig. 19 representative data for  $^n\text{Ne}$  and  $^{22}\text{Ne}$  are shown. On this scale the data for  $^{20}\text{Ne}$  fall indistinguishably close to the  $^n\text{Ne}$  curve.

Measurements from 20.3°K to the t.p. on  $^n\text{Ne}$  in good agreement with these have been reported by Grilly,<sup>184</sup> and nearer the t.p. by Henning and Otto.<sup>185</sup> For the range of his data, Grilly gives the sublimation pressure curve:  $\log_{10} P(\text{mm}) = 6.89224 - 110.809T^{-1} + 5.4348 \times 10^{-3}T$ . Long standing vapor-pressure measurements of Crommelin and Gibson<sup>186</sup> and Keesom and Haantjes<sup>187</sup> from about 15°K to the t.p. are in satisfactory agreement with extrapolated modern values. Representative data of all these workers have been plotted on Fig. 19 and connected with a smooth curve.

The only reported vapor pressure measurements for Rn are those of Gray and Ramsay,<sup>188</sup> from the triple point to the critical point.

As already noted, a sensitive test of solid state theories is calculation and comparison with experiment of differences in properties of isotopic solids; this is especially powerful for the monatomic solids we are discussing here. For the solid (and liquid) the vapor-pressure ratio of two isotopes, most commonly  $^{20}\text{Ne}$  and  $^{22}\text{Ne}$ , can be measured as a function of  $T$ , extreme care being necessary to assure that the slowly attained equilibrium associated with isotopic diffusion through low-temperature solids obtains. The isotopic vapor-pressure difference, which is associated with differences in zero-point energy, is especially large for such light molecules.

Early measurements of the ratio were made by Keesom and Haantjes.<sup>189</sup> Since pure isotopic solids are very difficult to prepare, suitably enriched isotopic mixtures were used, corrections being made from the theory of ideal solutions. The vapor pressure at constant temperature was found to vary linearly, with negative slope, with the average atomic weight of the isotopic mixture. More accurate measurements of the vapor-pressure ratio of these two Ne isotopes between 16°–30°K have been recently reported by Bigeleisen and Roth<sup>182,183</sup>

<sup>182</sup> E. G. Roth and J. Bigeleisen, *J. Chem. Phys.* **32**, 612 (1960).

<sup>183</sup> J. Bigeleisen and E. Roth, *J. Chem. Phys.* **35**, 68 (1961).

<sup>184</sup> E. R. Grilly, *Cryogenics* **2**, 1 (1962).

<sup>185</sup> F. Henning and J. Otto, *Physik. Z.* **37**, 633 (1936).

<sup>186</sup> C. A. Crommelin and R. O. Gibson, *Commun. Kamerlingh Onnes Lab. Univ. Leiden* **17**, 185b (1927).

<sup>187</sup> W. H. Keesom and J. Haantjes, *Physica* **2**, 460 (1935).

<sup>188</sup> R. W. Gray and W. Ramsay, *J. Chem. Soc.* **95**, 1073 (1909).

<sup>189</sup> W. H. Keesom and J. Haantjes, *Physica* **2**, 986 (1935).

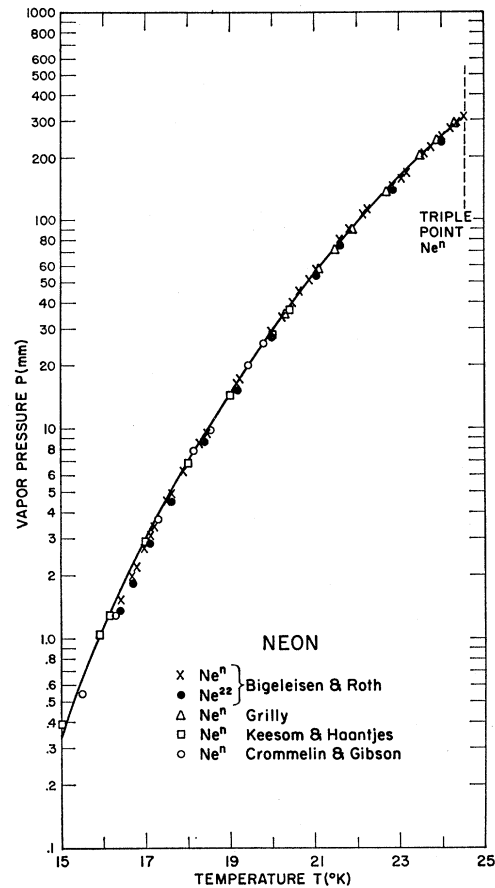


FIG. 19. Vapor pressures of solid normal Ne and  $^{22}\text{Ne}$  as functions of temperature. The solid curve is the vapor pressure of  $^n\text{Ne}$ ; blackened circles represent the data on  $^{22}\text{Ne}$ . Bigeleisen and Roth (Ref. 183) have also determined the vapor pressure of  $^{20}\text{Ne}$ ; on the scale shown this data cannot be distinguished from the  $^n\text{Ne}$  curve.

in substantial agreement with the earlier work, and a steady-state flow method has been used to measure the vapor-pressure ratio between 72°K and the t.p. of  $^{36}\text{Ar}$  and  $^{40}\text{Ar}$  by Boato *et al.*<sup>190</sup> Clusius, Schleich, *et al.*<sup>191</sup> have recently reported experimentally determined t.p. pressures and temperatures for these two Ar isotopes (footnote h of Table II).

The theoretical and experimental situation has been discussed in a recent review on vapor pressures of isotopic molecules.<sup>192</sup> All of the data is in reasonable agreement with the long-standing equation, in which the primed and unprimed quantities represent the two isotopes

$$\ln (P'/P) = (3/40T^2) (\Theta_D'^2 - \Theta_D^2) + \dots \quad (42)$$

<sup>190</sup> G. Boato, G. Scoles, and M. E. Vallauri, *Nuovo Cimento* **23**, 1041 (1962).

<sup>191</sup> K. Clusius, K. Schleich, F. Endtinger, R. Bernstein, and M. Vogelmann, *J. Chim. Phys.* **60**, 66 (1963).

<sup>192</sup> J. Bigeleisen, *J. Chim. Phys.* **60**, 35 (1963).

derived in the limit of a harmonic Debye lattice in equilibrium with an ideal vapor. Johns<sup>193</sup> has derived a somewhat different relation

$$\ln (P'/P) = \frac{3}{2} \ln (M'/M) + (f' - f)/kT, \quad (43)$$

where  $f'$  and  $f$  are the free energies per mole of the isotopes, by considering an Einstein lattice and taking account of anharmonicity. His calculations were applied to the Ne data of Keesom and Haantjes assuming a (6, 14) potential and are in improved agreement with experiment. The  $\Theta_D$  values derived from Eq. (42) are in general not as accurate as those derived from other thermodynamic data owing to the model approximations. An improved expression<sup>192</sup> for  $\ln (P'/P)$  taking account of nonideality in the vapor gives better fit to experimental data although anharmonicity in the lattice vibrations still precludes accurate  $\Theta_D$  determinations.

Casanova *et al.*<sup>194</sup> have examined Eq. (43) and found that varying potential and potential parameters does not further improve agreement of  $\ln (P'/P)$  with the data on Ne and Ar. The principal theoretical difficulties are connected with taking due account of both anharmonicity and coupling among molecules. Calculated isotopic vapor-pressure ratios for the systems  $^{78}\text{Kr} - ^{86}\text{Kr}$  and  $^{128}\text{Xe} - ^{136}\text{Xe}$  were obtained from application of the quantum mechanical law of corresponding states. No sublimation pressure experiments on either of these isotopes have yet been reported, although relative differences in vapor pressure of the two systems  $^{82}\text{Kr} - ^{86}\text{Kr}$  and  $^{130}\text{Xe} - ^{136}\text{Xe}$  have been measured<sup>195</sup> at the respective boiling points and found to be in qualitative agreement with the quantum-mechanical law of corresponding states.

Vapor-pressure curves of rare-gas liquids from the triple points to the critical points follow the expectations of the law of corresponding states. For Ar, Kr, and Xe, a single equation in the reduced variables describes the curves excellently<sup>196</sup> and the vapor pressure of Ne deviates from this universal curve in the manner expected due to quantum effects. In view of the closeness of microscopic structure between the liquid and solid states of rare gases near the triple point, universal sublimation-pressure curves may be expected to obtain for a short distance below the triple point.

### 3. Thermal Conductivity

The theory of thermal-energy conduction in solids at low temperatures has been the subject of much sophisticated development,<sup>197,198</sup> review,<sup>199</sup> and discussion. It is only recently, however, that experimental data have

<sup>193</sup> T. F. Johns, *Phil. Mag.* **3**, 229 (1958).

<sup>194</sup> G. Casanova, R. Fieschi, and N. Terzi, *Nuovo Cimento* **18**, 837 (1960).

<sup>195</sup> V. N. Grigoryev, *Ukrayin. Fiz. Zh. (U.S.S.R.)* **7**, 739 (1962).

<sup>196</sup> C. E. Hamrin and G. Thodos, *J. Chem. Phys.* **35**, 899 (1961).

<sup>197</sup> R. Peierls, *Ann. Physik* **395**, 1055 (1929).

<sup>198</sup> G. Leibfried and E. Schlömann, *Nachr. Akad. Wiss. Göttingen* **2a**, 71 (1954).

<sup>199</sup> P. Carruthers, *Rev. Mod. Phys.* **33**, 92 (1961).

become available on thermal conductivity ( $\lambda$ ) for rare-gas solids. We here discuss very briefly some of the salient points of the theory first, and then in more detail, applications to the experiments on rare-gas solids. Some recent extensions of the law of corresponding states are used to give the thermal conductivity for Xe approximately; no experimental data are available for Xe. Thermal conductivity of rare-gas solids has been discussed by Dobbs and Jones<sup>1</sup> who, although handicapped by the absence of data, except for Ar, anticipated the application of the law of corresponding states, and also by Hollis Hallett<sup>8</sup> who gives the experimental results clearly.

In metals heat may be conducted by both electrons (at room temperatures a large contribution) and phonons (at room temperatures a smaller contribution) and it is also necessary to consider several kinds of interactions among these. In dielectric solids the problem is somewhat simpler. In the absence of free electrons, thermal energy in the solid can only go into the normal lattice vibrations, i.e., only phonons carry the energy. In the harmonic approximation, i.e., the potential energy of a molecule displaced from its equilibrium lattice position is quadratic in the displacement, all higher order terms being negligible, no energy transfer among the lattice modes is possible and thus no thermal equilibrium can be attained. This means that there is no interaction between phonons, and thermal energy is carried at approximately the speed of sound through the crystal. Under these conditions neither temperature gradients nor even temperature in the usual sense can be spoken of.

Proper qualitative account of the role of coupling among the lattice modes due to anharmonicity in giving a finite thermal conductivity for all real solids was given by Peierls,<sup>197</sup> who showed that for high  $T$  the finite  $\lambda$  comes from Umklapp processes. These are three-phonon interactions in which the difference between the propagation vectors of the incoming phonons (or phonon) and that of the resultant phonon (or phonons) is proportional to a vector in the reciprocal lattice. For  $T \gg \Theta_D$  this mechanism gives  $\lambda \propto T^{-1}$ , a result which had been given earlier by Debye. This law is in good agreement with experiment and indeed the proportionality extends for rare-gas solids down to much lower  $T$  than expected ( $T \approx \Theta_D/3$  for Ar). As  $T$  is lowered further, fewer phonons are available with sufficiently high energies to effect Umklapp and  $\lambda$  in a perfect crystal rises, becoming proportional to  $T^{-\nu} \exp(\Theta_D/2T)$ ,  $\nu \approx 1$ , if scattering from crystal boundaries may be neglected. The constant of proportionality between  $\lambda$  and  $T^{-1}$  in the region  $T \gg \Theta_D$  has been independently calculated by several workers and the results are generally equivalent. We use here the result of Leibfried and Schlömann,<sup>198</sup>

$$\lambda = 12ma_0k^3\Theta_D^3/5\gamma^2h^3T \quad (44)$$

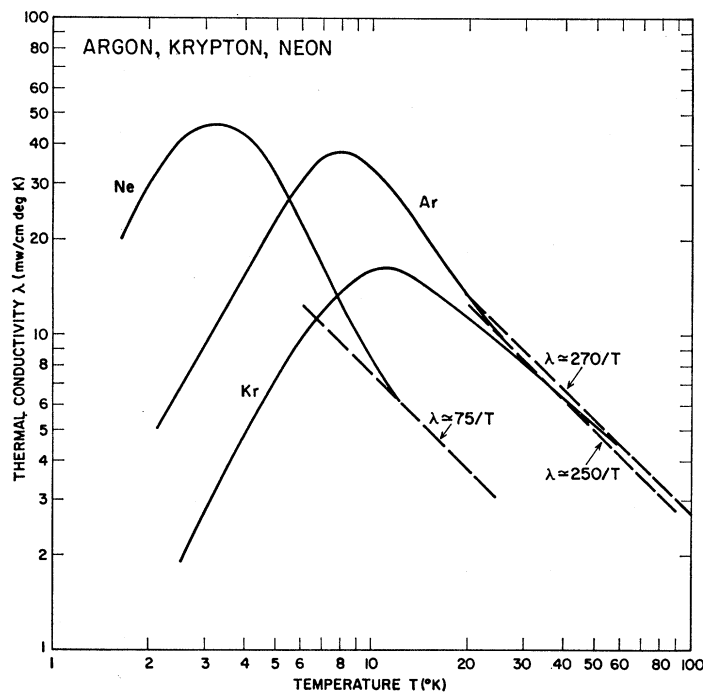


FIG. 20. Experimental thermal conductivities  $\lambda$  of solid Ar, Kr, and Ne, as functions of  $T$ . These curves have been drawn from those of White and Woods (Ref. 200). Data points are here omitted but  $\lambda$  was measured from  $2^\circ\text{K}$  up to near the triple point temperatures for all three substances. To the right of the conductivity maxima  $\lambda$  is limited principally by Umklapp processes, and the high  $T$  behavior  $\lambda = B/T$  is shown in the broken curves. These experimental values of  $B$  are in reasonable agreement with theory (see text). To the left of the maxima  $\lambda \propto T^2$ , characteristic of phonon scattering from dislocations. For Ar below  $10^\circ\text{K}$ ,  $\lambda$  showed large variations for different sources of gas and is therefore to be regarded as approximate.

where  $\gamma$  is Grüneisen's constant and  $m$  is the molecular mass. This equation is derived from an extension to three dimensions of a linear chain with nearest-neighbor central-force interactions.

Thermal conductivities of rare-gas solids have been measured by White and Woods<sup>108,200</sup> who give curves for Ar, Kr, and Ne, from  $2^\circ\text{K}$  to their triple points. A single determination  $\lambda = 2.6 \pm 0.4$  mW/cm  $^\circ\text{K}$  at  $80^\circ\text{K}$  for Ar is due to Lawrence *et al.*<sup>201</sup> The experimental procedures both for forming the polycrystalline solids and for measuring  $\lambda$  are quite different but the results are in agreement. Both experiments measure the temperature gradient  $\nabla T$  associated with a measured

TABLE VI. Thermal conductivity  $\lambda$  of solid-rare gases. The first two columns give the coordinates  $(\lambda, T)$  of the maximum on the  $\lambda(T)$  curve. The third column gives the thermal conductivity for the solid at the triple point. The entries for Ne, Ar, and Kr, have been read from the experimental curves of White and Woods and calculated from the asymptotic form  $\lambda = B/T$  of these curves (see Fig. 20 or Ref. 200). Entries for Xe, for which no experimental data are available, have been calculated from the law of corresponding states.

	$\lambda_{\text{max}}$	$T$	$\lambda(\text{solid})$ at t.p. mW/cm $^\circ\text{K}$
Ne	47 mW/cm $^\circ\text{K}$	3.4 $^\circ\text{K}$	3.1
Ar	38	8.2	3.0
Kr	17	11.5	2.3
Xe	24	16.1	2.0

<sup>200</sup> G. K. White and S. B. Woods, *Phil. Mag.* **3**, 785 (1958).

<sup>201</sup> D. J. Lawrence, A. T. Stewart, and E. W. Guptill, *Can. J. Phys.* **37**, 1069 (1959).

heat flux  $\mathbf{Q}$  and directly apply the equation which defines  $\lambda$ :  $\mathbf{Q} = -\lambda \nabla T$ . The results of White and Woods for Ar, Kr, and Ne, have been combined on Fig. 20 and selected numerical values read from the curves are shown in Table VI.

All three of the curves of Fig. 20 may be seen to terminate at their high  $T$  ends as the dotted lines for which  $\lambda \propto T^{-1}$ , characteristic of Umklapp processes. For Ar this proportionality sets in at about  $25^\circ\text{K}$  ( $\approx 0.31\Theta_D$ ) and  $10$  mW/cm  $^\circ\text{K}$ , for Kr at about  $60^\circ\text{K}$  ( $\approx 0.95\Theta_D$ ) and  $4.5$  mW/cm  $^\circ\text{K}$ , and for Ne at about  $12^\circ\text{K}$  ( $\approx 0.19\Theta_D$ ) and  $6.4$  mW/cm  $^\circ\text{K}$ . If reasonable values are substituted for the constants in Eq. (44) and if it is abbreviated  $\lambda = BT^{-1}$  then Eq. (44) gives theoretically expected values of  $B$ . By comparison with the experimental data then<sup>200</sup>:

$$\text{for Ar: } B_{\text{th}} \approx 464, \quad B_{\text{exp}} \approx 250 \quad \text{mW/cm}$$

$$\text{for Kr: } B_{\text{th}} \approx 509, \quad B_{\text{exp}} \approx 270 \quad \text{mW/cm}$$

$$\text{for Ne: } B_{\text{th}} \approx 98, \quad B_{\text{exp}} \approx 75 \quad \text{mW/cm.}$$

Theoretical values for  $B$  are thus from 30–90% higher than experimental values, Kr is in worst agreement. Considering the experimental and theoretical uncertainties, this general agreement must be regarded for the present as satisfactory. For studying the details of Umklapp processes the rare-gas solids are thus as well suited as alkali halides, for which in formulas like Eq. (44)  $B_{\text{th}}/B_{\text{exp}}$  varies from 1–2.5, and better than diamond, germanium, and silicon, for which the ratio

may be 5 or larger.<sup>202</sup> An important disadvantage of rare-gas solids as noted before, is the difficulty in obtaining good quality, large, single crystals.

As  $T$  decreases further,  $\lambda$  rises faster than  $T^{-1}$  since phonons sufficiently energetic to take part in Umklapp processes become scarcer as noted above; the probability of such processes falls approximately as  $\exp(-\Theta_D/2T)$ , and the phonon mean-free path increases. On Fig. 20 this rise in  $\lambda$  is evident for Ar and Ne although  $\lambda$  is rather smaller than expected. For Kr,  $\lambda$  rises more *slowly* than  $T^{-1}$ . This is apparently the result of a decrease in mean-free path due to phonon scattering from imperfections in the Kr crystals. As the temperature decreases still further, scattering from imperfections in the crystals becomes increasingly important and  $\lambda$  reaches a maximum (see Table VI) and then finally decreases with decreasing  $T$ , falling to zero at 0°K. In these experiments  $\lambda \propto T^2$  below the maximum. The phonon mean-free path  $l$  may be roughly estimated from the formula (derived for an attenuated gas)

$$\lambda = \frac{1}{3} C v l, \quad (45)$$

in which  $C$  is a specific heat per unit volume and  $v$  is approximately the velocity of sound.

For the data shown  $l \approx 10^{-4}$  cm at 2°K. These are surprisingly small mean-free paths even for crystals imperfect as those used here. In general, the poor quality of the crystals especially after the straining attending cooling, as remarked by White and Woods, makes interpretation of the results at low  $T$  extremely difficult. The polycrystalline solids were carefully annealed and growth conditions were varied without changing  $\lambda$ . For Ar from different sources, appreciable spread was found in  $\lambda$ , especially for  $T$  to the left of  $\lambda_{\max}$ .

For  $T < T(\lambda_{\max})$  the increased thermal resistivity is due to scattering from imperfections; for good quality crystals one may from the form of  $\lambda(T)$  (for this region generally  $\lambda \propto T^n$ ) study in principle the nature of the lattice defects and other imperfections present in the solid. The problem of phonon scattering is thoroughly discussed in the recent review of low-temperature thermal conductivity in solids by Carruthers.<sup>199</sup> The effects on  $\lambda$  of several kinds of departures from perfection in the crystal are discussed there, in particular scattering from strain fields due to dislocations ( $\lambda \propto T^2$ ) and point defects (vacancies), scattering due to mass differences in the lattice (isotope effect), and scattering from crystal boundaries. However, much needs to be done experimentally in improving the quality of rare-gas crystals in order for knowledge of their low temperature  $\lambda$  behavior to add to understanding of these processes.

<sup>202</sup> G. K. White, S. B. Woods, and D. K. C. MacDonald, *Annexe Bull. Inst. Intern. Froid* **2**, 91 (1956).

Although no experimental studies of the variation of  $\lambda$  with pressure in the solid-rare gases are available (such studies have however been carried through for He), it is interesting to note that at high  $P$  the outer electrons of rare-gas molecules, especially heavier ones, will be transferred into a conduction band.<sup>203</sup> High electrical conductivities near this region have already been found for Ar. In the presence of conduction electrons thermal conduction in rare-gas solids would involve prototype electron-energy transport and phonon-electron collisions.

A recent electron-spin resonance study<sup>204</sup> on impurities in Ar and Kr matrices at liquid helium temperatures indicates that energy absorbed by the lattice may be transferred to the impurity molecules by migration of electron holes in the rare-gas lattice.

Keyes<sup>205</sup> has made an interesting application of the quantum law of corresponding states to  $\lambda$  for rare-gas solids. He defines a reduced thermal conductivity  $\lambda^*$  as

$$\lambda^* = \lambda / (k/\sigma^2) (\epsilon/m)^{\frac{1}{2}}. \quad (46)$$

If the law is applicable one expects (in the  $\Lambda^* = 0$  limit)  $\lambda^* = \lambda^*(T^*)$  neglecting dependence on  $P^*$ . In the range of the experiments  $P^*$  is small. When the data on Ar, Kr, Ne, and H<sub>2</sub>, are plotted as  $\lambda^*$  vs  $T^*$ , the points in general follow a universal curve remarkably well. At high  $T^*$  ( $T^* \geq 0.3$ ) the behavior of this universal reduced curve is  $\lambda^* \approx 12/T^*$  in accordance with expectations. At  $T^*$  below  $\lambda_{\max}^*$  ( $T^* \leq 0.07$ ), the universal curve behaves as  $\lambda^* \approx 7 \times 10^4 T^{*2}$ , the variation characteristic of phonon scattering from dislocations.

The behavior of  $\lambda^*$  for  $0.07 \leq T^* \leq 0.3$  is also interesting. In this region the data for the different substances separate and the largest values of  $\lambda^*$  occur for the lightest molecules (highest  $\Lambda^*$ ). In this region a more significant energy than  $\epsilon$  may be the minimum energy for phonons to take part in Umklapp processes and it is thus perhaps more reasonable to define a new  $T^*$  in which  $T$  is reduced by division by  $\Theta_D$ , or  $\Lambda^*$ , which is proportional to  $\Theta_D$ . As a test of this hypothesis Keyes plotted  $\lambda^* \Lambda^*$  vs  $T^*/\Lambda^*$  and showed that the data in this region does indeed now fall on a universal curve for which an approximate formula is

$$\lambda^* \Lambda^* \approx 20 [\exp(\Lambda^*/2T^*) - 1]. \quad (47)$$

Notice that the exponential dependence in Eq. (47) suggests that of Peierls. We have used these general principles to calculate  $\lambda$  for Xe and this is shown on Table VI along with some experimental data for the other rare-gas solids.

<sup>203</sup> B. J. Alder, in *Solids Under Pressure*, edited by W. Paul and D. M. Warschauer (McGraw-Hill Book Co., Inc., New York, 1963), pp. 396-8. B. J. Alder and M. Van Thiel, *Phys. Letters* **7**, 317 (1963).

<sup>204</sup> W. V. Bouldin, R. A. Patten, and W. Gordy, *Phys. Rev. Letters* **9**, 98 (1962).

<sup>205</sup> R. W. Keyes, *J. Chem. Phys.* **31**, 452 (1959).

### C. Specific Heat

Morrison and his co-workers<sup>170,171</sup> have recently described an adiabatic calorimeter suitable for accurate measurement of heat capacity and other thermodynamic properties in the difficult region below 10°K and continuously up to room temperature. The major source of uncertainty in the  $T < 10^\circ\text{K}$  region is due to the temperature scale, but in their comprehensive experiments on Ar and Kr the uncertainties in  $C_p$ , the specific heat at constant pressure, are at most 2% and decrease steadily to 0.2% above 20°K. From 20°K to the triple points the uncertainty increases to 0.5%. In Fig. 21 their  $C_p$  results for solid Ar, Flubacher *et al.*,<sup>171</sup> and for solid Kr, Beaumont *et al.*,<sup>99</sup> between about 2°K and the triple points are shown in comparison with some earlier measurements. All reported rare-gas-solid heat capacity experiments measure  $C_{\text{sat}}$ , the specific heat of the solid under its saturated vapor pressure.  $C_{\text{sat}}$  is thermodynamically connected to  $C_p$  by

$$C_p - C_{\text{sat}} = T(\partial V/\partial T)_P(\partial P/\partial T)_{\text{sat}}. \quad (48)$$

The relative difference between  $C_p$  and  $C_{\text{sat}}$  is only about 0.1% and may thus usually be neglected. Heat capacity data on solid Ar between 10°–80°K of Clusius,<sup>24</sup> part of an early study including also Kr, Ne, and later Xe, fall about 2% lower than the modern values for  $T > 25^\circ\text{K}$  and at lower  $T$  are rather more widely scattered. Measurements with estimated uncertainties of 0.5% between 16°–35°K of Figgins *et al.*<sup>206,207</sup> fall within the combined experimental uncertainty.

Heat capacity determinations of solid Kr have also been reported by Clusius *et al.*,<sup>24,208</sup> from 10°K–t.p. and by Eucken and Veith<sup>209</sup> between 10°–80°K. Selected data of these workers are shown on Fig. 21 in comparison with the smoothed curve of the recent work discussed above.<sup>99</sup> As in the case of Ar the earlier data scatter about 4% at  $T \lesssim 20^\circ\text{K}$  but increase in accuracy with increasing  $T$ . The experiments of Clusius are especially distinguished by the techniques he developed for purifying all the rare gases. Present day technology makes available Ar and Kr better than 99.999% pure, Ne and Xe perhaps 99.99% pure, so that for most experiments the impurity effects which were so troublesome to pioneer workers with rare gases are hopefully absent.

Partly owing to these difficulties in purification, the heat capacity of solid Xe over a wide temperature range has been measured apparently only by Clusius and Riccoboni.<sup>210</sup> A smooth curve through their data

<sup>206</sup> E. R. Dobbs, B. F. Figgins, and G. O. Jones, *Suppl. Nuovo Cimento* **9**, 32 (1958).

<sup>207</sup> B. F. Figgins, *Proc. Phys. Soc. (London)* **76**, 732 (1960).

<sup>208</sup> K. Clusius, A. Kruis, and F. Konnertz, *Ann. Physik* **33**, 642 (1938).

<sup>209</sup> A. Eucken and H. Veith, *Z. Physik. Chem.* **B34**, 275 (1936).

<sup>210</sup> K. Clusius and L. Riccoboni, *Z. Physik. Chem.* **B38**, 81 (1937).

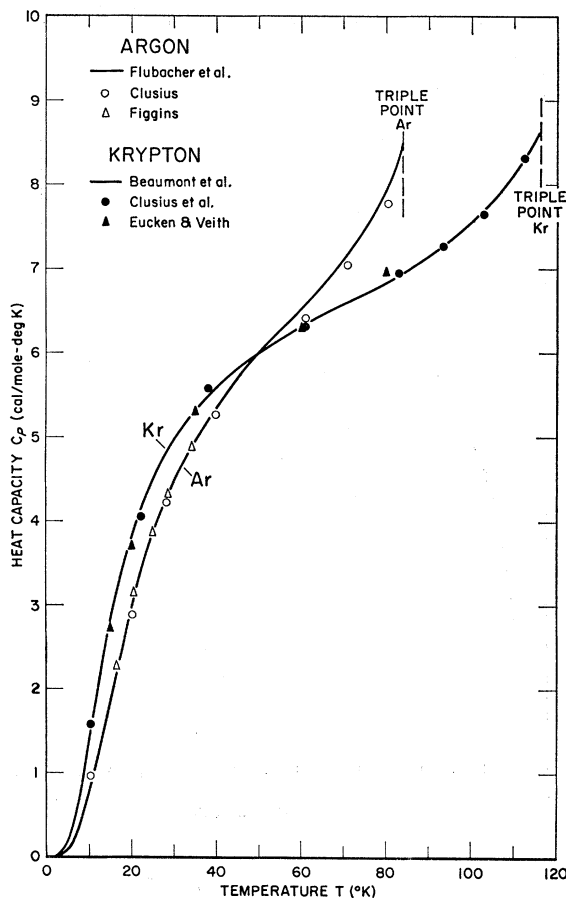


FIG. 21. Experimental heat capacity  $C_p$  or  $C_{\text{sat}}$  (cal/mole deg K) for solid argon and solid krypton as function of temperature. The plotted data are experimentally determined heat capacities at saturated vapor pressure  $C_{\text{sat}}$ .  $C_{\text{sat}}$  differs from  $C_p$  by only about 0.1% or less in the region of the curves. The estimated error in the solid curves is about 2% for lowest temperatures, decreasing to 0.2% for  $T > 20^\circ\text{K}$ , and then increasing for  $T > 60^\circ\text{K}$  to about 0.5% near the triple points (Refs. 99 and 171). The rapid rise of heat capacity near the t.p. which is apparent on both curves is probably the result of lattice vacancies.

for  $C_{\text{sat}}$  (or  $C_p$ ) between 10°K and the triple point is shown in Fig. 22.  $C_v$ , the specific heat at constant volume, may be calculated from  $C_p$  using

$$C_p - C_v = \beta^2 T / \rho \chi_T, \quad (49)$$

where  $\beta$  is the volume coefficient of thermal expansion, and  $\chi_T$  is the isothermal compressibility.  $C_v$  has been calculated from 0°K–t.p. for solid Xe using this equation and the resultant  $C_v(T)$  is shown on Fig. 22. Values of  $\beta$  were taken from Fig. 7, those of  $\rho$  from Fig. 3, and  $\chi_T$  were taken from recent measurements of bulk modulus of solid Xe of Packard and Swenson.<sup>35</sup>

In Fig. 23,  $C_p$  data of Clusius, Flubacher, *et al.*<sup>211</sup> on the two principal Ne isotopes are plotted. Measure-

<sup>211</sup> K. Clusius, P. Flubacher, U. Piesbergen, K. Schleich, and A. Sperandio, *Z. Naturforsch.* **15a**, 1 (1960).

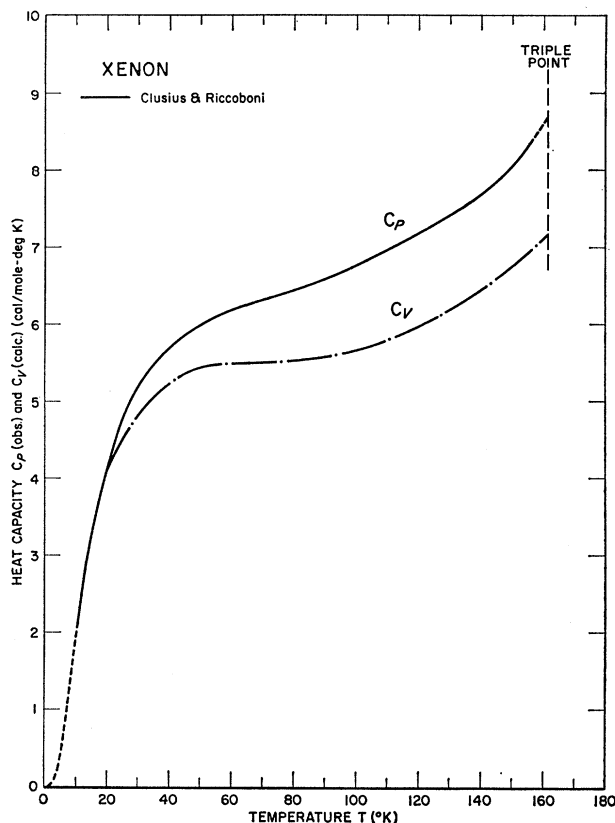


FIG. 22. Experimental heat capacity  $C_p$  or  $C_{\text{sat}}$  (cal/mole deg K) and calculated heat capacity  $C_v$  for solid xenon as function of temperature. The solid curve is drawn through experimental measurements of  $C_{\text{sat}}$  (or  $C_p$ ) between about 10°–157°K of Clusius and Riccoboni (Ref. 210). It has been extrapolated down to 0°K assuming  $\Theta_D = 55^\circ\text{K}$  and up to the triple point.  $C_v$  was calculated from the equation  $C_v = C_p - \beta^2 T / \rho \chi_T$  using experimental data for all quantities on the right hand side of the equation. The rapid rise of observed heat capacity near the t.p. may be the result of lattice vacancies in the solid and is reflected in the calculated  $C_v$ .

ments for  $^{20}\text{Ne}$  extend from 9°K up to the t.p., for this isotope 24.66°K, and measurements for  $^{22}\text{Ne}$  extend from 8°K up to its t.p. 24.84°K. Determinations<sup>24,176,212</sup> of  $C_p$  for pure normal Ne (90.9%  $^{20}\text{Ne}$ , 0.3%  $^{21}\text{Ne}$ , 8.8%  $^{22}\text{Ne}$ ) are very close to those for  $^{20}\text{Ne}$ . An approximate curve of  $C_v$  for  $^{20}\text{Ne}$  has been calculated from

$$C_p - C_v = A C_p^2 T, \quad (50)$$

where  $A$  is a constant determined from Eq. (49) at any fixed temperature as  $A = \beta^2 / \chi_T \rho C_p^2$ . Using values of  $\beta$  and  $\rho$  at 16°K from Figs. 8 and 4 and taking  $\chi_T$  (16°K) to equal the single experimentally determined value  $4.02 \times 10^{-3}$  cm<sup>3</sup>/cal (at 4°K) gives  $A = 2.79 \times 10^{-3}$  mole/cal. The use of Eq. (50) may not be rigorously justified over the whole  $T$  range since it assumes the validity of Grüneisen's rule. A more reliable estimate of  $C_v$  would of course be possible with measurements of  $\chi_T(T)$ .

$C_v$  and  $\Theta_D$  for Ar and Kr have been estimated by Beaumont *et al.*<sup>99</sup> from Eq. (49) and the  $C_p$  data of Fig. 21. The resultant  $\Theta_D(T)$  curves for  $T < 40^\circ\text{K}$  are shown on Fig. 24 and may be profitably compared. Above 40°K, estimated  $(C_p - C_v)$  values approach 10% of experimental  $C_p$ 's and are thus uncertain. In addition

$C_p(T)$  data show the effects of lattice vacancy formation, i.e., an unexpectedly rapidly rising  $C_p$ . This is especially pronounced near the t.p. for Ar and Kr (Fig. 21) and also is apparent for Xe (Fig. 22). In Fig. 22, for which the  $C_v$  curve has been calculated from the  $C_p$  data right up to the t.p., the rise in  $C_p$  due to vacancy formation is reflected in  $C_v$ . Vacancy effects, which have also been observed in vapor pressure experiments as already remarked, represent nonvibrational contributions to thermodynamic properties and must be theoretically accounted for by special methods. We discuss some of these briefly later in this section.

The  $\Theta_D$  curves for Ar and Kr are in remarkably good agreement with those calculated by Leighton<sup>213,1</sup> from the frequency spectrum.  $\Theta_D$  (Kr) shows a sharper minimum in the region of about 8°K than  $\Theta_D$  (Ar) and at higher  $T$  it rises more slowly. Since the zero-point energy for Ar is a larger fraction of lattice energy than for Kr these differences may be interpreted as the result of anharmonicity.<sup>99</sup> Notice that at least for  $T \lesssim 40^\circ\text{K}$  anharmonicity decreases  $C_v$  but the effect of lattice vacancies above 40°K is to increase  $C_p$ . It is to be emphasized, however, that independent calculations<sup>131</sup> indicate that anharmonicity increases  $C_p$ . This question has not been satisfactorily resolved.

<sup>212</sup> K. Clusius, Z. Physik. Chem. **B4**, 1 (1929).

<sup>213</sup> R. B. Leighton, Rev. Mod. Phys. **20**, 165 (1948).

In their recent work, Horton and Leech<sup>131</sup> systematically calculated  $C_v(T)$ ,  $\Theta_D(T)$ , and Grüneisen constants for Ne, Ar, Kr, and Xe for  $T \leq \Theta_D/2$  in the harmonic approximation as functions of: the repulsive exponent  $n$  and potential parameters  $\epsilon$  and  $r_0$  in Eq. (16), and the number of interacting neighbors. Some of their general conclusions are: (a) Calculated  $\Theta_D$ 's for Ne show greater sensitivity to variation of the number of interacting neighbors than  $\Theta_D$ 's for the heavier rare-gas solids but are less sensitive to variation of  $n$ . (b) The inclusion of interactions with atoms

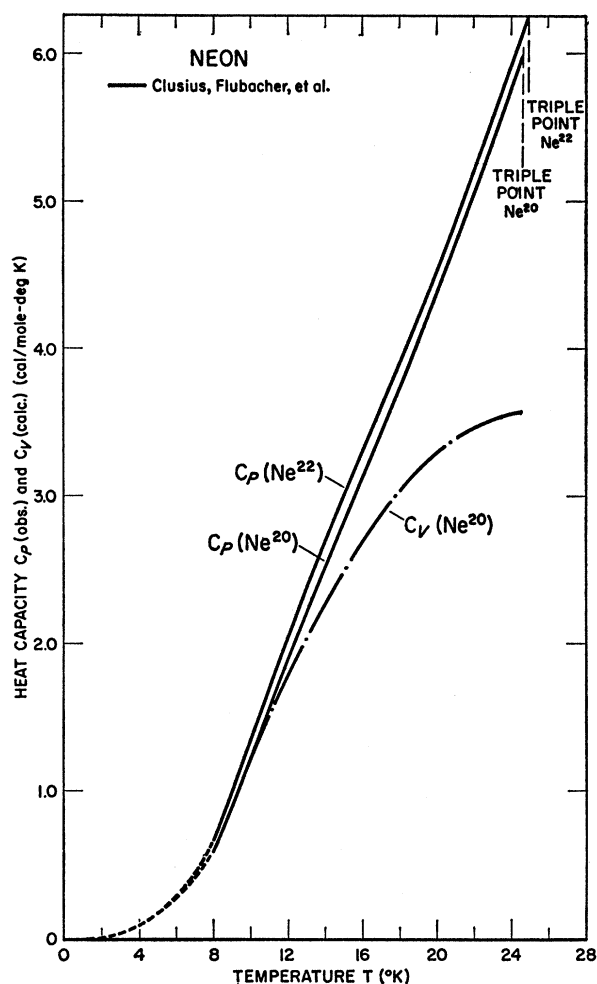


FIG. 23. Experimental heat capacity  $C_p$  or  $C_{sat}$  (cal/mole deg K) for solid neon 20 and neon 22 and calculated  $C_v$  for solid neon 20, all as functions of temperature. The solid curves are drawn through experimental measurements of  $C_{sat}$  (or  $C_p$ ), between about 8°K and the triple points, of Clusius, Flubacher, Piesbergen, Schleich, and Sperandio (Ref. 211). The t.p. for  $^{20}\text{Ne}$  has ( $P, T$ ) coordinates (325.10 mm, 24.66°K) and those of  $^{22}\text{Ne}$  are (327.73 mm, 24.84°K). The solid curves have been extrapolated to 0°K assuming  $\Theta_D(^{20}\text{Ne}) = 66.7^\circ\text{K}$  and  $\Theta_D(^{22}\text{Ne}) = 65.2^\circ\text{K}$ .  $C_v$  has been calculated approximately for  $^{20}\text{Ne}$  from  $C_v = C_p - \beta^2 T / \rho \chi T$  and  $C_v = C_p - A C_p^2 T$  ( $A$  const), using available experimental data. The heat capacities for normal Ne are very close to  $C_p$  and  $C_v$  for  $^{20}\text{Ne}$ .

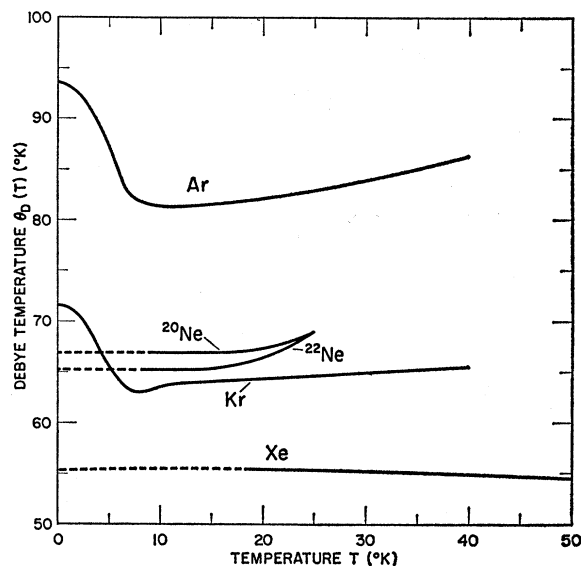


FIG. 24. Debye temperature  $\Theta_D$  (°K) for Ar, Kr, Xe,  $^{20}\text{Ne}$ , and  $^{22}\text{Ne}$ , as functions of temperature. References for the curves are: Ar and Kr (Ref. 99), Xe (Ref. 35),  $^{20}\text{Ne}$  and  $^{22}\text{Ne}$  (Ref. 211). All of these  $\Theta_D(T)$  are derived from heat capacity measurements and therefore refer to a temperature dependent molar volume.

beyond the first- and second-nearest neighbors gives an appreciable contribution to calculated  $\Theta_D$ 's, becoming more important with increasing  $T$ . (c) Increasing  $n$  raises  $\Theta_D(T)$  but does not change the shape of  $\Theta_D(T)$ . The results of this calculation for Ar and Kr do not in general agree very well with the specific heat data of Fig. 21 and the  $\Theta_D(T)$  curves of Fig. 24 except at very low  $T$ . The source of the disagreement is apparently the combined result of exaggeration to the effect of distant neighbors given by Eq. (16) and the neglect of anharmonicity.

Shown on Fig. 24 is  $\Theta_D(\text{Xe})$  as estimated by Packard and Swenson<sup>35</sup> from earlier entropy data<sup>210</sup> and extrapolated from 20°–0°K. The characteristic sharp drop of about 15% in  $\Theta_D$  with increasing  $T$  just above 0°K, derived for the basic case of central forces between nearest neighbors in an fcc lattice<sup>213</sup> is not evident in the extrapolated Xe curve although apparent for both Ar and Kr. From theoretical considerations<sup>35,131</sup> and analogy with  $\Theta_D(\text{Ar})$  and  $\Theta_D(\text{Kr})$  behavior,  $\Theta_D(\text{Xe})$  near 0°K is expected to be about 65°K. Debye temperatures for  $^{20}\text{Ne}$  and  $^{22}\text{Ne}$  from the heat capacity data of Clusius, Flubacher, *et al.*<sup>211</sup> are also shown in Fig. 24. Since the measurements extend only down to about 8°K any behavior of  $\Theta_D$  below this disappears in the extrapolation. Anharmonic effects in this region are expected to be most pronounced for Ne and its isotopes since the ratios of zero-point energy to static-lattice energy are higher than for any other rare-gas solids. The zero-point energy for Ne may be considered to cause melting in the lattice at a temperature so low that  $C_p$  for the solid

shows no tendency to level out at the t.p. (Fig. 23). This is in marked contrast to  $C_p$  curves for the other rare-gas solids (Figs. 21 and 22). Classically, in the approximation of a harmonic lattice with no vacancies,  $C_v \rightarrow 3R$  at temperatures above  $\Theta_D$ . This is the cause of the decreasing slope in  $C_v$  for Xe on Fig. 22. The apparent leveling off of  $C_v$  for  $^{20}\text{Ne}$  (Fig. 23), however, is probably spurious, the result of approximations in computing  $C_v$ .

Many theoretical aspects of thermodynamics of rare-gas solids have been thoroughly discussed by Dobbs and Jones<sup>1</sup> and most recently by Horton and Leech.<sup>131</sup> We here restrict ourselves to brief discussion of the effects of vacancies and anharmonicity on thermodynamic properties.

### 1. Vacancy Effects

In thermal equilibrium the number  $n$  of vacancies in a crystal of  $N$  atoms is<sup>214</sup>

$$n = N \exp(-g_s/kT), \quad (51)$$

in which  $g_s = h - Ts$  is the Gibbs free energy for creation of a single vacancy;  $h$  and  $s$  are, respectively, the enthalpy and the entropy for a vacancy. The effect of  $n$  vacancies on the observed  $C_p$  is an increase

$$\Delta C_p = (\partial nh / \partial T)_P = nh^2/kT^2. \quad (52)$$

The second equality holds at higher  $T$  where  $h$  and  $s$  are independent of  $T$ . Beaumont *et al.*<sup>99</sup> have estimated  $\Delta C_p$  for Ar and Kr by extrapolating their  $C_p$  data near the t.p. (Fig. 21) and obtain for vacancies in Ar between 45°–83°K,  $h = 1280$  cal/mole of vacancies, and for Kr between 60°–115°K,  $h = 1770$  cal/mole vac., to within about 10% in both cases. The corresponding experimental estimates for the number of vacancies are

$$n/N (\text{Ar}) = (30 \pm 20) \exp(-1280/RT)$$

and

$$n/N (\text{Kr}) = (30 \pm 20) \exp(-1770/RT).$$

Near the triple points these give vacancy concentrations of about 1.5% in the solids. Evidence for vacancy formation in experimental vapor pressure data has been discussed by Salter.<sup>168</sup>

Kanzaki<sup>145</sup> has analyzed the general problem of point defects in a static (0°K) fcc lattice and presents a formalism for calculating the displacement field  $\xi_i(\mathbf{r})$  of the molecules in the relaxed lattice around the point defect, and the associated lattice energy and volume changes. This technique has been extended by Nardelli and Chiarotti<sup>215</sup> to vacancies in a vibrating lattice

( $T > 0^\circ\text{K}$ ), in particular to Ar between 0°–80°K assuming an Einstein model with two-body (6, 12) central-potential interaction. At  $T \lesssim 60^\circ\text{K}$  the displacement field oscillates in sign, e.g., at 0°K, at which the theoretical concentration of vacancies is  $2 \times 10^{-22}$ , the nearest neighbors are displaced inward toward the vacancy by  $|\xi| \approx 0.02 \text{ \AA}$  but the second-nearest neighbors are displaced outward by  $|\xi| \approx 0.01 \text{ \AA}$ . At higher  $T$  the displacements are all outward although still oscillatory, at 80°K for which on this model the vacancy concentration is  $5 \times 10^{-5}$ , for the nearest neighbors  $|\xi| \approx 0.01 \text{ \AA}$ , for second-nearest neighbors  $|\xi| \approx 0.02 \text{ \AA}$ , and for third-nearest neighbors  $|\xi| \approx 0.004 \text{ \AA}$ . The calculated changes of volume in the lattice due to a vacancy are small, at 0°K,  $\Delta v = -0.007a_0^3$ , and at 80°K,  $\Delta v = +0.005a_0^3$  where  $a_0$  is the temperature-dependent lattice parameter. The volume of the absent molecule is much larger in contrast, i.e.  $a_0^3/4$ . From these considerations the free energy  $f_s$  to create a vacancy in Ar was calculated for  $T$  from 0°–80°K. In the high  $T$  region the result<sup>214, 215</sup> is  $f_s$  (cal/mole vac.) =  $2540 - 6RT$  so that the theoretically predicted value at the Ar t.p. temperature is 1540 cal/mole vac., about 20% larger than the experimentally reported  $f_s$ . The discrepancy is considerably larger (70%) if a recently improved experimental estimate taken from Morrison's  $C_p$  data is used,<sup>214</sup> i.e.,  $f_s = 1820 - 5.5 RT$  for Ar (900 cal/mole vac. at t.p. for Ar).

Difficulties in properly accounting for the observed thermodynamic effects of vacancies in solid Ar with a two-body potential and the necessity of considering many body forces in the theory have been pointed up by Foreman and Lidiard<sup>214</sup> with their calculation of  $C_v$  using an anharmonic Einstein lattice and a (6, 12) potential. The results may be compared with a  $C_v$  taken from experimental  $C_p$  data, corresponding thermal expansivity and compressibility data, and Eq. (49), as has been done on Fig. 22 for Xe. This calculation gives good agreement with the measured  $C_v$  from 40°–60°K but above this a  $\Delta C_v$  due to vacancy formation becomes increasingly important:

$$\Delta C_v = \frac{n}{kT^2} \left( h - \frac{\beta_0 v T}{\chi r_0} \right) \left( h - \frac{\beta v T}{\chi r} \right), \quad (53)$$

where  $v$  is the free volume of vacancy formation and the subscript zero refers to the vacancy-free solid. Values for  $f_s$  obtained in this way are in well-defined disagreement with experiment by about 25%.

Jansen<sup>216</sup> has extended earlier work by calculating the corrected energy of vacancies in solid Ar using the short range three-body exchange forces described earlier<sup>66</sup> (see I.C) In the static lattice the energy of a vacancy is reduced when these forces are taken into account so that at 0°K the ratio of vacancy energy to total cohesive energy is about 0.7 whereas if pair po-

<sup>214</sup> A. J. E. Foreman and A. B. Lidiard, *Phil. Mag.* **8**, 97 (1963).

<sup>215</sup> G. F. Nardelli and A. Repanai Chiarotti, *Nuovo Cimento* **18**, 1053 (1960).

<sup>216</sup> L. Jansen, *Phil. Mag.* **8**, 1305 (1963).

tentials only were considered the ratio would be about one. Since the earlier two-body interaction calculations<sup>215</sup> showed very little lattice relaxation the energy of vacancy formation for them may be taken as the cohesive energy. The ratio at 0°K of this (pair) cohesive energy to the (three-body) vacancy formation energy is 1.9. These corrections are of the right sign and of about the right magnitude so that they may be expected to explain the differences between experimental and theoretical  $f_S$  at higher  $T$ . Finally, Foreman<sup>217</sup> has estimated the volume of a vacancy in Ar including the three-body interactions of Jansen and Zimring. He finds the elastic relaxation per vacancy to be about 0.25 molecular volumes, much increased over relaxation in the two-body interaction model, and the volume of a vacancy would thus be 0.75 molecular volumes, i.e.,  $3a_0^3/16$ .

## 2. Anharmonicity and Grüneisen's Constant

The problem of calculating thermodynamic properties including anharmonicity effects is formidable and no entirely satisfactory treatment is available. Henkel<sup>218,219</sup> has developed an elegant approach for taking into account small anharmonicities in the Einstein model of crystals. He supposes that when a particle is displaced from its equilibrium position at the origin to a point  $(x, y, z)$  its potential energy becomes<sup>220</sup>

$$V(x, y, z) = P_0/2 + P_2(x^2 + y^2 + z^2) + P_4(x^4 + y^4 + z^4). \quad (54)$$

The dependence of  $P_0$ ,  $P_2$ , and  $P_4$  on volume and potential parameters is obtained by inverse power sums over all particles in an infinite lattice. In order to get the energy levels from which the partition function  $Q$  may be calculated the potential of Eq. (54) is substituted into the time independent Schrödinger equation. If  $P_4$  is sufficiently small this reduces to the problem of the perturbed three-dimensional harmonic oscillator which may be solved by separation of variables. The resultant partition function for the atom is

$$Q = \sum_j \exp(-\epsilon_j/kT) = \exp(-P_0/2kT) \times \exp(-3W/2kT) \left\{ \sum_{n=0}^{\infty} \exp[-k^{-1}T^{-1}(nW + n^2Y)] \right\}^3 \quad (55)$$

where

$$W = \hbar(2P_2/m)^{1/2} + Y; \quad Y = 3\hbar^2 P_4/4mP_2.$$

<sup>217</sup> A. J. E. Foreman, *Phil. Mag.* **8**, 1211 (1963).

<sup>218</sup> J. H. Henkel, Ph.D. thesis, Brown University, 1954.

<sup>219</sup> J. H. Henkel, *J. Chem. Phys.* **23**, 681 (1955).

<sup>220</sup> J. W. Leech, *Can. J. Phys.* **27**, 1067 (1959), notes that for the *one-dimensional* anharmonic chain model, which can be solved exactly, it can be shown that cubic terms in the displacement are very important in the analog of Eq. (54).

In the limit of a small perturbing anharmonic term  $V \ll W$ , and a good approximation to  $F = -NkT \ln Q$  may be obtained with an expansion of only a few terms of the infinite sum in Eq. (55).

Comparison of this model with experimental data for Ar has been carried through by Henkel using a (6, 10) potential, and subsequently by Zucker<sup>221</sup> using an improved (6, 12) potential. Zucker compared Henkel's anharmonic Einstein model with a harmonic quasi-Debye model for crystalline Ar, i.e., a Debye model in which  $\Theta_D$  is taken as a function of  $V$  so that  $\beta$  and  $\chi_T$  may be calculated. The differences between the models are small at low  $T$  ( $T \lesssim \Theta_D/5$ ) but at higher  $T$  the differences become larger and the anharmonic model gives values for  $\rho(T)$ ,  $\beta(T)$ ,  $C_v(T)$ ,  $C_p(T)$ ,  $\chi_T(T)$ , and  $\chi_T(P)$  in better agreement with experiment. In general the anharmonic lattice is denser, has smaller thermal expansivity, smaller isothermal compressibility, and smaller specific heats than the harmonic lattice. Agreement with experiment is very good for not too low  $T$  for such an admittedly crude model. For  $C_p$  the predictions of the anharmonic model<sup>219</sup> fall between 1–2½% lower than experimental  $C_p$  data (Fig. 21) between 20°–60°K. At lower  $T$  the Einstein model is generally inaccurate as has been noted and for  $T \gtrsim 60^\circ\text{K}$  where the deviations are largest, vacancy effects become important in the experiments. Henkel's model has also been applied remarkably successfully on solid-state properties of Ne by Johns<sup>193</sup> who used it to calculate from first principles the vapor-pressure ratio of <sup>20</sup>Ne to <sup>22</sup>Ne in agreement with experiment.

Anharmonic contributions to thermodynamic properties at low  $T$  of fcc Debye solids have been recently investigated by Flinn and Maradudin.<sup>222</sup> The contributions to  $F$  and  $\Theta_D$  appear as terms in  $\phi^{\text{III}}(r_0)$  and  $\phi^{\text{IV}}(r_0)$  and in Pb, to which the model is applied, the calculated anharmonicity effects on  $\Theta_D$  are about 1%. Sufficiently reliable  $\phi(r)$  are now available for rare-gas solids so that this model could probably be profitably applied to them.

Grüneisen's equation of state is<sup>1</sup>

$$PV + VU'_0(V) = \gamma E_{\text{vib}} \quad (56)$$

in which  $U_0(V)$  and  $E_{\text{vib}}$  are, respectively, the non-thermal (static lattice) and thermal contributions (including  $E_z$ ) to internal energy  $E$ . The term on the right is more generally given by

$$\gamma E_{\text{vib}} = \sum_j \gamma_j \hbar \nu_j \left\{ \frac{1}{2} + 1/[\exp(\hbar \nu_j/kT) - 1] \right\} \quad (57)$$

in which  $\nu_j$  are the lattice frequencies and

$$\gamma_j = -d \ln \nu_j / d \ln V. \quad (58)$$

Equation (56) may be derived from the assumption that the  $\gamma_j$ 's in Eq. (58) are all equal and functions of

<sup>221</sup> I. J. Zucker, *Phil. Mag.* **3**, 987 (1958).

<sup>222</sup> P. A. Flinn and A. A. Maradudin, *Ann. Phys.* **22**, 223 (1963).

TABLE VII. Grüneisen's constant  $\gamma$  for rare-gas solids. For Ar and Kr, tabulated values are for  $\gamma = \beta/\rho\chi_S C_p$  using  $\beta$ ,  $\rho$ , and  $C_p$  data taken from figures in the text and  $\chi_S$  from Refs. 1 and 99 and the law of corresponding states. For Ne and Xe, tabulated values are for  $\gamma = \beta/\rho\chi_T C_v$  using  $\beta$ ,  $\rho$ , and  $C_v$  data taken from figures in the text. For Xe, data for  $\chi_T$  were taken from Ref. 35. For Ne,  $\chi_T$  was estimated from a single value at 4°K (Refs. 248 and 8) and the law of corresponding states. Constants obtained from extrapolated data are bracketed.

$T(^{\circ}\text{K})$	5	10	15	20	40	60	80	110	140
$\gamma(\text{Ne})$	4.16	2.85	2.69	2.68					
$\gamma(\text{Ar})$				1.78	2.87	2.83	[2.21]		
$\gamma(\text{Kr})$				2.05	2.27	2.42	2.33	[1.76]	
$\gamma(\text{Xe})$				1.95	2.91	3.06	2.88	[2.47]	[1.88]

$V$  alone and under these conditions we have for the Grüneisen constant  $\gamma$

$$\gamma = \beta/\rho\chi_T C_v = \beta/\rho\chi_S C_p \quad (59)$$

in which  $\chi_T$  and  $\chi_S$  are, respectively, isothermal and adiabatic compressibilities.<sup>1</sup> Grüneisen's rule states that at low  $T$ , say  $T < \Theta_D$ ,  $\beta$  is proportional to  $C_p$  and  $C_v$ . Generally the  $\gamma_i$ 's in Eq. (58) may differ widely and  $\gamma$  as defined by Eq. (59) varies both with  $V$  and  $T$ . The behavior of  $\gamma(V, T)$  in particular as a measure of anharmonicity, has been much discussed for rare-gas solids both experimentally and theoretically.

Table VII shows values of  $\gamma$  computed at several  $T$  from Eq. (59) with experimental data on  $\beta$  (Figs. 5–8),  $\rho$  (Figs. 1–4), and  $C_p$  and  $C_v$  (Figs. 21–23). Except for Xe for which rather complete data on  $\chi_T(T)$  is available<sup>35</sup> and Ar for which  $\chi_S(T)$  has been reliably deduced from experimental data,<sup>99</sup> compressibilities have been estimated with heavy reliance on the principle of corresponding states. This assumption, viz. that  $\chi_S(T)/\chi_S(0)$  is the same function of  $T/T_{tp}$  for all rare-gas solids has only been tested, over limited temperature ranges, for Ar and Kr. For this reason and also because  $\beta$  is in general not accurately known, the tabulated values of  $\gamma$  are to be regarded as approximate and theoretical deductions about  $\gamma$  cannot be rigorously tested until more data is available. Clusius, Flubacher, *et al.*<sup>211</sup> have obtained the following single values ( $T=16^{\circ}\text{K}$ ) of  $\gamma$  from Eq. (59) for Ne isotopes,  $\gamma(^{20}\text{Ne})=4.09$ ,  $\gamma(^{22}\text{Ne})=4.24$ .

Barron<sup>48,223,224</sup> has discussed the temperature variation of  $\gamma$  by using Born-von Kármán lattice dynamics. According to this model the principal variation in  $\gamma$  independent of the crystal should occur at temperatures of the order of  $0.2\Theta_D$  in qualitative agreement with experimental data on metals. For rare-gas crystals in which the molecules interact with a Lennard-Jones ( $m, n$ ) potential, the behavior of  $\gamma(T)$  may be more quantitatively determined. For a (6, 12) potential considering all neighbor interactions,  $\gamma_{\infty}(T$  sufficiently above  $0.2\Theta_D)=2.96$  and  $\gamma_0(T$  sufficiently below  $0.2\Theta_D)=2.82$ . Some general qualitative agreement

with experimental  $\gamma$ 's may be seen from the  $\gamma$  for Ar, Kr, and Xe in Table VII in which  $\gamma$  has a high and more or less constant value (about 3 for Ar and Kr) at  $40^{\circ}$ – $60^{\circ}\text{K}$  and falls sharply near  $20^{\circ}\text{K}$ . This kind of behavior for  $\gamma(\text{Ar})$  has been previously discussed.<sup>1,225</sup> The fall of  $\gamma$  at  $T > 60^{\circ}\text{K}$  and the anomalous behavior of  $\gamma(\text{Ne})$  is not accounted for since the theory breaks down at higher  $T$  and for large zero-point energies. A recent calculation of  $\gamma$  and an extension of the equation of state to define and calculate higher order Grüneisen constants for solid Ar and other lattices has been reported by Arenstein *et al.*<sup>226</sup> in generally good agreement with Barron's work.

Savvinykh<sup>227</sup> has calculated the equation of state of ideal crystals in a harmonic lattice approximation taking oscillation frequencies explicitly into account. The isotherms,  $C_p(T)$ , and  $C_v(T)$  given by this detailed model are in excellent agreement with results given by the simpler Grüneisen model and both are in good agreement with experiment. The theoretical volume dependence of  $\gamma$  has been studied for several kinds of Grüneisen constants by Vashchenko and Zubarev.<sup>228</sup> It may be shown from their result for Ar that  $\gamma$  is approximately a linear function of molar volume in agreement with the experimental observations of Packard and Swenson<sup>35</sup> who concluded that for  $T > \Theta_D$ ,  $\gamma$  is a linear function of molar volume at constant  $T$  for Xe.

#### D. Zero-Point Properties

On Table VIII are collected modern values for several zero-point properties of rare-gas solids, e.g.,  $\Theta_{D0}$ , the Debye temperatures extrapolated to  $0^{\circ}\text{K}$  (see III.C);  $\rho_0$  and  $a_{00}$ , respectively, the densities and lattice parameters extrapolated to  $0^{\circ}\text{K}$  (see I.A); and  $\chi_0$ , the compressibilities extrapolated to  $0^{\circ}\text{K}$  (see III.E). The quantum parameters  $\Lambda^*$  (see III.B.1) are, essentially, temperature independent. Heats of sublimation  $L_0$ , zero-point energies  $E_z$ , and the static-lattice

<sup>225</sup> C. Domb and I. J. Zucker, *Nature* **178**, 484 (1956).

<sup>226</sup> M. Arenstein, R. D. Hatcher, and J. Neuberger, *Phys. Rev.* **131**, 2087 (1963).

<sup>227</sup> S. K. Savvinykh, *Fiz. Metal. i Metalloved.* **6**, 400 (1958).

<sup>228</sup> V. Ya. Vashchenko and V. N. Zubarev, *Fiz. Tver. Tela* **5**, 886 (1963) [English transl.: *Soviet Phys.-Solid State* **5**, 653 (1963)].

<sup>223</sup> T. H. K. Barron, *Ann. Phys.* **1**, 77 (1957).

<sup>224</sup> T. H. K. Barron, *Proc. Seventh Internat. Conf. Low Temp. Phys.*, Toronto, 1960, pp. 655–670.

TABLE VIII. Zero-point and related properties.

	Latent heats (cal/mole)				Zero pt. energy <sup>m</sup> ( $E_z$ ) (cal/mole)	Density at 0°K ( $\rho_0$ ) (g/cm <sup>3</sup> )	Lattice parameter at 0°K ( $\bar{a}_0$ ) (Å)	Compressibility at 0°K ( $\chi_0$ ) (cm <sup>2</sup> /dyne)	Quantum parameter <sup>t</sup> ( $\Lambda^* = h/\sigma(m\epsilon)^{1/2}$ )
	Debye Temp. (°K) at 0°K $\Theta_D$	Sublimation at 0°K $L_0$	Sublimation at t.p. $L_s$	Fusion at t.p. $L_f$					
Ne	66.6 <sup>a</sup>	448 <sup>e,f,g</sup>	511 <sup>f,i</sup>	80.1 <sup>f,k</sup>	154 <sup>n</sup>	1.508 <sup>o</sup>	4.4620 <sup>o,p</sup>	$10 \times 10^{-11s}$	0.574
Ar	93.3 <sup>b</sup>	1846 <sup>b</sup>	1861 <sup>b</sup>	284.5 <sup>l</sup>	187 <sup>b</sup>	1.769	5.312 <sup>q</sup>	$3.98 \times 10^{-11b}$	0.184
Kr	71.7 <sup>b</sup>	2666 <sup>b</sup>	2579 <sup>b</sup>	392.0 <sup>b</sup>	145 <sup>b</sup>	3.094	5.644 <sup>q</sup>	$3.88 \times 10^{-11b}$	0.105
Xe	55 <sup>o,d</sup>	3828 <sup>b</sup>	3450 <sup>i</sup>	548.5 <sup>o</sup>	123 <sup>d</sup>	3.782	6.131 <sup>q,r</sup>	$2.8 \times 10^{-11d}$	0.0637

<sup>a</sup> Interpolated value obtained from  $\Theta_{D0}(^{20}\text{Ne}) = 66.7^\circ\text{K}$  and  $\Theta_{D0}(^{22}\text{Ne}) = 65.2^\circ\text{K}$  as measured in Ref. 211. K. Clusius (Ref. 24) has measured  $C_p$  for pure  $^{20}\text{Ne}$  and found  $\Theta_D(^{20}\text{Ne}) = 64^\circ\text{K}$ ,  $T \approx 10^\circ\text{K}$ .

<sup>b</sup> Reference 99.

<sup>c</sup> Reference 210.

<sup>d</sup> Reference 35.

<sup>e</sup> Reference 212.

<sup>f</sup> Reference 24.

<sup>g</sup> Reference 176.

<sup>h</sup> Reference 137.

<sup>i</sup> Reference 184.

<sup>j</sup> Calculated from Clausius-Clapeyron Eq. (10) with data from Ref. 8 and this paper.

<sup>k</sup> For the principle isotopes of Ne:  $L_f(^{20}\text{Ne}) = 79.20$  cal/mole,  $L_f(^{22}\text{Ne}) = 79.74$  cal/mole, and interpolated  $L_f(^{20}\text{Ne}) = 79.3$  cal/mole; Ref. 211.

<sup>l</sup> Reference 171.

<sup>m</sup>  $E_z = 9R\Theta_{D\infty}/8$ , Ref. 229.

<sup>n</sup> Reference 211.

<sup>o</sup> For the principal isotopes of Ne:  $a_{00}(^{20}\text{Ne}) = 4.4622 \text{ \AA}$ ,  $\rho_0(^{20}\text{Ne}) = 1.494 \text{ g/cm}^3$ ;  $a_{00}(^{22}\text{Ne}) = 4.4536 \text{ \AA}$ ,  $\rho_0(^{22}\text{Ne}) = 1.653 \text{ g/cm}^3$ .

<sup>p</sup> Reference 39.

<sup>q</sup> Reference 28.

<sup>r</sup> Reference 37.

<sup>s</sup>  $T = 4^\circ\text{K}$ , Reference 249.

<sup>t</sup> Calculated from  $\epsilon$  and  $\sigma$  values on Table III.

energies  $U_0$ , all at 0°K are connected by

$$E_0 = -L_0 = U_0 + E_z, \quad (60)$$

from which  $U_0$  can be found from tabulated  $L_0$  and  $E_z$ .  $E_z$  was calculated, using modern estimates of  $\Theta_{D\infty}$ , from the equation  $E_z = 9R\Theta_{D\infty}/8$  as developed by Domb and Salter.<sup>229,1</sup>  $\Theta_{D\infty}$  is the limiting value of  $\Theta_D$  at high temperatures although from theoretical considerations  $\Theta_D \rightarrow \Theta_{D\infty}$  rapidly for  $T > \Theta_D/5$ . The influences of this expression for the zero-point energy on internal energy, equilibrium volume, and especially on elastic constants all at 0°K have been examined by Salter<sup>230</sup> and others.<sup>231</sup> Wallace<sup>63</sup> has recently analyzed errors in using this expression by considering anharmonic corrections, beginning with terms in  $T^4$ , to the free energy  $F$  at 0°K. He found that the true zero-point energy is less than  $9R\Theta_{D\infty}/8$  but that the relative difference is 1% or less as long as the powers in the  $(m, n)$  potential are large enough, i.e., short-range forces.

Among the latent heats in Table VIII, the heat of fusion at the t.p.  $L_f$  is determined directly from experiment. The heats of sublimation at the t.p. and 0°K, respectively,  $L_s$  and  $L_0$  are generally calculated from experimental data on  $C_p$  and heats of vaporiza-

tion using standard thermodynamic relations, e.g.,<sup>99</sup>

$$L_0 = L_s(T) - \int_0^T C_p(\text{gas}) dT + \int_0^T C_p(\text{solid}) dT + RPT^2 \left( \frac{dB}{dT} \right), \quad (61)$$

in which  $B$  is the second-virial coefficient; the term in  $(dB/dT)$  is a correction for gas imperfection. Vapor pressure measurements [see III.B.2, Eq. (37)] have also been used to determine  $L_s$  and  $L_0$ .

There have been several rather successful theoretical approaches to the zero-point properties of rare-gas solids, usually from a combination of quantum-mechanical first principles and the principle of corresponding states (see III.B). Bernardes<sup>232</sup> has calculated the molar volume  $V_0$  and total lattice energy  $E_0 = -L_0$  at 0°K for Ar, Kr, Xe, and Ne, in substantial agreement with experiment in this manner. Bernardes's general procedure was to find the volume-dependent energy  $E_0(V)$  in the Schrödinger equation using an experimentally determined (6, 12) potential and suitable Heitler-London variational wavefunctions. The product wavefunction for the solid is composed of single-particle wavefunctions for the ground and first-excited states of a particle in a spherical box. This absence of correlation among the atoms is a characteristic of the

<sup>229</sup> C. Domb and L. Salter, *Phil. Mag.* **43**, 1083 (1952).

<sup>230</sup> L. Salter, *Phil. Mag.* **45**, 360 (1954).

<sup>231</sup> T. H. K. Barron and M. L. Klein, *Proc. Phys. Soc. (London)* **82**, 161 (1963).

<sup>232</sup> N. Bernardes, *Phys. Rev.* **112**, 1534 (1958).

Einstein crystal and indeed further refinement could be obtained by including explicit correlation terms. The calculation takes into account two contributions to  $E_0$  due to quantum effects, viz. the correction  $\Delta U_0$  to the static potential energy necessary to account for motion of the lattice molecules around their static sites, and the zero-point kinetic energy. Both contributions are approximately equal in magnitude and have the same sign (plus); for Ne their combined magnitude<sup>232</sup> is 28% of  $U_0$ , for Ar 10%, for Kr 5.6%, and for Xe 3.7%. The equilibrium molar volume  $V_0$  at 0°K is calculated from the zero-point equation of state:

$$P_0 = - (dE_0(V)/dV)_{V=V_0}, \quad (62)$$

taking  $P_0=0$  at  $V=V_0$  to determine the equilibrium volume  $V_0$ . Substitution of  $V_0$  back into  $-E_0(V)$  gives  $L_0$ . Zero-point compressibility and the  $P(V)$  isotherm may be obtained from the more general

$$P = - (dE_0(V)/dV)_{T=0^\circ\text{K}}.$$

Bernardes<sup>160,233</sup> has also calculated several zero-point properties in their explicit dependence on the quantum parameter  $\lambda = \hbar/\sigma(2m\epsilon)^{1/2}$  in an application of the variational technique to the classical law of corresponding states (in the classical limit of no zero-point energy,  $\lambda=0$ ). In the usual reduced units  $E^* = E/N\epsilon$ ,  $V^* = V/N\sigma^3$ ,  $P^* = P\sigma^3/\epsilon$ ,  $K_T^* = -V^*(dP^*/dV^*)_{T^*}$ , he obtains (0°K)

$$E_0^* = -8.61(1 - 5.34\lambda + 16\lambda^2), \quad (63a)$$

$$V_0^* = 0.916(1 + 2.02\lambda + 5\lambda^2), \quad (63b)$$

$$K_0^* = 75(1 - 9.4\lambda + 28\lambda^2), \quad (63c)$$

$$P^* = (24.3V^{*-5} - 28.9V^{*-3}) + 114\lambda V^{*-10/3}, \quad (63d)$$

along with analogous expressions for longitudinal sound-wave velocity, Debye temperature, and Grüneisen's constant<sup>233</sup> ( $\gamma=2.83$ ). Agreement with experiment for Eqs. (63a, b, and c) is very good for all the rare-gas solids including Ne, although not so good as  $\lambda$  increases, as for deuterium and lighter molecules. The experimental comparison of Eq. (63c) for the reduced initial bulk modulus  $K_0^*$  is displayed on Fig. 15 (the ordinate axis is  $K_0^*/75$  and  $\lambda = \Lambda^*/2\pi\sqrt{2}$ ). A comparison of experimental  $P$ ,  $V$  data with Eq. (63d) shows<sup>233</sup> reasonable agreement for Ne and Xe but not for Ar.

Zucker<sup>161</sup> in an extension in the Einstein model of the work of Salter<sup>230</sup> has derived a reduced equation of state and expressions analogous to (63a) and (63b) for  $E_0^*$  and  $V_0^*$  at 0°K as functions of  $\Lambda^*$  by taking explicit account of the anharmonic terms of the fourth and sixth order in displacement components in the potential of Eq. (54). A plot of the function  $F_0^*(\Lambda^*)$  is shown on Fig. 16. Incorporation of anharmonic terms into the

equation of state makes it possible to take satisfactory account of large zero-point vibrations up to and including those in  $^4\text{He}$ . A quantum-mechanical variational principle technique which takes some account of correlation between molecules has been described by Yoshimori and Matsubara.<sup>234</sup> In this treatment the wavefunction for the solid is taken as a generalization of that for an assembly of harmonic oscillators:  $\psi \propto \exp[-(a \text{ quadratic form in the displacements of nearest neighbors in the lattice})]$ . The coefficients in the quadratic form are taken as the variational parameters. Analysis is carried through using both a harmonic potential and also using a potential with small anharmonicity (Ne). For Ne including anharmonicity and a suitable (exp, 6) two-body potential,  $L_0=445$  cal/mole; ignoring anharmonicity increases this by 2%, all in excellent agreement with the tabulated  $L_0$ .

Nosanow and Shaw<sup>235</sup> have made a more refined iterative computer calculation of  $E_0$  in the Schrödinger equation for rare-gas solids using self-consistent Hartree wavefunctions. Their physical assumptions about the lattice are the same as those of Bernardes, viz., single-particle wavefunctions spherically symmetric about static lattice sites, and the resultant  $L_0$ 's are slightly closer to experimental values.<sup>232</sup> Since this calculation is the optimum one with such a wavefunction, one can estimate from the experimental comparison that correlation and symmetry effects in the lattice account for about 5% of  $E_0$  in Ne and less in the other solids. It is worth noting that the self-consistent potential for the crystals turns out to be well approximated by a harmonic oscillator potential when the mean-square deviation  $\delta^2$  of an atom<sup>160</sup> from its lattice site,  $\delta^2 = 0.121\lambda\sigma^2(1+6.1\lambda)$ , is small. For lighter molecules—e.g., He—the self-consistent potential is more nearly a square well.

The general idea of molecules localized in spherical boxes and acted on by a spherically averaged potential due to all other molecules in the lattice is familiar from the cell model of liquids.<sup>236</sup> The approximation holds better the smaller the actual displacements of the molecules from their lattice sites, but near the boundary of the cell the field is decidedly nonspherically symmetric so application to molecules with small  $\Lambda^*$  is limited. Hurst and Levelt<sup>237</sup> have extended the cell model to calculate  $E_0$ ,  $E_2$ , and the equation of state of rare-gas solids at 0°K with an anharmonic Einstein theory.

Total static potential energy is obtained from a specially calculated sphericalized potential in the

<sup>234</sup> A. Yoshimori and T. Matsubara, *J. Phys. Soc. Japan* **9**, 465 (1954).

<sup>235</sup> L. H. Nosanow and G. L. Shaw, *Phys. Rev.* **128**, 546 (1962).

<sup>236</sup> J. M. H. Levelt and R. P. Hurst, *J. Chem. Phys.* **32**, 96 (1960) and references given there, especially J. E. Lennard-Jones and A. F. Devonshire, *Proc. Roy. Soc. (London)* **A163**, 53 (1937).

<sup>237</sup> R. P. Hurst and J. M. H. Levelt, *J. Chem. Phys.* **34**, 54 (1961).

<sup>233</sup> N. Bernardes and C. A. Swenson, in *Solids Under Pressure*, edited by W. Paul and D. M. Warschauer, pp. 101–136.

variable  $\rho$  (reduced displacement from static-lattice position):

$$V(\rho) = 4\epsilon \sum_{n=0}^{\infty} B_{2n} \rho^{2n},$$

in which the  $B$ 's are constants determined from the intermolecular potential and lattice structure. Zero-point energy per molecule is the ground-state eigenvalue in the Schrodinger equation:

$$-(\hbar^2/2m\sigma^2) \nabla^2 \psi + [4\epsilon \sum_{n=1}^{\infty} B_{2n} \rho^{2n} - e_0] \psi = 0.$$

Zero-point properties are calculated from  $U_0 + E_z$  in the standard manner using Eq. (62). No adjustable parameters are needed in this calculation and the use of (6, 12) potentials obtained from second-virial coefficients leads to generally good agreement with experiment from Xe through He.

Gombás and Kunvári<sup>238</sup> have assumed that the high symmetry of lattice sites in rare-gas solids allows consideration of the molecules as localized, spherical, electron gases. Using the statistical theory of the atom, the equation of state Eq. (62) for an atom is obtained;  $E_0$  and  $V$  in this case the energy and volume of an atom, and  $P(V)$  curves at 0°K are calculated for the solids.

Dugdale and MacDonald<sup>239</sup> have proposed from a Debye consideration of the solids the nonlinear differential equation:  $y = v(x) + a(y'')^{\frac{1}{2}}$ , to describe zero-point properties. In this equation:  $y = E_0/N\epsilon$ ,  $v = \phi(r)/\epsilon$ ,  $x = r/\sigma$ , and  $a \propto \Lambda^*$ . Although a limited iterative solution of the equation gives good values for  $E_0$ ,  $V_0$ , and  $\Theta_D$ , a continuation of the iteration<sup>240</sup> diverges for  $a > 0$  ( $E_z > 0$ ) and  $r > 0$ . The behavior of the equation in the limit  $a \rightarrow 0$  is apparently nonphysical, and the equation has no solutions which are physically acceptable over the whole range of  $r$ . Therefore, although the equation has some physical significance, it is not entirely suitable for investigating zero-point properties.

### E. Compressibility

Although the  $P$ - $V$ - $T$  surfaces of rare-gas solids have been much studied experimentally (e.g., see II), knowledge is limited of the surfaces themselves and especially of their important derivatives: isothermal compressibility  $\chi_T(P, T) = -V^{-1}(\partial V/\partial P)_T$ , volume expansion coefficient  $\beta(P, T) = V^{-1}(\partial V/\partial T)_P$  (see I.B), and "thermal pressure"<sup>241</sup>  $(\partial P/\partial T)_V$ . We here discuss experimental compressibility determinations and some of their theoretical aspects.

<sup>238</sup> P. Gombás and O. Kunvári, Acta Phys. Acad. Sci. Hungary **5**, 339 (1955).

<sup>239</sup> J. S. Dugdale and D. K. C. MacDonald, Phil. Mag. **45**, 811 (1954).

<sup>240</sup> M. E. Fisher and I. J. Zucker, Proc. Cambridge Phil. Soc. **57**, 107 (1961).

<sup>241</sup> F. Simon and F. Kippert, Z. Physik. Chem. **135**, 113 (1928).

The adiabatic compressibility  $\chi_S(P \approx 0, T)$  of solid Ar under its own vapor pressure has been determined from measurements of the velocity of longitudinal ultrasonic waves<sup>105, 242</sup>  $v_l$ , and more satisfactorily, from measurements of both  $v_l$  and the velocity of transverse ultrasonic waves<sup>106</sup>  $v_t$ . From these  $\chi_S$  may be obtained from:

$$\chi_S = 1/\rho(v_l^2 - \frac{4}{3}v_t^2), \quad (64)$$

and from  $\chi_S$ ,  $\chi_T$  may be calculated with:

$$\chi_T = \chi_S(1 + \beta T \gamma). \quad (65)$$

The velocities have been measured between about 60°K and the triple-point temperature on polycrystalline solids, of approximate grain size 0.1 mm, condensed from the vapor into a resonance chamber in which plane ultrasonic waves of known frequency are typically<sup>105, 106</sup> excited by a quartz-crystal transducer. The thickness of the Ar solid may be varied and measured at successive standing wave resonances to determine the velocities. Measurements of this kind as of all elastic properties, are best carried out on single crystals but strain free homogeneous polycrystals are suitable for ultrasonic velocity determinations as long as the wavelength is large compared to grain size, in these experiments typically  $\lambda \approx 1$  mm. Even when these conditions are satisfied, attenuation, about 0.6 cm<sup>-1</sup> at 1.5 Mc,<sup>242</sup> and possible dispersion at the grain boundaries along with other effects of microscopic and macroscopic imperfection in the solid, limit the accuracy of the results. Smoothed values of the velocities are:  $v_l(60^\circ\text{K}) = 1420$  m/sec,  $v_l(84^\circ\text{K}) = 1290$  m/sec and  $v_t(60^\circ\text{K}) = 750$  m/sec,  $v_t(84^\circ\text{K}) = 705$  m/sec. The ratio  $v_t/v_l = 0.54$  is approximately constant over this range. Theoretical predictions of  $v_l$  by Dobbs<sup>243</sup> using Henkel's Einstein model of the crystal are somewhat larger than these and outside the experimental error. The ratio  $v_t/v_l$  however has been accurately calculated<sup>244</sup> from low-temperature lattice dynamics and consideration of the important problem of properly averaging single crystal  $v_l$  and  $v_t$  values to get expected velocities through a solid of randomly-oriented crystallites. An expert discussion of elastic constants of solid Ar may be found in the review of Dobbs and Jones.<sup>1</sup>

Fig. 25 shows  $\chi_T$ 's at low  $P$  as functions of  $T$ , as far as they are known for rare-gas solids. The data originate in the ultrasonic velocity experiments discussed above and other experiments to be discussed below. As has been pointed out by Beaumont *et al.*<sup>99</sup> the extrapolation of  $\chi_S$  for Ar to 0°K given by Barker and Dobbs<sup>106</sup> assumes a  $\Theta_{D0}$  determined from elasticity data much smaller than the more reliable  $\Theta_{D0}$  from specific-heat

<sup>242</sup> E. W. Guptill, C. K. Hoyt, and D. K. Robinson, Can. J. Phys. **33**, 397 (1955).

<sup>243</sup> E. R. Dobbs, J. Chem. Phys. **24**, 477 (1956).

<sup>244</sup> T. H. K. Barron and C. Domb, Phil. Mag. **45**, 654 (1954).

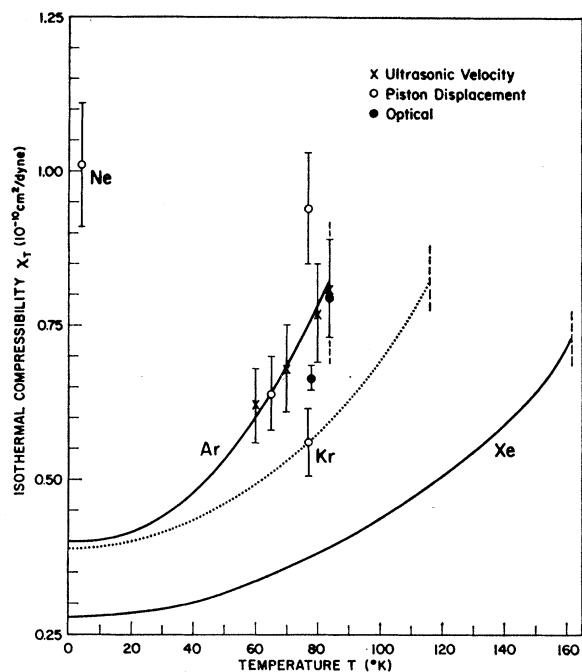


FIG. 25. Isothermal compressibilities  $\chi_T = -(1/V)(\partial V/\partial P)_T$  at low pressure as functions of temperature for solid Ne, Ar, Kr, and Xe. Ne: The single point at 4°K is from experimental data of Ref. 249. Ar: From 0°–50°K the  $\chi_T$  curve is calculated from  $\chi_S$ , Ref. 99, extrapolated from theory and ultrasonic velocity data. The ultrasonic velocity data, as at higher  $T$ , are from Ref. 106, piston displacement data are from Ref. 249, and optical data are from Ref. 246. Kr: From 0°–50°K the  $\chi_T$  curve is estimated from theory at 0°K and the law of corresponding states applied to  $\chi_S$  of Ar, Ref. 99. From 50°K–t.p. the curve is extended with the law of corresponding states applied to  $\chi_T$  of Ar modified to pass through the single experimental point, Ref. 248. Xe: This curve is from experimental piston displacement data of Packard and Swenson, Ref. 35. The uncertainty varies from about 6% at the low temperature end to 12% near the triple point.

data. It has recently been shown<sup>245</sup> that even for an anharmonic crystal these two  $\Theta_{D0}$ 's should be equal. Thus the  $\chi_T$  curve for Ar on Fig. 25 is calculated from the theoretical-experimental extrapolation<sup>99</sup> using Eq. (65). The two optically determined  $\chi_T$ 's shown for Ar at higher  $T$  are from the recent interesting measurements of  $P$  and  $T$  dependence of the solid Ar index of refraction by Smith and Pings.<sup>246,247</sup> Since the compressibility of Kr has apparently been measured only at a single temperature, the  $\chi_T$  curve for Kr on Fig. 25 has been roughly estimated from the law of corresponding states applied to the Ar curve.

The earliest measurements of  $P$ - $V$ - $T$  surfaces for rare-gas solids at high  $P$  are due to Simon and Kipert,<sup>241</sup> who found, for Ar in the region of the t.p.,  $(\partial P/\partial T)_V = 38$  atm/°K up to about 500 atm. Subse-

quent experiments, for example those of Stewart<sup>248,249</sup> have generally been direct determinations of  $\chi_T$  by measuring the change in  $V$  with both increasing and decreasing  $P$  of a compacted sample in an isothermal pressure chamber,  $(\partial V/\partial P)_T$ . In the necessary  $P$  and  $T$  range many of the fluids which are otherwise preferred for transmitting hydrostatic pressures solidify or else have large compressibilities themselves. It is therefore generally most convenient to take data on rare-gas solids at temperatures for which they are sufficiently plastic (low shear strength) to serve as satisfactory pressure transmitters themselves. Extrusion experiments<sup>248</sup> show that Ne at 4°K, Ar at 65° and 77°K, and Kr at 77°K, are sufficiently plastic but at 4°K neither Ar nor Kr could be extruded. The largest source of error in the piston displacement technique is friction between the piston and walls of the chamber, i.e., the plot of piston displacement vs  $P$  for increasing and decreasing pressure shows a hysteresis loop. As noted earlier (see II), this is effectively minimized, however, by suitable averaging.

Stewart's<sup>248,249</sup> determinations of  $\chi_T(P)$  for Ar, Kr, and Ne, at the above temperatures is shown on Fig. 26 along with some isolated measurements of Lahr, Eversole, and Williams<sup>87</sup> along the melting curves of Ar and Xe. The  $P$  and  $T$  dependence of isothermal bulk

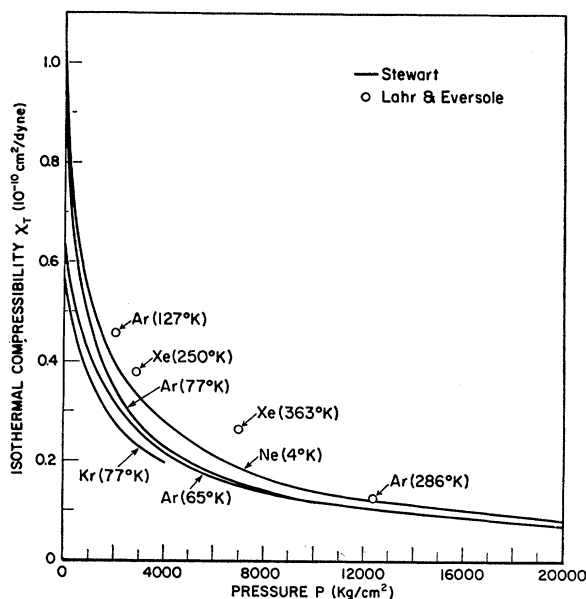


FIG. 26. Experimental isothermal compressibilities  $\chi_T = -(1/V)(\partial V/\partial P)_T$  as functions of pressure for solid rare gases. The curves for Ne (4°K), Ar (65°K), and Ar (77°K), are plotted from data of Ref. 249; Kr (77°K) is plotted from data in Ref. 248. For all the curves the approximate error is 10%. The isolated circles are plotted from  $\chi_T$  data for the solid phase along the melting line with approximate error 6%, Ref. 87.

<sup>245</sup> T. H. K. Barron and M. L. Klein, Phys. Rev. 127, 1997 (1962).

<sup>246</sup> B. L. Smith and C. J. Pings, J. Chem. Phys. 38, 825 (1963).

<sup>247</sup> B. L. Smith and C. J. Pings, Physica 29, 555 (1963).

<sup>248</sup> J. W. Stewart, Phys. Rev. 97, 578 (1955).

<sup>249</sup> J. W. Stewart, J. Phys. Chem. Solids 1, 146 (1956).

modulus  $K_T (= \chi_T^{-1})$ , and other thermodynamic properties, for Xe has been experimentally studied up to about 20 000 kg/cm<sup>2</sup> in recent piston displacement work of Packard and Swenson<sup>35,233</sup> and the general theory of pressure dependence of thermodynamic properties, about which relatively little is known, discussed (see, especially, Fig. 3 in Ref. 35). High-pressure isotherms for rare-gas solids generally fit well an equation given by Birch<sup>250</sup>:

$$P = \frac{3}{2} \chi_{T0} (V_0/V)^{5/3} \{ (V_0/V)^{2/3} - 1 \} \{ 1 - \xi [(V_0/V)^{2/3} - 1] \} \quad (66)$$

in which  $\chi_{T0}$  and  $V_0$  are, respectively, the isothermal compressibility and volume at zero pressure, and  $\xi$  is an adjustable characteristic parameter. Values of  $\chi_{T0}$  obtained by fitting data to this equation by Stewart<sup>248,249</sup> and by Packard and Swenson<sup>35</sup> are shown on Fig. 25 for Ne, Ar, Kr, and Xe. Since the lowest  $P$  at which the isotherms are determined is usually still quite high, some error is introduced in the long extrapolation.

The only rare-gas solid for which  $\chi_T$  data is available from both ultrasonic velocity as well as piston displacement experiments is Ar and from Fig. 25 it is clear that near the t.p. the two sets of data are in poor agreement. This difficulty has been much discussed<sup>106,248,249</sup> and is apparently a fundamental one possibly due to differences in microstructure between melt-grown and vapor-grown crystals. Although the piston displacement experiments use polycrystalline solids condensed from the melt under conditions which may favor formation of voids and vapor snakes (see II.B) and hence non-compactness in the solids, Stewart<sup>248,249</sup> has shown that compressing the solids to 4000 kg/cm<sup>2</sup> before taking data leads to reproducible results and, further, compressing the solids to 19 000 kg/cm<sup>2</sup> before taking data does not change the results. This implies that the samples were compact during data taking. An interesting and relevant theoretical problem, the effect of vacancies and other lattice defects on  $\chi_T$  of rare-gas solids, is difficult and has not yet been quantitatively discussed in the literature.

Analyses and predictions of  $\chi_T$  for rare-gas solids have been given by several of the thermodynamic and statistical mechanical approaches discussed earlier. Compressibility may be straightforwardly determined from theoretical equation of state isotherms by taking another volume derivative of  $F$ , i.e.,  $\chi_T^{-1} = V(\partial^2 F / \partial V^2)_T$ . The  $V$  dependence of  $F$  or of  $\nu_i$ , the lattice frequencies, is the problem of Grüneisen's law, also discussed earlier. Since  $\chi_T$ 's for rare-gas solids have not been so accurately determined experimentally as, say,

<sup>250</sup> F. Birch, *J. Geophys. Res.* **57**, 227 (1952).

specific heats and vapor pressures, we forego a detailed theoretical treatment here. In the interests of completeness however we briefly treat some rather recent very interesting contributions to the theory of elasticity and compressibility in these solids.

Davies and Parke<sup>251</sup> have extended Grüneisen's equation of state, Eq. (56), to

$$V/\chi_T = V^2 U_0''(V) + \gamma' E_{\text{vib}} - \gamma^2 T C_v, \quad (67)$$

in which again  $U_0$  and  $E_{\text{vib}}$  are nonthermal (static lattice) and thermal contributions to the internal energy, and  $U_0(V)$  is determined for a quasiharmonic lattice, a good approximation for Ar when  $T < 40^\circ\text{K}$ . The new constant  $\gamma' = (V^2/\nu_i)(\partial^2 \nu_i / \partial V^2)$  averaged over  $i$ , is a so called "second" Grüneisen constant obtainable from  $T$  dependence of  $\chi_T$ ; for Ar  $\gamma' \approx 10$ . Still higher-order Grüneisen constants appear in the coefficients of the expansion of  $F$  as a power series in dilatation,  $(V - V_0)/V_0$ . The theory gives  $C_p(T)$  and  $\beta(T)$  as well as  $\chi_T(P, T)$  in good agreement with experiment and with several other harmonic and anharmonic theories. For  $T > 40^\circ\text{K}$  the theoretical treatment of Zucker<sup>221</sup> which specifically considers anharmonic terms gives better agreement with experiment. In an extension of this work including zero-point energy and all neighbor interactions in Ar at  $0^\circ\text{K}$ , Parke<sup>252</sup> has calculated  $v_l$  and  $v_t$ , respectively, 1567 m/sec and 877 m/sec, and hence  $v_t/v_l = 0.56$ , for ultrasonic waves in a polycrystal. A semi-empirical treatment of Ar due to Kalinin<sup>253</sup> which assumes a Debye model for the crystal with  $U_0 = A \exp(-Bx^3) - Cx^{-2}$ ,  $A$ ,  $B$ , and  $C$  adjustable parameters and  $x = V/V_0$ , has been used to fit equation of state data satisfactorily from  $20^\circ$ – $80^\circ\text{K}$ . David and Hamann<sup>254</sup> have shown that at not too high pressures, say  $P < 10^4$  kg/cm<sup>2</sup>, and not too low temperatures, say  $T > 40^\circ\text{K}$ , the solid Ar  $P$ - $V$ - $T$  surface may be obtained from application to simple molecular solids of the Lennard-Jones and Devonshire liquid model.

#### ACKNOWLEDGMENTS

The author would like to thank all of his many correspondents who very generously provided him with reprints, preprints, and reports of work in progress. Floyd A. Mauer and Sigurd Larsen each very kindly read the entire manuscript and offered helpful comments and suggestions. He is also, particularly, indebted to Antoinette A. Pollack for indispensable help, especially with translations and library work.

<sup>251</sup> R. O. Davies and S. Parke, *Phil. Mag.* **4**, 341 (1959).

<sup>252</sup> S. Parke, *J. Phys. Chem. Solids* **23**, 267 (1962).

<sup>253</sup> V. A. Kalinin, *Zh. Eksperim. i Teor. Fiz.* **34**, 229 (1958) [English transl.: *Soviet Phys.-JETP* **7**, 158 (1958)].

<sup>254</sup> H. G. David and S. D. Hamann, *J. Chem. Phys.* **38**, 3037 (1963).

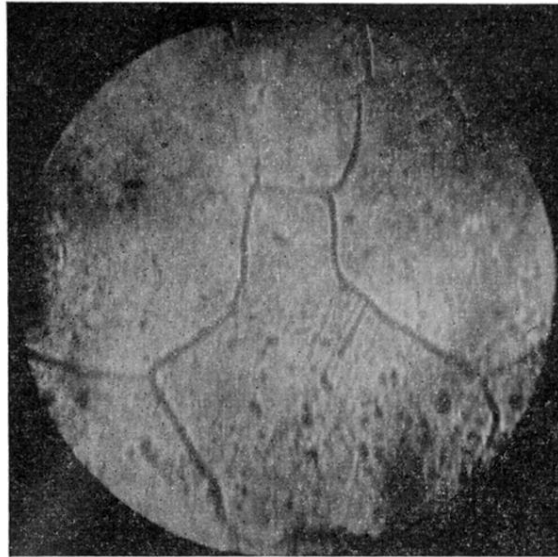


FIG. 12. Thermally etched surface of polycrystalline Ar grown from the melt. The heavy lines are grain boundaries. Notice also the striations on grain faces; these are probably twin boundaries or slip planes. Field diameter is 2 mm.